Development of Geopolymer-Carbon Composite for Wastewater Treatment

Lívia Firmani Silva

Thesis submitted to

Escola Superior de Tecnologia e Gestão

Instituto Politécnico de Bragança

Master Degree in

Chemical Engineering

Supervisors:

Prof. Dr. Helder Teixeira Gomes

Prof. Dr. Edilaine Regina Pereira

Bragança

2026

Development of Geopolymer-Carbon Composite for Wastewater Treatment

Lívia Firmani Silva

Thesis submitted to **Escola Superior de Tecnologia e Gestão** of **Instituto Politécnico de Bragança** under the framework of the Master's Degree in Chemical Engineering, and the double diploma with the **Universidade Tecnológica Federal do Paraná - Campus Campo Mourão**

Supervisors:

Prof. Dr. Helder Teixeira Gomes

Prof. Dr. Edilaine Regina Pereira

Bragança

2026

ACKNOWLEDGEMENTS

I begin by thanking God for guiding and supporting me throughout my Master's degree. I am also deeply grateful to my family, who never spared any effort to ensure I had the best opportunities and made it possible for me to be here today. I express my gratitude to my father, Elvis, for always teaching me to see life in a positive way; to my mother, Amônica, for teaching me the value of life and for being my intercessor; and to my brother, Murilo, who may not realize it, but who constantly teaches me about dedication and loyalty.

To my college partner and now my boyfriend, Gustavo, I sincerely thank you for supporting me throughout this journey we have always dreamed of. Thank you for being my partner, for comforting me even from afar, and for sharing yet another important experience with me. To all my friends, especially my lifelong friends Lívia and Bruna; the friends who were my home during college, Bianca and Natálli; my companions on this journey, Lorena and Luiz Eduardo; and all my friends who shared this experience with me here, on the other side of the ocean, my sincere thanks for the support and for the best conversations.

I sincerely thank my supervisors, Professor Helder Teixeira Gomes, from the Polytechnic Institute of Bragança (IPB), and Professor Edilaine Regina Pereira, from the Federal University of Technology of Paraná (UTFPR), Londrina campus, for the research opportunity and for all the support throughout this year. I am especially grateful to M.Sc. Ana Paula Ferreira, for being my mentor, for all the knowledge shared, for the opportunities granted, and for the trust placed in my work. I also thank the entire research group, especially Dr. Adriano Silva and Dr. Fernanda Roman, for all their support throughout the research process. I thank my professors at UTFPR, Campo Mourão campus, for their teaching and dedication, especially Professors Karla Silva and Marcelo Real Prado, for conveying their passion for Chemical Engineering and contributing to the development of my critical thinking.

Finally, I thank all those who were not mentioned by name, but who are part of this achievement.

This work was supported by national funds through FCT/MCTES (PIDDAC): CIMO, UIDB/00690/2020 (DOI: 10.54499/UIDB/00690/2020) and UIDP/00690/2020 (DOI: 10.54499/UIDP/00690/2020); and SusTEC, LA/P/0007/2020 (DOI: 10.54499/LA/P/0007/2020). The authors are grateful to Sociedade Ponto Verde for the financial support through the project "Avaliação de Ciclo de Vida de materiais geopoliméricos obtidos a partir da valorização de resíduos sólidos urbanos".

ABSTRACT

The quality of wastewater treatment and the discharge of treated effluents remain major environmental issues, particularly due to the release of contaminants of emerging concern into aquatic environments as a result of insufficient tertiary treatment in wastewater treatment plants. Among these contaminants of emerging concern, pharmaceuticals such as carbamazepine, are frequently detected in wastewater and poses potential risks to water quality. In this context, the present study investigates the development of geopolymer and geopolymer-carbon composite subjected to a zeolitization process, produced from waste-derived materials. Fly ash was used as the primary precursor for geopolymer synthesis, while activated carbon was obtained from grape pomace. Comprehensive characterization was performed to assess the composition, structure, and surface properties of the synthesized materials. X-ray diffraction analysis revealed the presence of major crystalline phases, including quartz, hematite, and calcite, as well as the formation of zeolitic phases (Na-faujasite) in GP_HT2.0, whereas GP_AC_HT2.0 exhibited only calcite and gehlenite phases. Fourier Transform Infrared Spectroscopy spectra confirmed the presence of Si–O–T groups in the inorganic (FA, GP_M, GP_ HT1.0, GP_ HT1.5, GP _HT2.0, and GP_HT2.5) materials and carbon-related (–CH_2 and –CH_3 groups, C–O and C–O–C) bonds in the organic (WGP, AC_WGP, GP _AC, and GP _AC_HT2.0) materials. Additionally, acid–base characterization demonstrated the high basicity of all samples. BET analysis revealed a specific surface area of 427 $m^2\ g^{-1}$ for AC, 30 $m^2\ g^{-1}$ for GP_M, 181 $m^2\ g^{-1}$ for GP _HT2.0, 48 $m^2\ g^{-1}$ for GP_AC, and 139 $m^2\ g^{-1}$ for GP_AC_HT2.0. Equilibrium analysis showed that the Langmuir model effectively described the adsorption process, indicating favorable conditions and strong affinity between the adsorbents and the adsorbate. Kinetic studies confirmed that all materials followed a pseudo-second-order model, the maximum adsorption capacities were determined as 4.2, 29.4, 39.7, and 30.6 mg g^{-1} for GP_M, GP _HT2.0, GP_AC, and GP_AC_HT2.0, respectively.

Keywords: Solid waste valorization; Circular economy; Geopolymer; Wastewater treatment; Contaminants of emerging concern; Carbamazepine.

RESUMO

A qualidade do tratamento de águas residuais e a descarga de efluentes tratados continuam a representar importantes desafios ambientais, particularmente devido à liberação de contaminantes de preocupação emergente em ambientes aquáticos como resultado da insuficiência do tratamento terciário em estações de tratamento de águas residuais. Entre esses contaminantes de preocupação emergente, fármacos como a carbamazepina são frequentemente detectados em águas residuais e representam potenciais riscos à qualidade da água. Nesse contexto, o presente estudo investiga o desenvolvimento de um geopolímero e de um compósito geopolímero–carbono submetidos a um processo de zeolitização, produzidos a partir de materiais derivados de resíduos. A cinza volante foi utilizada como principal precursor para a síntese do geopolímero, enquanto o carvão ativado foi obtido a partir do bagaço de uva. Uma caracterização abrangente foi realizada para avaliar a composição, estrutura e propriedades superficiais dos materiais sintetizados. A análise por difração de raios X revelou a presença de fases cristalinas majoritárias, incluindo quartzo, hematita e calcita, bem como a formação de fases zeolíticas (Na-faujasita) em GP_HT2.0, enquanto GP_AC_HT2.0 apresentou apenas as fases calcita e gehlenita. Os espectros de Espectroscopia no Infravermelho com Transformada de Fourier confirmaram a presença de grupos Si–O–T nos materiais inorgânicos (FA, GP_M, GP_HT1.0, GP_HT1.5, GP_HT2.0 e GP_HT2.5) e de ligações relacionadas ao carbono (grupos $–CH_2$ e $–CH_3$, C–O e C–O–C) nos materiais orgânicos (WGP, AC_WGP, GP_AC e GP_AC_HT2.0). Adicionalmente, a caracterização ácido–base demonstrou a elevada basicidade de todas as amostras. A análise BET revelou áreas superficiais específicas de 427 $m^2\ g^{-1}$ para AC, 30 $m^2\ g^{-1}$ para GP_M, 181 $m^2\ g^{-1}$ para GP_HT2.0, 48 $m^2\ g^{-1}$ para GP_AC e 139 $m^2\ g^{-1}$ para GP_AC_HT2.0. A análise de equilíbrio mostrou que o modelo de Langmuir descreveu adequadamente o processo de adsorção, indicando condições favoráveis e forte afinidade entre os adsorventes e o adsorvato. Os estudos cinéticos confirmaram que todos os materiais seguiram o modelo de pseudo-segunda ordem, e as capacidades máximas de adsorção foram determinadas como 4.2; 29.4; 39.7; e 30.6 mg g^{-1} para GP_M, GP_HT2.0, GP_AC e GP_AC_HT2.0, respectivamente.

Palavras-chave: Valorização de resíduos sólidos; Economia circular; Geopolímeros; Tratamento de águas residuais; Contaminantes de preocupação emergente; Carbamazepina.

LIST OF FIGURES

LIST OF TABLES

LIST OF ABBREVIATIONS

AC	Activated carbon
BET	Brunauer–Emmett–Teller method
CBZ	Carbamazepine
CECs	Contaminants of emerging concern
CNHS	Carbon, nitrogen, hydrogen and sulfur elemental analysis
FA	Fly ash
FT-IR	Fourier transform infrared spectroscopy
GP	Geopolymer
ID	Intraparticle diffusion model
pH	Hydrogen potential
pH_{PZC}	pH at the point of zero charge
PFO	Pseudo-first order model
PSO	Pseudo-second order model
SEM	Scanning electron microscopy
TGA	Thermogravimetric analysis
UV-VIS	Ultraviolet–visible spectroscopy
UWWTD	Urban wastewater treatment directive
WGP	Winery grape pomance
WWTPs	Wastewater treatment plants
XRD	X-ray diffraction
XRF	X-ray fluorescence

NOMEMCLATURE

C_0	Initial concentration of contaminant in solution (mg L^{-1})
C_{eq}	Equilibrium concentration of contaminant in solution (mg L^{-1})
k_1	Pseudo-first order rate constant (min^{-1})
k_2	Pseudo-second order rate constant (g mg^{-1} min^{-1})
k_F	Freundlich adsorption constant (L g^{-1})
k_{id}	Intraparticle diffusion rate constant (mg g^{-1} $min^{-0.5}$)
k_L	Langmuir adsorption constant (L mg^{-1})
n_F	Freundlich intensity parameter
q_{eq}	Adsorption capacity at equilibrium (mg g^{-1})
q_{max}	Maximum adsorption capacity of the adsorbent (mg g^{-1})
q_t	Adsorption capacity at time (mg g^{-1})
r^2	Coefficient of determination
S_{BET}	BET specific surface area (m^2 g^{-1})
S_{ext}	External surface area (m^2 g^{-1})
$S_{Langmuir}$	Langmuir-specific surface area (m^2 g^{-1})
S_{mic}	Microporous surface area (m^2 g^{-1})
t	Time (min)
V_T	Total pore volume (cm^3 g^{-1})

TABLE OF CONTENTS

1. INTRODUCTION

Water security has increasingly attracted global attention since the United Nations International Conference on Water, held in Mar del Plata, Argentina, in 1977, which formally recognized that all people, regardless of development status, have the right to access drinking water in quantities and quality sufficient to meet basic needs [1]. This challenge has directed societal and scientific efforts toward the development of advanced water treatment technologies across all stages [2], including membrane filtration [3], adsorption [4], and advanced oxidation [5], as well as the use of materials such as zeolites [6], activated carbons (ACs) [7], and ceramic membranes [8]. These approaches target a broad spectrum of pollutants, from contaminants commonly addressed in early treatment stages, such as suspended solids [9], and organic matter [10], to more persistent and emerging pollutants detected in advanced treatment, including heavy metals [11], dyes [12], pharmaceuticals [13], and personal care products [14].

Among these technologies, adsorption has been recognized as a particularly promising alternative due to its versatility for integration with other treatment systems, operational simplicity, effectiveness under mild conditions, and high pollutant removal efficiency [15]. Common adsorbents include porous inorganic materials and carbon-based solids, which are valued for their high surface area, tunable surface chemistry, and strong affinity for a wide range of contaminants. However, the production of conventional adsorbents often involves costly precursors and energy-intensive processes, highlighting the growing need for alternative materials derived from low-cost and abundant resources while maintaining comparable adsorption performance [16,17].

Within this context, geopolymers (GP), aluminosilicate-based materials [18] synthesized through the alkaline activation of industrial by-products [19], have emerged as an alternative to the adsorption process due to their cost-effective production [20], straightforward synthesis methods [21], low environmental footprint [22], high durability [23], excellent thermal and chemical stability [24], and capacity for functional adaptation [25].

GP are typically produced from silica and alumina-rich materials, such as fly ash (FA) [26], blast furnace slag [27], or metakaolin (MK) [28], forming a three-dimensional inorganic polymer network under alkaline conditions [29]. Among these precursors, FA stands out for

its global availability [30], low cost [31], and high reactivity [32], making it one of the most relevant sources for synthesis of GP. These materials exhibit a combination of mechanical strength [33], tunable porosity [34], and ion-exchange capacity [35], which have enabled their application beyond the construction sector [36], particularly in the waste water treatment containing lead [37], cobalt [38], methylene blue (MB) [39], crystal violet dye [40], acetaminophen and gallic acid [41], and phenol [42].

Recent research efforts have increasingly focused on tailoring the physicochemical properties of fly ash-based geopolymers (FA-GP) to enhance their performance as adsorbents [43], catalysts [44], or filtration matrices [45]. Parameters such as precursor composition, alkaline activator ratio [46], curing conditions [47], and thermal post-treatments [48] play a crucial role in defining surface area [49], pore size distribution [50], and active site for pollutant interaction [51].

To improve the performance of GPs in the adsorption process, certain methodologies, such as zeolitization, have been gaining increasing attention [52]. For instance, He *et al*. [53] produced a FA-GP zeolite using LiOH and after hydrothermal treatment (HT) achieved a surface area of 30.19 $m^2\ g^{-1}$. Khalid *et al.* [22] produced GP using FA and sodium silicate and NaOH as the alkaline activating solution, and reported a maximum S_{BET} of 90 $m^2\ g^{-1}$ for a zeolitized GP containing the analcime phase after 24 h of HT at 100 °C using 8 M NaOH. De Rossi *et al.* [54] prepared GPs based on biomass FA (75 wt%) and MK (25 wt%). Then, the samples were cured in hydrothermal conditions in hermetic glass container for 3, 7 and 28 days at 60 °C. Such a treatment caused the formation of zeolite Na–P1 and faujasite regardless the curing time, however, the higher time of the treatment enhanced their formation.

Current studies generally report findings related to the composition of geopolymeric zeolites following more conventional routes, such as the use of FA, NaOH, and sodium silicate precursors for GP production followed by zeolitization, or more distinct approaches, such as incorporating natural or synthetic zeolites into the precursor geopolymeric matrix [55] and forming zeolites directly within the matrix under curing conditions at elevated temperatures [56]. However, to date, no study has investigated the production of these geopolymeric zeolites incorporating adsorbent materials, such as AC, nor examined the optimal point of zeolite formation through variation of NaOH concentration during HT and verified whether it is proportional to the surface area. All studies found in literature have focused on the removal of compounds such as heavy metals [57] and dyes [58], e.g. this reveals a significant gap regarding the treatment of contaminants of emerging concern [59].

Therefore, to address this gap, the present work focuses on the development of innovative zeolite–carbon composite GP for removal of emerging contaminants, such as carbamazepine (CBZ). The materials were characterized for textural, chemical, and thermal properties.

2. STATE-OF-THE-ART

2.1. WATER SECURITY AND EMERGING CONTAMINANTS

2.2.1 Water Security: Current Challenges

Access to safe drinking water is an essential necessity and a fundamental human right [60]. The availability of freshwater is steadily decreasing, as both its quality and quantity decline due to population growth and to the discharge of untreated wastewater into water bodies [61]. If urban wastewater is not properly collected and treated, it can become one of the main sources of water pollution [62]. Globally, 80% of wastewater is discharged directly into the environment, affecting the quality of water resources, leading to clean water scarcity, and contributing to the spread of diseases [63].

In 2015, the United Nations General Assembly adopted the Sustainable Development Goals (SDGs), comprising 17 goals and numerous targets aimed at achieving sustainable development by 2030. Since then, sustainability has gained increasing attention worldwide [64]. Wastewater management plays a crucial role in achieving universal access to water and sanitation, as outlined in SDG 6 [65]. Proper wastewater management can contribute to the protection of water resources and reduce competition for already scarce water [66]. Wastewater treatment is essential, as it is responsible for degrading pollutants found in water and ensuring that it can be safely discharge into the environment [67]. By removing undesirable impurities such as bacteria and viruses [68], organic micropollutants [69] and excess nutrients [70].

Across Portuguese territory, there are 465 urban areas, composed of households and industries, which generate approximately 13 million population equivalents (p.e.) of wastewater daily, equivalent to 2.61 million cubic meters per day [71]. The country has 492 wastewater treatment plants (WWTPs), of which 8 only apply primary treatment (in Portugal's Madeira Archipelago), 394 continue to biological treatment, and 90 apply biological treatment with nitrogen and phosphorus removal [71]. Currently, 57.5% of mainland Portugal suffers from water shortages, and only 10% of treated wastewater is reused [72].

The Urban Wastewater Treatment Directive (UWWTD) is responsible for monitoring the quality of urban wastewater within the European Union by establishing quality parameters and requirements [73]. It sets standards for the collection, treatment, and discharge of urban wastewater, as well as wastewater from specific industrial sectors, aiming to minimize the potential negative environmental impacts associated with wastewater discharge [74].

Wastewater treatment in Portugal is regulated by Directive 91/271/EEC and transposed into Portuguese law by Decree-Law 11/2023, which imposes maximum limits on nutrients such as nitrogen (10 – 15 mg L^{-1}) and phosphorus (below 2 mg L^{-1}) in effluents and stipulates that tertiary treatment must be used, where necessary, by the receiving body or water resources [75,76]. The latest UWWTD (3019/2024/UE) mandates that, by 2045, tertiary treatment must be implemented in treatment plants with a load equal to or greater than 150 000 p.e., alongside quaternary treatment aimed at removing at least 80% of micropollutants including pharmaceuticals (antibiotics, antidepressants, hormones, etc.), personal care products (UV filters, synthetic fragrances, etc.), per- and polyfluoroalkyl substances (PFAS), industrial chemicals, among others [77].

Water reuse has shown promising results in minimizing water stress, as it increases available water resources while closing the loop between water supply and wastewater disposal [78]. To validate the quality of treated water and the success of the treatment plant, it is necessary to create a tailor-made solution for each case, adapted to local needs, available funds, and competent technologies [79].

2.2.2 Contaminants of Emerging Concern

Contaminants of emerging concern (CECs) represent a wide and growing range of substances regularly found in water [80], which are referred to as “emerging” due to their recent recognition in different natural environments [81]. These compounds represent micropollutants with uncertain effects but have the potential to cause harmful reproductive, neurological, and immunological impacts in humans and animals [82]. Among them are cosmetics [83], pesticides [84], personal care products [85], pharmaceuticals [86], hormones [87] and microplastics [81]. Pharmaceutical products have been recognized as environmental contaminants in aquatic environments for over 40 years [88]. Therefore, concern about CECs is growing, considering that they are widely used by the entire population and there are no regulations to control their concentrations in wastewater after treatment [89].

Even with the current wastewater treatment processes considered necessary, WWTPs are still not equipped to effectively remove contaminants of emerging concern CECs [90]. Since these pollutants are resistant to conventional wastewater treatment processes, this leads to their bioaccumulation [91]. Therefore, the concern with developing technologies that eliminate or reduce the concentration of these contaminants becomes a priority for monitoring water quality [88]. CECs reach aquatic systems through various contamination pathways, for instance, organic pollutants from agricultural activities enter water bodies via surface and subsurface runoff; landfills and dumpsites release leachates that infiltrates the soil and reaches

groundwater; and untreated domestic, hospital, and industrial wastewater directly discharges contaminants into rivers and lakes [92].

The removal efficiency of CECs presents a significant challenge for conventional wastewater and drinking water treatment facilities, as these systems were never designed to address such small concentration and diverse pollutants [93]. Additionally, contamination levels may vary depending on seasonal fluctuations and climatic conditions, which must also be considered [94].

Examples of CECs are sulfamethoxazole (SMX) and CBZ, which are reported as endocrine-disrupting chemicals (EDCs) and can enter water systems after excretion by humans and animals [95]. When present in water, CECs have significant effects on human health, potentially disrupting hormonal functions and impacting animal species [96]. These effects can be observed at relatively low concentrations, as pharmaceutical products are designed to be biologically active at low doses [97].

CECs are found in many items used daily by the entire population, and preventing their spread is challenging [98]. Silva *et al.,* [99] conducted a study in northern Portugal, analyzing river water both upstream and downstream of a WWTP discharge. The study revealed that the presence of pharmaceuticals in the watercourse increased after effluent release. Upstream and downstream concentrations, respectively, were detected for azithromycin (5.49 and 189.77 ng $POCIS^{-1}$ day^{-1}), CAF (9.21 and 15.33 ng $POCIS^{-1}$ day^{-1}), CBZ (12.75 and 244.76 ng $POCIS^{-1}$ day^{-1}), fluoxetine (2.61 and 222.49 ng $POCIS^{-1}$ day^{-1}) and SMX (0.43 and 25.33 ng $POCIS^{-1}$ day^{-1}) (ng $POCIS^{-1}$ day^{-1} is a measurement that reflects the amount of contaminant retained per day by the passive sampling device POCIS (polar organic chemical integrative sampler), allowing for estimation of its presence in the water). As observed, the effluent from treatment systems contains a variety of CECs and their transformation by-products [100]. Therefore, it is crucial to develop a treatment method that prioritizes the effective and safe removal of CECs from wastewater and reduces environmental and health problems [101].

2.1.2.1. Carbamazepine

CBZ is an anticonvulsant drug primarily used in the treatment of epilepsy and bipolar disorder [102]. It is a molecule with remarkable chemical stability and a highly complex organic structure (Figure 1), which makes it difficult to degrade or remove through conventional processes [103]. The removal efficiency of CBZ in conventional biological WWTPs is indeed low, typically below 30% [104].

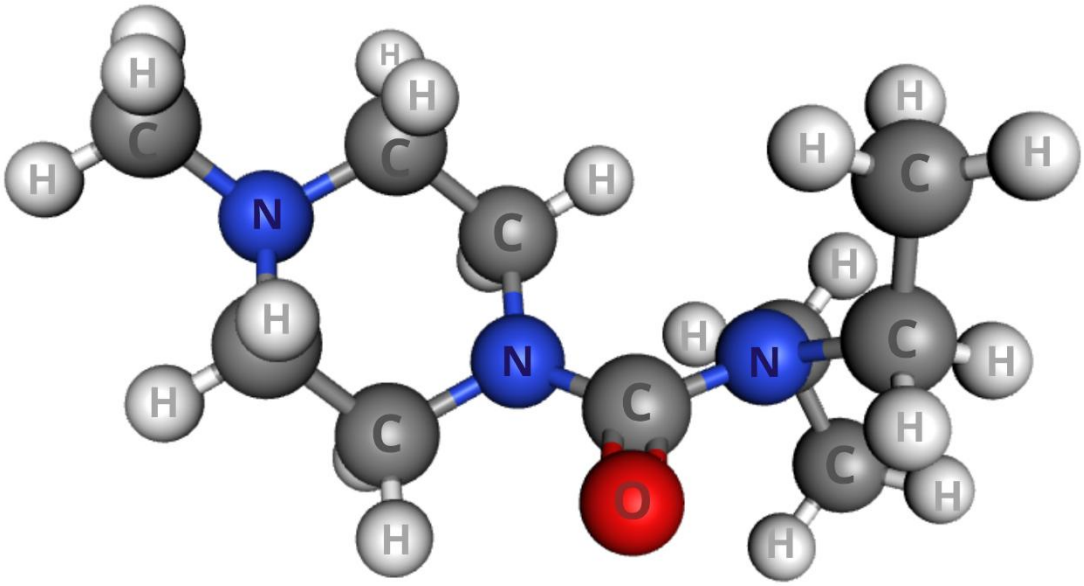

Figure 1: Carbamazepine Molecule (adapted [105]).

CBZ is a pharmaceutical compound systematically detected in various water matrices, especially in urban wastewater, where it is found at concentrations ranging from 0.1 to 3 μg L^{-1} [106]. Although the drinking water equivalent level (DWEL) of CBZ is higher (5.7 μg L^{-1} in Europe) than the concentrations found in hospital wastewater, prolonged exposure to lower levels over time can still have harmful effects [107]. CBZ has been found to be much more difficult to degrade using biological systems compared to other antibiotics, such as SMX, and endocrine-disrupting compounds, because of its highly complex organic structure [103].

2.2. WASTEWATER TREATMENT STRATEGIES

2.2.1 Conventional Treatment

Current WWTPs are not designed to remove CECs and microplastics (MPs), so it is necessary to understand current removal procedures in order to develop effective technologies [108]. In general, wastewater treatment involves three main stages [109], as shown in the Figure 2.

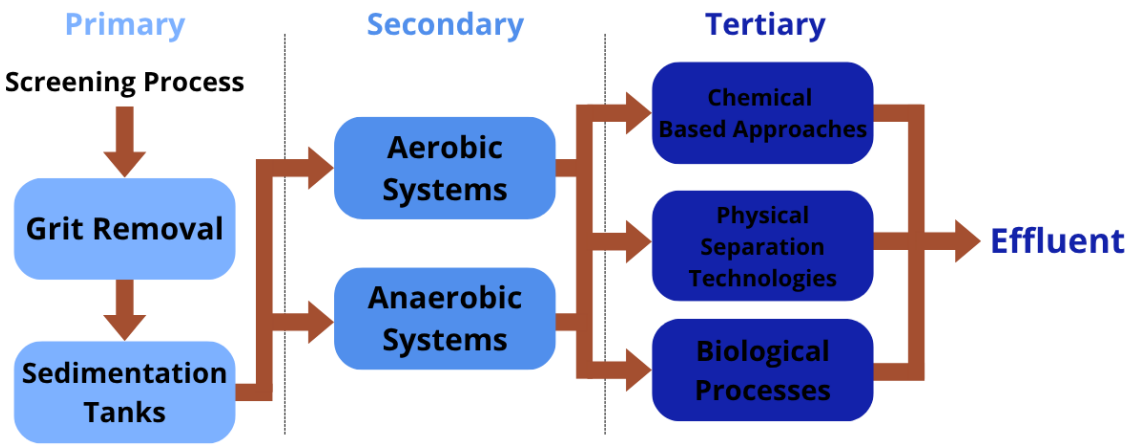

Figure 2: Steps of Traditional Wastewater Treatment (adapted [95,110]).

Primary treatment, which can be considered preliminary treatment, is responsible for removing 60 to 80% of solid materials from wastewater, such as wood, sand, rags, sludge, plastic particles, and wire, leaving only solids in the form of dissolved matter [111]. In general, the flow is passed through screening, sand chambers, and primary settling tanks [112].

The secondary treatment degrades the biological content of organic matter present in the wastewater using aerobic systems such as microbial biofilms and activated sludge, which can be integrated with anaerobic systems through reactors such as UASB (Up-flow Anaerobic Sludge Blanket), EGSB (Expanded Granular Sludge Bed), and AFFR (Anaerobic Fluidized Film Reactor), responsible for converting organic matter into biogas and sludge [95,113].

Tertiary treatment is designed to remove toxic compounds, including phosphorus and nitrogen compounds, that are not removed in the previous stages, ensuring that wastewater can be discharged into the environment and is of sufficient quality to be reused [114]. The removal techniques are selected based on the characteristics of the target contaminants, with the most commonly employed methods being ozonation [115], UV radiation [116], chlorination [117], and reverse osmosis [117]. The main objective of this stage is to ensure that the final product does not contain any toxic compounds that could be harmful to living beings [118].

Conventional methods focus mainly on eliminating pollutants such as heavy metals and organic compounds [119]. Therefore, the traditional three-stage treatment design of WWTPs cannot fully guarantee the removal of CECs [120]. A study showed that implementing a sequential treatment process can significantly improve CE removal from 50% (with conventional treatments) to 80% [121].

2.2.2 Quaternary Treatment

One of the main goals of the academic community is to develop effective and sustainable solutions for wastewater treatment in WWTPs, with a focus on the efficient removal of CECs. In this context, sequential treatments, still under development, have been referred to as quaternary or advanced treatment, representing an additional stage to conventional technologies [122]. Nevertheless, existing technologies for removing micropollutants from wastewater that are available include ion exchange [123], supercritical fluid extraction [124], adsorption [125], among others. Each process has its own specificities regarding efficiency, environmental impact, and economic viability, which in most cases limit the practical application of these methods [126]. Wastewater treatment facilities must process large volumes of wastewater daily, necessitating treatment technologies that are both efficient and high throughput [127].

Ion exchange treatment is technically effective and widely studied for specific contaminants, but its broader application in wastewater is limited by pre-treatment requirements, regeneration brine management, resin durability, and large-scale cost [128]. Supercritical fluids, in turn, can effectively remove or destroy contaminants, but the combination of extreme operating conditions, high equipment costs, and issues related to corrosion and scaling has hindered their widespread adoption in wastewater treatment [129,130].

Another effective alternative for the degradation of micropollutants is the ozonation process, which achieves removal in approximately 10 minutes, with the contact time inversely related to the ozone dose [131]. The main drawbacks of ozonation lie in the formation of toxic by-products during wastewater treatment, such as bromate. To reduce the risk of toxicity in the ozonated effluent, post-treatment, such as a biological filter, may be required [132]. In addition, implementing ozonation increases energy demand due to the need for ozone generation from oxygen. Therefore, beyond the initial capital investment, the selection of ozonation as a treatment option must also take into account the rise in operational costs [133].

2.2.3 Cost-Effective and Sustainable Alternatives

Adsorption is one of the most widely used techniques to remove various pollutants from wastewater due to its effectiveness, simplified and economical method, and high regeneration capacity [134]. The adsorption method has emerged as a strategic approach to remove CECs due to its accessibility, rapid applicability, and absence of sludge or harmful substance accumulation during and after the process [135,136]. The adsorption technique

involves the adsorption of the adsorbate to the surface of the adsorbent and the interaction between adsorbate and adsorbent is influenced by the species involved [137], as shown in Figure 3.

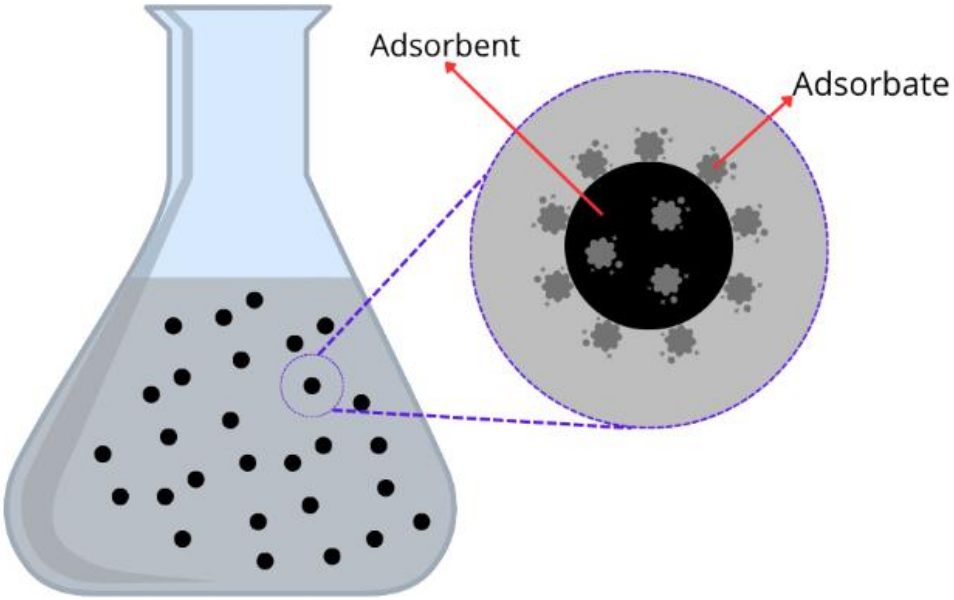

Figure 3: Graphical representation of the adsorption process (adapted [98]).

Adsorbents, whether in their native form or after chemical modification, have an extensive surface area with functional groups, pore size distribution, and a well-developed porous structure, ensuring successful adsorption [137]. With regard to the elimination of CECs, the adsorption process can be through chemical or physical interactions, and these processes can be distinguished based on Table 1 [138].

Table 1: Difference between physical adsorption and chemical adsorption (adapted [138]).

Physical Adsorption	Chemical Adsorption
Van der Waal force of attraction is involved	Chemical bond is involved
The adsorption is considered a reversible process	The adsorption is considered an irreversible process
It does not require activation energy	Activation energy is needed
The adsorption occurs at lower temperatures	The adsorption occurs at higher temperatures
It produces a multilayer	It produces a monolayer

A wide range of adsorbents — such as GPs [139], zeolites [140], biochars [141], ACs [142], resins [143], FA [144], chitosan [145], and others — are employed for the removal, mainly of heavy metals [146], dyes [138], and other pollutants, from wastewater [126].

Among these, chitosan is the second largest natural polymer and has a structure that allows strong interactions with heavy metals and enables chemical modifications to improve adsorption performance [147]. Chitosan dissolves in acidic solutions [148], does not have

good mechanical stability, and can increase the concentration of ammoniacal nitrogen in treated effluents [149]. Biochars are generated by pyrolysis of biomass feedstock and has unique characteristics, such as specific surface area, cation exchange capacity, and many oxygen-containing groups [150]. On the other hand, biochars may contain various toxic substances, such as polyaromatic hydrocarbons, dioxins, and heavy metals [151].

Natural zeolites are porous hydrated aluminosilicate materials that contain pores ranging from macropores to mesopores. They originate from the alteration of volcanic glass under varying geochemical conditions and temperatures [152]. They belong to the mineral family and are distinguished by their crystalline structure [153]. Synthetic zeolites vary in their Si/Al ratio and can be produced from various raw materials rich in silica and aluminum [154]. Due to their complex formation conditions, unstable chemical composition, and the presence of impurities, natural zeolites exhibit inferior performance compared to synthetic ones, which limits their application in industrial processes [155].

The procedures developed for zeolite production mimic the HT environmental conditions under which they would naturally form [156]. In other words, HT techniques involve temperatures and pressures above ambient levels [153], along with the need for an alkaline medium, a solvent, and a source of alumina and silica [157]. Various solid wastes such as coal FA [158], coal gangue [159], rice husk [160] and alum sludge [161] have also been explored as sources of silica-aluminum for zeolite synthesis. Given their low cost and widespread availability, these solid wastes are considered suitable and sustainable silica–alumina precursors for the synthesis of zeolites [155].

2.2.4 Activated Carbons: Properties and Applications

Commercially available ACs are typically derived from fossil-based, non-renewable resources, making their use environmentally unsustainable. To align with circular economy principles, renewable raw materials can be employed in ACs production, to reduce environmental impact [162]. Carbonaceous precursors such as wood [163], almond shells [164], fruit pits [165], agricultural residues [166], and winery waste [167], among many others, are commonly used for ACs production, providing a sustainable disposal option for these residual biomasses as opposed to common practices like open-air burning and waste dumping [168,169].

The conversion of biomass into porous carbon materials is done through a carbonization process, which can be HT carbonization [170] or pyrolysis [171]. The most common way to convert biomass into porous carbon materials, such as ACs, is through pyrolysis followed by activation. The main stage of pyrolysis occurs at 250 – 500 °C, during

which the biomass releases condensable volatile fractions such as CO_2, CO, CH_4, and H_2, undergoing significant mass loss. The slow decomposition phase of residual material typically takes place at temperatures above 500 °C for any biomass not fully pyrolyzed [172]. Pyrolysis alone results in low specific surface areas and pore volumes, so activation is necessary to enhance these properties. Chemical activation involves agents like potassium hydroxide [173], sodium hydroxide [174], phosphoric acid [175], among others, which promote corrosion, hydrolysis, oxidation, or dehydration reactions. Due to these chemical treatments, thorough washing and drying are required afterward to remove any residual chemicals. Physical activation refers to the use of gases such as air, water vapour, CO_2 or combustion gases to activate the precursor material after pyrolysis at temperatures between 800 and 1000 °C. In this process, gas oxidation plays a key role by blocking, then reopening and further expanding the pores of the carbonized material [172,176].

Through careful selection of waste materials, preparation methods, and adsorption conditions, these renewable-source ACs have demonstrated superior adsorption performance compared to their commercial counterparts [169]. Fine and porous particles offer higher adsorption capacity but also increase the risks of pore blockage and particle friction. Practical regeneration processes for adsorbents remain lacking; therefore, adsorbents need to be replenished after saturation [177].

AC is the most commonly used adsorbent for removing pollutants from wastewater due to its high surface area, stability, and durability. This material contains functional groups such as carbonyl, carboxyl, phenolic, and quinone groups, which enhance its adsorption capacity for pollutants [178]. Studies show the potential of using wine industry waste to obtain AC, whether using grape wood [179], stems [180], seeds [181,182], or pomace [183]. AC produced from grape seed waste for the removal of paracetamol, prepared via chemical activation with H_3PO_4, exhibited a well-developed porous structure and a specific surface area of 543 $m^2\ g^{-1}$, along with a maximum adsorption capacity of 17.3 mg g^{-1} [184]. The production of AC from grape pomace for the removal of antibiotics from wastewater was also studied, with chemical activation using hydrochloric acid. This resulted in a surface area of 44.23 $m^2\ g^{-1}$ and in an adsorption capacity of 17.38 mg g^{-1} [185].

2.2.4.1. Geopolymers: Composition, Synthesis and Functionalization

GPs, also known as alkali-activated ceramics, are novel inorganic polymers that exhibits properties comparable to ceramics while being environmentally friendly. It utilizes solid waste materials (material rich in silicon and aluminum), producing no CO_2 emissions during manufacturing, and has a low cost [186]. Are relatively new inorganic materials

characterized by suitable mechanical properties and low carbon footprint [187]. Because they are synthesized from residual raw materials such as coal FA [188], steel slag [189] and mining waste [190], GPs emerge as alternative adsorbents with significant environmental relevance [191]. FA is considered coal combustion waste, resulting in water, air, and soil pollution if not properly treated. It is deposited in landfills and ash ponds [144,192]. It is considered a natural adsorbent with very high carbon content, a hydrophilic surface (adsorption capacity), and a porous structure, composed mainly of SiO_3 and Al_2O_3 [193].

GPs are amorphous inorganic polymers typically composed of a three-dimensional network material formed by $[SiO4]^{4-}$ (silicon-oxigen) and $[AlO4]^{5-}$ (aluminium-oxigen) tetrahedra sharing bridging oxygens [194]. Their raw materials undergo a depolymerization–condensation gel network process, during which the negative charge is balanced by alkali metal ions supplied by an activator [195]. Typically, the activators consist of sodium (Na) and potassium (K), whose ionic radii and charge density significantly influence the degree of polymerization, microstructure, and properties [34,196].

The GPs formation reaction, attractive because it occurs at room temperature [197], typically follow three stages: first, the dissolution of the aluminosilicate raw material in an alkaline solution, releasing silicon-aluminum complexes; second, the diffusion of these complexes leading to a gel system where polymerization reactions take place; and finally, the gradual evaporation of water from the gel phase, resulting in consolidation and hardening [34,198].

GPs are primarily used in environmental and waste management, particularly for the immobilization of heavy metals [199], wastewater treatment [21,200], and the recycling of industrial waste [201]. As research on GPs advanced, their application gradually shifted toward energy-related purposes [23], namely carbon capture and storage [202] and geothermal applications [203]. In addition, GPs have been applied in biomedical applications [204] and have gained significant attention in civil engineering due to their greater durability in corrosive environments compared to cement-based materials [205].

The use of GPs as adsorbents has been explored in various morphological forms, such as powders [206], microspheres [207], porous monoliths [208], membranes [209] and even as zeolitic structures [210]. GP monoliths are typically obtained by shaping and cutting cured GP blocks into specific geometries and dimensions. They exhibit porous structures with high surface area and low water flow resistance, characteristics that provide high adsorption efficiency and ensure performance comparable to or even superior to powdered GPs [187].

2.2.4.2. Geopolymer–Carbon Composite: Development and Performance

Studies have reported the excellent performance of GP in various wastewater treatment applications. Yang *et al.* [211], demonstrated the efficiency of a GP in water purification, specifically in the removal of Rhodamine B (RB) and Nickel (II) (Ni(II)). The GP achieved removal rates of 99 and 92% for 10 mg L^{-1} of each compound, respectively, and maintained its performance even after five cycles. A GP-based tubular membrane proposed by Wang *et al.* [212], achieved a removal efficiency of 98% in an atmosphere filled with smoke haze containing particulate matter (2.5 μm) with concentrations above 1000 μg m^{-3}.

Their structural characteristics resemble those of zeolitic materials, but GPs exhibit lower adsorption capacities due to their amorphous or semi-crystalline nature, which lacks uniform micropores [213]. One approach briefly presented in literature to improve the adsorptive properties of GPs is their incorporation with AC. Some studies indicate that, given the lower adsorption capacity of GPs, combining them with AC leads to improved pollutant filtration by increasing surface area and adsorption performance [214]. Nevertheless, the adsorption capacity of GPs can be further enhanced through strategies such as incorporation of additional adsorptive phases, like zeolites, or chemical modifications that optimize interactions between the geopolymeric matrix and target pollutant molecules [215]. GP adsorbents should exhibit high porosity due to their pore structure and maintain low resistance to water flow [187].

The transformation of GPs into zeolites (zeolitization) is more readily achieved when HT treatment is applied [216], and this is the main method currently used for zeolite synthesis [217]. The conversion of amorphous geopolymeric materials into zeolite composite materials has received significant attention, driven by the desire to create sustainable, high-performance materials from industrial waste [52]. The application of geopolymeric materials has been studied in a wide range of areas, including catalysis [218], CO_2 capture [219] and water purification involving heavy metals and dyes [220,221]. In a universe of 50 studies found on the production of GP, a survey was conducted on those that reported the synthesis of zeolites, the results being summarized in Table 2. The table compiles the main parameters, such as the GP precursor, variables involved in the HT, surface area, pollutant, and the adsorption capacity of the material.

Table 2: Summary of various studies on hydrothermal treatment of geopolymers.

Author	GP Precursor	Treatment	Surface Area (m^2 g^{-1})		Pollutant	Adsorption Capacity – qt (mg g^{-1})	Application
			Pre	Post			
He *et al.* [53]	FA + LiOH	HTC 180 °C, 24 h (LiOH 1 M)	13.36	30.19	Hexavalent chromium (Cr(VI))	-	Continuous
Qiu *et al.* [216]	FA + NaOH + sodium silicate	HTC 100 °C, 24 h (NaOH 2 M)	0.26	50.46	-	-	-
Manickam *et al*, [52]	FA + NaOH + sodium silicate	HTC 100 °C, 48 h (NaOH 1 M)	9.59	28	Methyl orange dye	5.19	Batch
Khalid *et al*, [22]	FA + NaOH + sodium silicate	HTC 100 °C, 24 h (NaOH 5 M)	-	90.3	Pb^{2+}	37.9	Batch
Wang *et al.* [222]	FA + H_2O_2 + sodium silicate	HTC 180 °C, 12 h (NaOH 1 M)	186.5	252	CO_2	2.06 mmol/g	Continuous
Liu *et al.* [223]	FA + NaOH + sodium silicate	HTC 70 °C, 24 h (NaOH 1 M)	1.07	174.35	-	-	-
Liu *et al.* [224]	FA + NaOH + H_2O_2 + sodium silicate + oleic acid	Direct curing 80 °C, 10 h	-	67.62	MB	50.7	Batch

For instance, He *et al*. [53] produced a GP zeolite using LiOH and after HT treatment achieved a surface area of 30.19 m^2 g^{-1}; Wang *et al*. [222] incorporated H_2O_2 into the synthesis; and Liu *et al*. [223] produced a geopolymeric zeolite at a lower temperature and achieved a surface area of 136.23 m^2 g^{-1}. However, no study to date has investigated the production of these geopolymeric zeolites incorporating adsorptive materials such as ACs.

3. OBJECTIVES

The main objective of this work is to valorize industrial (FA) and agricultural (grape pomace) residues through their conversion into value-added zeolitic and carbon-based materials, including zeolites synthesized by HT, and their application in the production and optimization of GP–carbon composite for the removal of contaminants of emerging concern (CECs) from wastewater.

- Synthesize GPs from FA;
- Produce ACs using pressed and distilled winery grape pomace (WGP);
- Develop GP-carbon composite;
- Apply HT treatment to convert GPs into zeolite-based structures;
- Characterize all materials, including all GPs, ACs and biomasses, to evaluate their physicochemical properties and functional performance;
- Perform batch adsorption experiments to assess the adsorption behavior and efficiency of the developed materials.

4. MATERIALS AND METHODS

4.1. REACTANTS

The reactants employed in this investigation are outlined below and classified according to their specific applications.

a) Production of geopolymers

- FA provided by SOGAMA (composition presented in Table 9);
- Sodium Hydroxide pearls (NaOH – 98% purity) provided by Labkem;
- Sodium Silicate (Na_2SiO_3 - Na_2O = 10.6% purity and SiO_2 = 26.5% purity) provided by Fisher Chemical;
- Hydrochloric acid (HCl - 37% purity) provided by VWR Chemicals.

b) Production of activated carbons

- WCP provided by winery Casa do Joa;
- Carbon dioxide (CO_2 – 99% purity) provided by AirLiquide;
- Nitrogen (N_2 – 99% purity) provided by Alphagaz™;
- Silica wool provided by Elemental Microanalysis.

c) Contaminant utilized in the simulation of wastewater

- Carbamazepine ($C_{15}H_{12}N_2O$ - 98% purity) provided by Thermo Scientific.

4.2. MATERIALS PRODUCTION

The production of all materials and the subsequent processes are presented in the flowchart shown in Figure 4. The detailed steps of each process are described in the sections below. The concentration to be applied to the GP incorporated with AC will be the one with the best efficiency for the GP, and its application will take into account the precursor GPs (pure and AC-containing) and their respective HT forms.

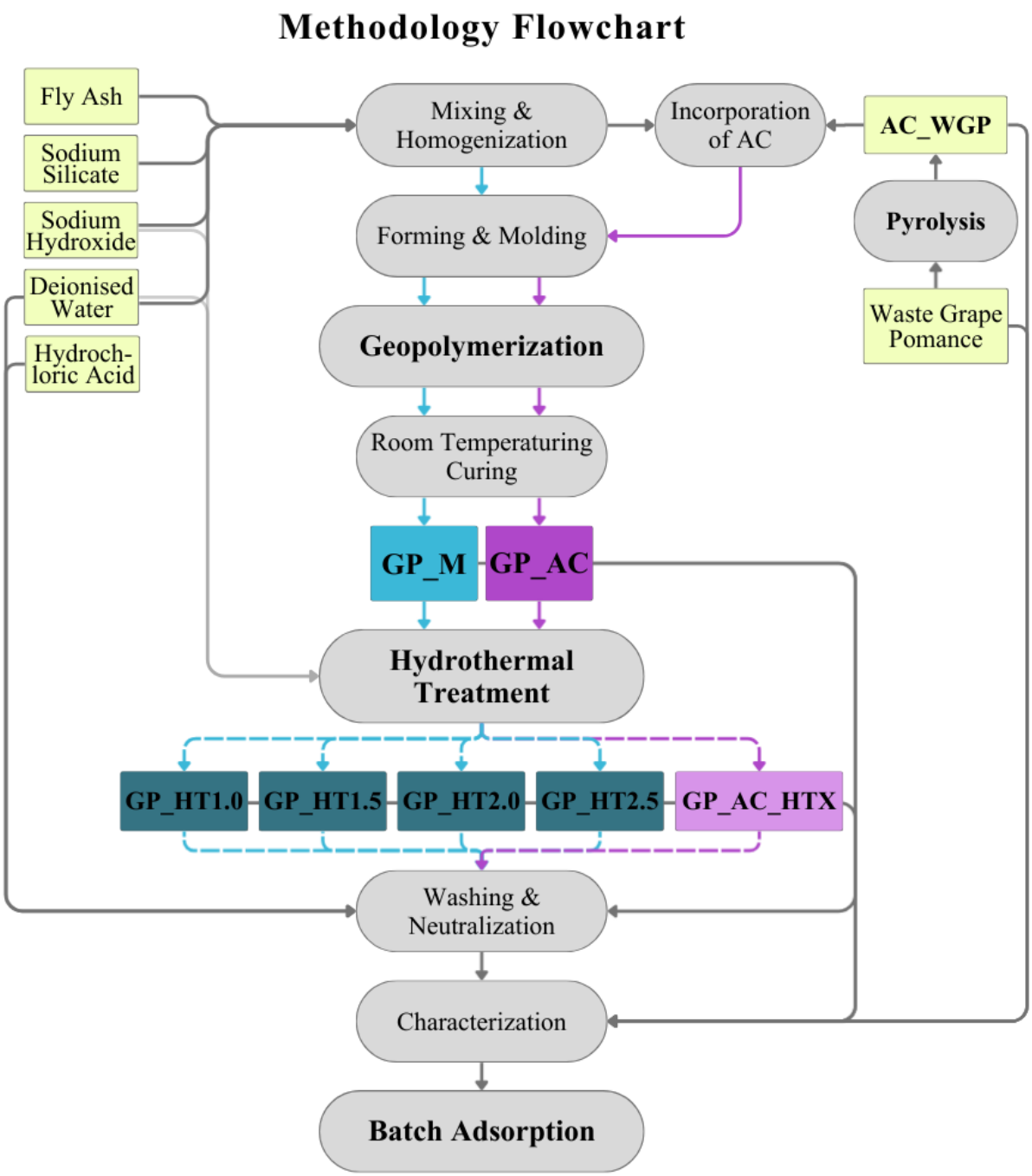

Figure 4: Methodology flowchart.

4.2.1. Geopolymers Production

The GP matrix (GP_M) refers to the base geopolymeric material prior to any post-treatment or modification. The GP_M was prepared by mixing 11.6 g of FA with an alkaline activating solution composed of 9.55 g of Na_2SiO_3 and 3 mL of 5 M NaOH, until a homogeneous paste was formed. The homogeneous paste was then poured into a silicone cubes mold with 2.55 cm edges, as show the Figure 5. The GP_M were then cured for 24

hours at room temperature. Finally, the sample were then thoroughly washed multiple times using 0.1 M HCl solution and distilled water, until the pH of the solution containing the materials was neutral. Following washing, the materials were dried for 24 hours at room temperature.

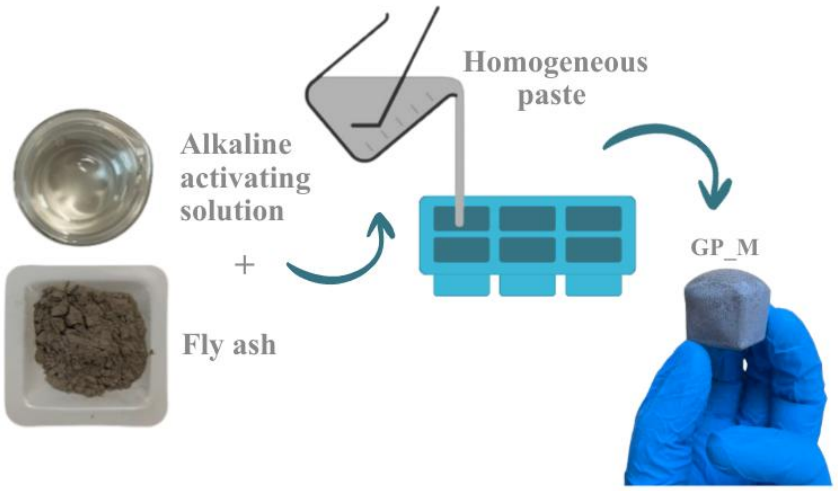

Figure 5: Schematic representation of GP_M synthesis.

4.2.2. Activated Carbon Production

10 g of WGP (ground and sieved to a particle size smaller than 250 µm) was placed in a tubular furnace with a nitrogen flow of 100 mL min^{-1} to produce AC. A heating ramp of 5 °C min^{-1} was applied, progressing through three temperature stages: 400 °C and 600 °C for 1 h each, followed by 800 °C for 4 h. At 800 °C, the nitrogen flow was replaced with CO_2 injection for 1 h to activate the carbon, following a procedure adapted from Ferreira *et al.* [41], which provided an optimal balance between surface area development and carbon yield for WGP. Nitrogen was then reintroduced and continued until the reactor cooled. The resulting material was labeled as AC_WGP, washed with distilled water, and dried overnight at 60 °C.

4.2.3. Geopolymer-Carbon Composite

A GP–carbon composite was obtained by incorporating 3.2 g of AC_WGP into the GP_M mixture prior to molding and curing, as show the Figure 6. The resulting materials was labeled as GP_AC and the mixture was cured for 24 h at room temperature. Finally, the sample were then thoroughly washed multiple times using 0.1 M HCl solution and distilled water, until the pH of the solution containing the materials was neutral. Following washing, the materials were dried for 24 hours at room temperature.

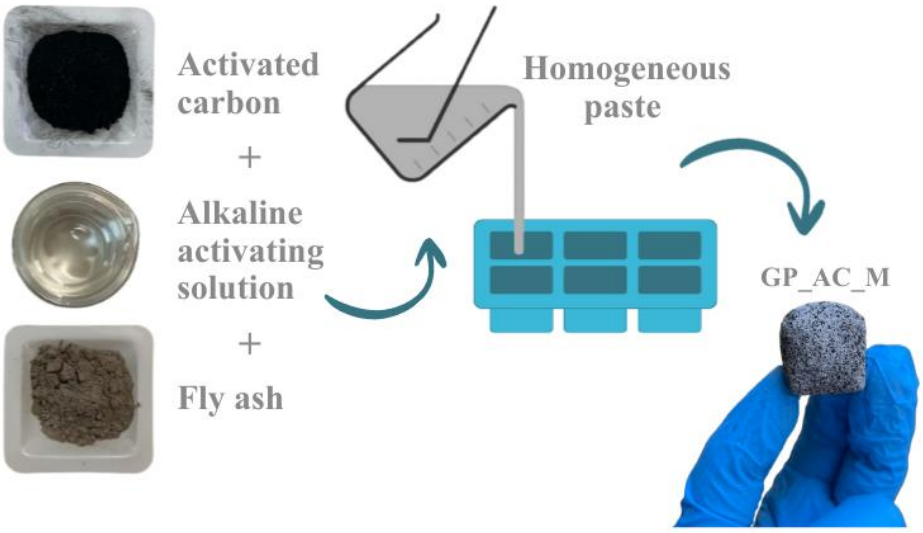

Figure 6: Schematic representation of GP_AC synthesis.

4.2.4. Hydrothermal Treatment

The GP_M precursor was subjected to HT to induce zeolitization the in 30 mL of NaOH solution at four different concentrations: 1.0, 1.5, 2.0 and 2.5 M. The resulting materials was labeled as GP_HT_1.0, GP_HT_1.5, GP_HT_2.0 and GP_HT_2.5, respectively. The HT treatment was be carried out in a Teflon vessel housed in a stainless-steel reactor (Model 249 M 4744–49, Parr Instrument Co., USA) at 70 °C for 24 h.

After identifying the NaOH concentration that led to the best performance for the GP_HT materials, the same HT procedure was applied only to the AC-incorporated GP using this optimized concentration. The resulting material was labeled as GP_AC_HT (NaOH concentration).

4.3. CHARACTERIZATION TECHNIQUES

4.3.1. Surface chemistry

4.3.1.1. X-ray diffraction

This technique involves directing X-rays at the sample and analyzing the resulting diffraction patterns, which provide information about the atomic arrangement and the crystallographic properties of the material. X-ray diffraction (XRD) measurements were conducted at room temperature using a PANalytical X'Pert Pro diffractometer equipped with an X'Celerator detector and a secondary monochromator in θ/2θ Bragg-Brentano geometry. This analysis was conducted at the Department of Chemical and Environmental Technology of Rey Juan Carlos University, Spain.

4.3.1.2. Fourier-transform infrared spectroscopy

The analysis of surface chemistry for the materials was tracked using Fourier Transform Infrared Spectroscopy (FT-IR), with a PerkinElmer FT-IR spectrophotometer UATR Two. The spectra were recorded from 450 to 4000 cm^{-1} with a resolution of 4 cm^{-1}. All measurements were conducted on solid samples at room temperature. This analysis was carried out at the Analytical Chemistry Laboratory of the IPB, Portugal.

4.3.1.3. Acid-base characterization

To assess the material's acid-base properties, various solutions were prepared and titrated to determine acidic and basic sites. For acidic sites, the samples (0.2 g) were mixed with NaOH (0.02 mol L^{-1}) and then titrated with HCl (0.01 mol L^{-1}). For basic sites, the samples were mixed with HCl (0.02 mol L^{-1}) and then titrated with NaOH (0.01 mol L^{-1}). Acidic site concentration was determined by the moles of NaOH consumed, while basic site concentration was determined by the moles of HCl consumed, both normalized to the sample mass. Equations (1) and (2) were used for sites calculations.

$$C_{acidic} = \frac{C_{NaOH} \cdot V_{NaOH} - C_{HCl} \cdot V_{HCl}}{m_{sample}} \quad (1)$$

$$C_{basic} = \frac{C_{HCl} \cdot V_{HCl} - C_{NaOH} \cdot V_{NaOH}}{m_{sample}} \quad (2)$$

where C_{acidic} and C_{basic} (mmol g^{-1}) represents the concentration of acidic or basic sites on samples's surface, C_{NaOH} and C_{HCl} (mmol L^{-1}) are the initial concentrations of NaOH and HCl, respectively, V_{NaOH} (L) is the volume of NaOH added during titration, V_{HCl} (L) is the volume of HCl added during titration, and m_{sample} (g) is the mass of the solid sample used.

To determine the point of zero charge (pH_{PZC}), nine dilutions of 50 mL of NaCl (0.01 mol L^{-1}) were prepared, and their pH was adjusted between 4 and 12 by adding NaOH (0.02 mol L^{-1}) or HCl (0.02 mol L^{-1}). To study pH effects on the material's adsorption performance, 0.2 g of the solid sample was added to each solution and stirred at 300 rpm and 25 ºC for 24 h. After filtration, the pH of the solutions was measured, and the final and initial pH values were plotted to determine the pH at which the surface charge of the adsorbent is zero [225]. The analysis was conducted at the Mountain Research Center of the IPB, Portugal.

4.3.2. Morphological Analysis

Scanning electron microscopy combined with energy dispersive spectroscopy (SEM/EDS) was conducted to investigate the morphological and microstructural features of the precursor material and GPs. The samples were analyzed using a FEI Quanta 400 SEM with a resolution of 4 nm, equipped with an Everhart-Thornley detector for backscattered and secondary electron contrast. This analysis was conducted at the Chemistry Center Vila Real of the University of Tras-dos-Montes and Alto Douro, Portugal.

4.3.3. Textural analysis

Textural analysis using the BET method is used to quantitatively determine the surface area of porous materials [226]. The textural properties were gathered upon analysis of N_2 adsorption-desorption isotherms at 77 K, obtained in a Quantachrome NOVATOUCH LX4 adsorption analyzer equipped with long cells with a bulb and outer diameter of 9 mm. Before the analysis, the samples were degasified for 16 h at 120 °C, following IUPAC recommendation. Total pore volume (V_T), BET specific surface area (S_{BET}), and Langmuir-specific surface area ($S_{langmuir}$) was be gathered using the Quantachrome TouchWinTM software. The external surface area (S_{ext}) and the micropore volume (V_{mic}) was be obtained by the t-method (thickness was calculated by employing the ASTM standard D-6556-01). The microporous surface area (S_{mic}) was determined as the subtraction of S_{ext} from S_{BET} and the average pore width (W_{mic}) by approximation ($W_{mic} = 4\ V_{mic}\ S_{mic}^{-1}$). The total pore volume (V_{Total}) was determined at p/p0 = 0.98. Calculations of those methods were all done using the TouchWinTM software v1.21. The analysis was conducted at the Mountain Research Center of the Bragança Polytechnic Institute (IPB), Portugal.

4.3.4. Thermogravimetric Analysis

Thermogravimetric Analysis (TGA) is a technique that measures the mass variation of a material as a function of temperature, aiming to assess its thermal stability and decomposition behavior. It determines the decomposition temperature, quantifies mass loss due to volatilization or chemical reactions, and analyzes the moisture and volatile content. Finally, TGA (TGA-DCS1, Mettler-Toledo, SAE) was performed in air atmosphere from 40 to 900 °C (heating rate 10 °C min^{-1}) to evaluate the mass loss for the samples during the synthesis procedure. This analysis was conducted at Rey Juan Carlos University, Spain.

4.3.5. Elemental and Chemical Composition

4.3.5.1. Elemental analysis CNHS

The chemical composition of WGP and AC_WGP was assessed by elemental analysis CHNS (carbon, hydrogen, nitrogen and sulfur), carried out in a Flash 2000 analyzer (Thermo Fisher Scientific, Massachusetts, USA) equipped with a thermal conductivity detector (TCD). This analysis was conducted at the Department of Chemical and Environmental Technology of the Rey Juan Carlos University, Spain.

4.3.5.2. X-ray fluorescence

X-ray fluorescence spectrometry (XRF) is an analytical technique that relies on the emission of characteristic fluorescence energies from atomic species when they are excited by incident X-rays [227]. The method is based on the interaction between primary X-rays, and the atoms present in the sample, leading to the excitation and subsequent emission of secondary (fluorescent) X-rays with energies characteristic of each element [228]. This process enables the qualitative and quantitative identification of a broad range of chemical elements. The chemical composition of samples was determined using a Malvern Panalytical Epsilon 4 energy-dispersive XRF spectrometer (Almelo, The Netherlands), equipped with a high-power generator operating at 15 W and 15 kV, and X-ray tubes with a silver anode. The measurements were carried out at the Department of Chemical and Environmental Technology of Rey Juan Carlos University, Spain.

4.4. ADSORPTIVE OF ADVANCED MATERIALS

4.4.1. Adsorption Kinetics

The study of kinetics in adsorption processes is essential to understand the rate at which contaminants are removed from solutions by adsorbents. Adsorption kinetics describe the time-dependent interaction between the adsorbate and the adsorbent, providing insights into the mechanisms of adsorption, the efficiency of the process, and the factors affecting the rate of adsorption [229].

The adsorbents were individually loaded (C_{ads} = 2.5 g L^{-1}) into a CBZ-contaminated model wastewater solution with an initial concentration of C_0 = 100 mg L^{-1}. The pH values of the solutions were measured prior to the experiments. The solutions were undergoing agitation on a magnetic stirrer at 300 rpm. At 13 distinct time intervals (0, 15, 30, 60, 120, 240, 300, 360 and 480 min), 2 mL aliquots were drawn from the solutions. This study was

employed three kinetic models: the pseudo-first order (PFO) model, the pseudo-second order (PSO), and the intraparticle diffusion (ID) model. The mathematical expressions are given in Table 3.

Table 3: Kinetic models equations.

Ref.	Models	Equilibrium	Linearized
Lagergren [230]	Pseudo-first order	$q_t = q_e(1 - e^{-k_1 t})$	$\ln(q_t - \mathrm{q_e}) = \ln q_e - \mathrm{k_1 t}$
Ho *et al.* [231]	Pseudo-second order	$q_t = \frac{q_e^2 k_2 t}{1 + q_e k_2 t}$	$\frac{\mathrm{t}}{q_t} = \frac{1}{q_e^2 k_2} + \frac{t}{q_e}$
Weber *et al.* [232]	Intraparticle diffusion	$q_t = k_{id} t^{1/2}$	$q_t = k_{id} t^{1/2} + I$

where qt is the adsorption capacity (mg g^{-1}) at time t (min), q_e is the adsorption capacity at equilibrium (mg g^{-1}), k_1 is the adsorption rate kinetic constant of the PFO model (min^{-1}), k_2 is the adsorption rate kinetic constant of the PSO model (g mg^{-1} min^{-1}), k_{id} is the ID rate constant (mg g^{-1} $min^{-0.5}$), and I is the intercept (mg g^{-1}).

4.4.2. Equilibrium Isotherms

Equilibrium isotherms describe the relationship between the concentration of adsorbate in solution and its concentration on the surface of the adsorbent at equilibrium. These isotherms are essential to understand how adsorbents interact with pollutants in environmental and industrial processes, providing insights into adsorption capacity, affinity, and the effectiveness of adsorption systems [229].

The selected adsorbents (C_{ads} = 2.5 g L^{-1}) were tested with six different concentrations for CBZ (5, 10, 20, 30, 40, 50, and 100 mg L^{-1}). The mixtures were agitated on a magnetic stirrer at 300 rpm at room temperature for 24 h, after which 2 mL aliquots were collected, filtered with 0.45 µm Polytetrafluoroethylene syringe filters, and stored for High Performance Liquid Chromatography (HPLC) analysis. Two isotherm fitting models for solid-liquid systems were evaluated, shown in the Table 4. The Langmuir isotherm describes monolayer adsorption on a homogeneous surface with a finite number of identical sites, while the Freundlich isotherm describes adsorption on heterogeneous surfaces with varying affinities [233].

Table 4: Equilibrium isotherms models equations.

Ref.	Models	Equilibrium	Linearized
Langmuir [234]	Langmuir	$q_{eq} = \frac{q_{max} K_L C_{eq}}{1 + K_L C_{eq}}$	$\frac{C_{eq}}{q_e} = \frac{1}{q_{max} K_L} + \frac{C_{eq}}{q_{max}}$
Vigdorowitsch *et al.* [235]	Freundlich	$q_{eq} = K_F C_{eq}^{1/n_F}$	$\log q_e = \log K_F + \frac{1}{n_F} \log C_{eq}$

where q_{eq} is the adsorption capacity at equilibrium (mg g^{-1}), q_{max} is the maximum adsorption capacity of the adsorbent (mg g^{-1}), C_{eq} is the equilibrium concentration (mg L^{-1}), K_L is the Langmuir adsorption constant (L mg^{-1}), K_F is the Freundlich constant (L g^{-1}), and n_F is the dimensionless Freundlich constant related to adsorption intensity, values in the range 1 to 10 represent favorable adsorption conditions.

4.5. ANALYTICAL METHOD

HPLC measurements involve two distinct analyses equipped with a UV-VIS detector (UV-2075 Plus) and a quaternary gradient pump (PU-2089 Plus). HPLC was used to analyze the contaminant under investigation (CBZ), and an Ultra BiPh 5 µm column (150 mm × 2.1 mm) was used for this analysis. The mobile phases were consisted of 60% ultrapure water with 0.1% formic acid and 40% acetonitrile, which share a detection wavelength of 285 nm, under an isocratic system operating at a flow rate of 0.3 mL min^{-1} and an acquisition time of 7.6 min. A calibration curve was constructed for CBZ to convert the integrated peak areas from the electrochemical signal into concentration units (APPENDIX).

5. RESULTS AND DISCUSSION

5.1. GEOPOLYMERS PRODUCTION

The mass balance of GPs production was determined based on mass and volume measurements. These variables were measured after the production of each batch and again after the washing step applied to the GPs. The corresponding values are presented in Table 5.

Table 5: The mass and volume throughout the membrane production process.

	Initial		**Post HT***				**Post Wash**			
	Mass (g)	**Volume (cm^3)**	**Mass (g)**	**Mass loss (%)**	**Volume (cm^3)**	**Volume loss (%)**	**Mass (g)**	**Mass loss (%)**	**Volume (cm^3)**	**Volume loss (%)**
GP_M	20.70 ± 0.20	25.94 ± 0.81	18.08 ± 0.72	12.7	25.55 ± 0.92	1.5	14.08 ± 0.15	22.1	23.40 ± 0.64	8.4
GP_AC	23.14 ± 0.06	28.57 ± 1.32	18.13 ± 0.33	21.6	25.53 ± 0.98	10.6	15.87 ± 0.52	12.5	24.33 ± 0.34	4.7

*The values were not separated according to HT concentration; the variation among the different concentrations was disregarded.

The mass and volume results of the GPs reveal significant changes throughout the different processing stages for both GP_M and GP_AC. Initially, the difference in mass (GP_M 20.70 g and GP_AC 23.14 g) and volume (GP_M 25.94 cm^3 and GP_AC 28.57 cm^3) of the materials is consistent with the incorporation of AC into the geopolymeric matrix.

After the HT, a more pronounced mass reduction was observed for GP_AC (21.6%) compared to GP_M (12.7%). Regarding volume for GP_M, the variations after HT (1.5%) were relatively small, suggesting that the treatment primarily promoted internal structural rearrangements and material loss, without significant collapse of the macroscopic structure. After the washing and neutralization step, both materials exhibited additional mass losses, which were more pronounced for GP_M (22.1%), while GP_AC showed a smaller loss (12.5%). The volume reduction observed after washing was moderate for both materials, reflecting pore emptying and increased surface exposure of the GP matrix due to the removal of unreacted material and excess alkaline activating solution [236].

Overall, these results demonstrate that each processing step distinctly affects the materials, highlighting the importance of carefully considering mass and volume balances in future studies, particularly for scaling up GP materials production, where material losses and dimensional variations can directly impact process feasibility and reproducibility.

In the literature, GP subjected to HT are rarely analyzed in terms of quantitative parameters such as the percentage of mass and volume losses observed in the present work. However, these parameters are highly relevant when considering process scale-up and real-world applications. For instance, in one of the few studies reporting such information,

Ramadan *et al.* [237] investigated the hydrothermal curing of GPs at 165 °C for 6 h and reported total mass changes of up to 10.87%.

5.2. CHARACTERIZATION OF MATERIALS

5.2.1. Surface Chemistry

5.2.1.1. X-ray Diffraction

The XRD patterns obtained for materials are displayed in Figure 7. Several crystalline phases are discernible using the software X′ Pert HighScore Plus in the diffractogram.

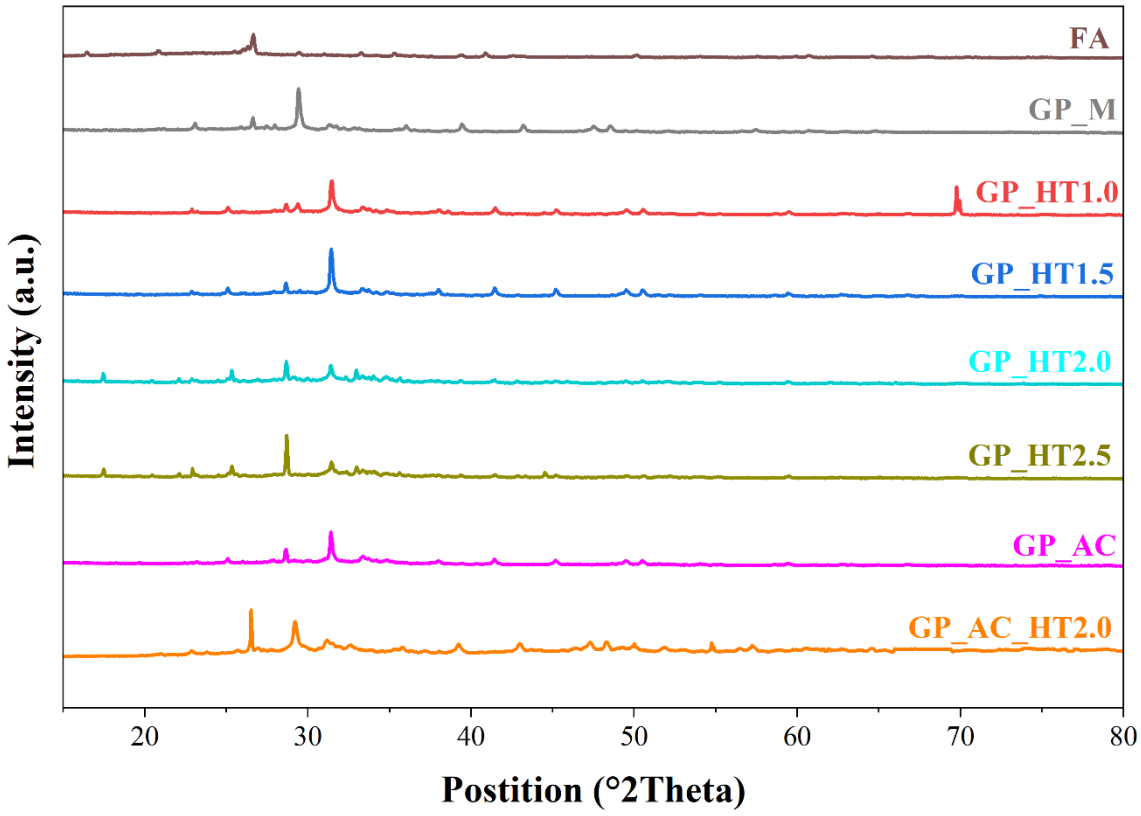

Figure 7: X-ray diffractogram of FA, GP_M, GP_HT1.0, GP_HT1.5, GP_HT2.0, GP_HT2.5, GP_AC, and GP_AC_HT2.0.

XRD analysis of the FA revealed several crystalline phases, including quartz (SiO_2: 2θ = 20.8º and 26.6º), mullite ($Al_6Si_2O_{13}$: 2θ = 26.4º, 33.2º and 35.3º), and hematite (Fe_2O_3: 2θ = 24.2º, 33.1, 35.6º and 49.5º). After geopolymerization without HT (GP_M), the diffractogram shows the persistence of quartz (2θ = 20.8° and 26.6°) and hematite (2θ = 24.2°, 33.1°, 35.6°, 49.5°). New crystalline phases appear, including calcite ($CaCO_3$; 2θ ≈ 29.4°), gehlenite ($Ca_2Al_2SiO_7$; 2θ ≈ 31.1°, 32.6°), and gismondine ($CaAl_2Si_2O_8{\cdot}4H_2O$; 2θ ≈ 15.2°, 27.1°).

These phases reflect partial dissolution of the FA and subsequent reorganization of aluminosilicate species within the GP [238].

The materials subjected to HT in Figure 7, GP_HT1.0 and GP_HT1.5, display very similar crystalline assemblages, with quartz (2θ = 20.8°, 26.6°), hematite (2θ = 24.2°, 33.1°, 35.6°, 49.5°), calcite (2θ ≈ 29.4°), gehlenite (2θ ≈ 31.1°, 32.6°), and enstatite ($MgSiO_3$; 2θ ≈ 30.0°, 35.0°). In GP_HT1.0, mullite (2θ = 26.4°, 33.2°, 35.3°) remains detectable, while GP_HT1.5 exhibits gismondine (2θ ≈ 15.2°, 27.1°). For the samples treated under higher alkalinity (GP_HT2.0 and GP_HT2.5), all phases observed in the HT conditions are retained: quartz (2θ = 20.8°, 26.6°), hematite (2θ = 24.2°, 33.1°, 35.6°, 49.5°), calcite (2θ ≈ 29.4°), enstatite (2θ ≈ 30.0°, 35.0°), gehlenite (2θ ≈ 31.1°, 32.6°), mullite (2θ = 26.4°, 33.2°, 35.3°), and gismondine (2θ ≈ 15.2°, 27.1°). Additionally, both samples show the formation of faujasite-Na (Na–X zeolite; 2θ ≈ 6.1°, 10.1°, 15.7°, 23.0°). The appearance of this zeolitic phase indicates intensified dissolution of Si and Al species and enhanced crystal growth under more alkaline hydrothermal conditions [239]. Faujasite is a crystalline aluminosilicate belonging to the zeolite family, characterized by a cubic FAU-type framework made of interconnected SiO_4 and AlO_4 tetrahedra. This structure forms a three-dimensional pore system with large supercages and 12-membered-ring windows [240,241]. The only study reporting Faujasite formation from FA-GP via in-situ HT is that of Liu *et al*., [242]. In their work, faujasite GPs were synthesized using a SiO_2/Al_2O_3 molar ratio of 4.0, a NaOH solution concentration of 1.0 M, and a crystallization period of 24 h at 70 °C.

For the AC-containing material (GP_AC), XRD analysis indicated the presence of the same phases as those identified in the geopolymeric materials, including quartz (2θ = 20.8º and 26.6º), calcite (2θ ≈ 29.4°), mullite (2θ = 26.4º, 33.2º and 35.3º), gehlenite (2θ ≈ 31.1°, 32.6°), gismondine (2θ ≈ 15.2°, 27.1°), and enstatite (2θ ≈ 30.0°, 35.0°). In the diffractogram of sample GP_AC_HT2.0, only the calcite (2θ ≈ 29.4°) and gehlenite (2θ ≈ 31.1°, 32.6°) phases were observed. In the study by Khan *et al*. [191], in which AC was incorporated into the GP matrix, XRD analysis in the 2θ range of 2–80° indicated that the obtained materials are predominantly amorphous, exhibiting a broad diffuse halo between 20–27° (2θ), characteristic of the amorphous nature of the geopolymeric matrix. In addition to the amorphous phase, residual crystalline phases were identified, with quartz being particularly prominent, as evidenced by peaks at approximately 2θ ≈ 20.8°, 26.5°, 50.2°, 60.1°, and 68.3°. Brushite and mullite phases were also observed in both samples. The presence of the amorphous phase associated with brushite confirms the formation of the incorporated material, while the quartz and mullite phases indicate the presence of unreacted FA.

5.2.1.2. Fourier Transform Infrared Spectroscopy

The FT-IR spectra of the inorganic samples are presented in Figure 8, allowing for the qualitative identification of the main functional groups present.

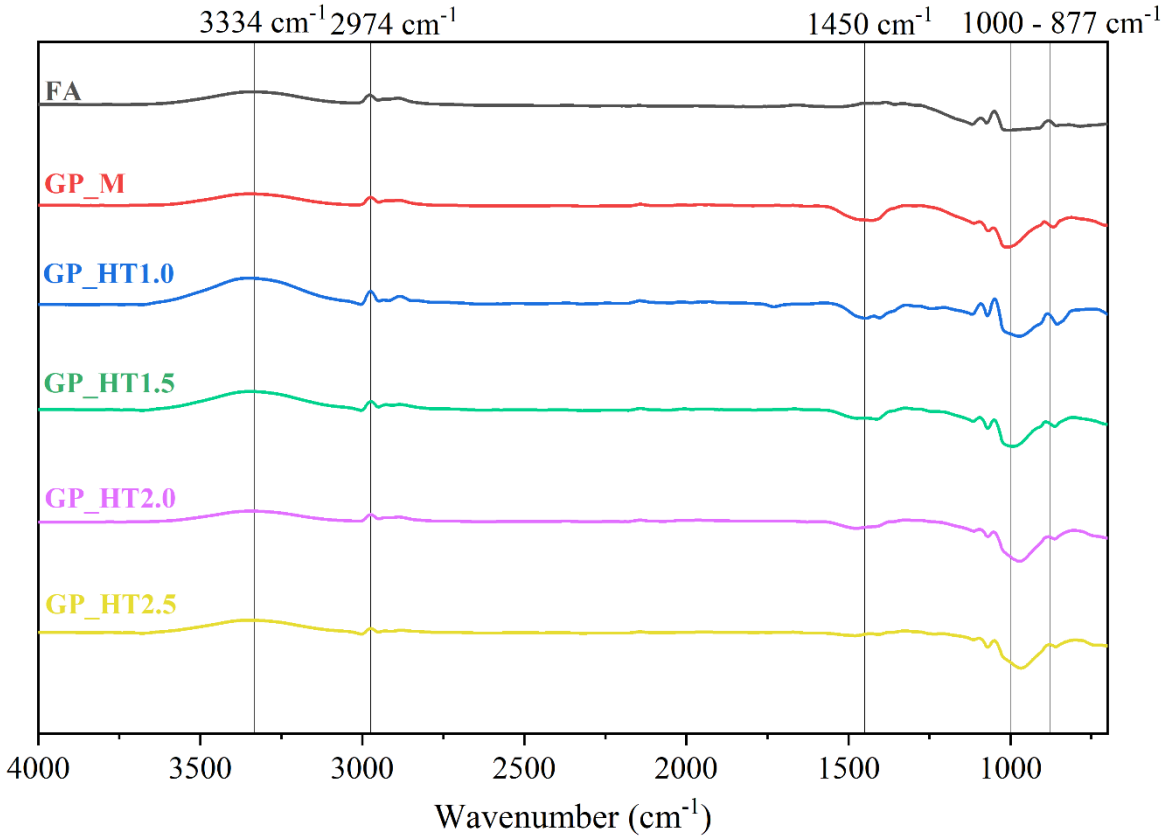

Figure 8: FT-IR spectra of the investigated inorganic materials.

In all analyzed samples, a broad band at approximately 3334 cm^{-1} was observed, indicating the presence of hydroxyl groups (-OH) in the GP matrix, which are attributed to weakly bound water molecules trapped in large cavities or adsorbed on the surface of the GPs [243,244]. The peak in 2974 cm^{-1} in samples can be attributed to C-H stretching vibrations [181], likely associated with residual organic species originating from the precursor materials, particularly considering their higher presence in the FA used as the raw material for the samples. In the spectra of both FA and GP samples, a peak at approximately 1450 cm^{-1} was observed, which is attributed to C-O bending vibrations associated with the CO_3^{2-} group [245]. It is believed that these bands formed due to the carbonation of the surface by atmospheric CO_2 [246]. Additionally, the band observed at 1000 cm^{-1} corresponds to the asymmetric stretching vibrations of Si-O-T (where T represents tetrahedral Al or Si), which is a characteristic feature of the aluminosilicate network [247]. Liu *et al.* [223] produced FA-GP and, after HT, obtained a faujasite-type GP. In both samples, bands between 3436 and 1640

cm⁻¹ were observed, corresponding to O–H stretching and H–O–H bending vibrations. The band around 1440 cm⁻¹ was associated with O–C–O stretching vibrations, while the broad bands in the 900–1030 cm⁻¹ region were attributed to asymmetric Al–O/Si–O stretching vibrations.

The FT-IR spectra of the organic materials are presented in Figure 9. The spectrum of the WGP sample is characteristic of lignocellulosic materials, showing a peak at 3330 cm⁻¹, attributed to the stretching vibrations of O–H bonds present in cellulose, hemicellulose, lignin, and adsorbed water [248].

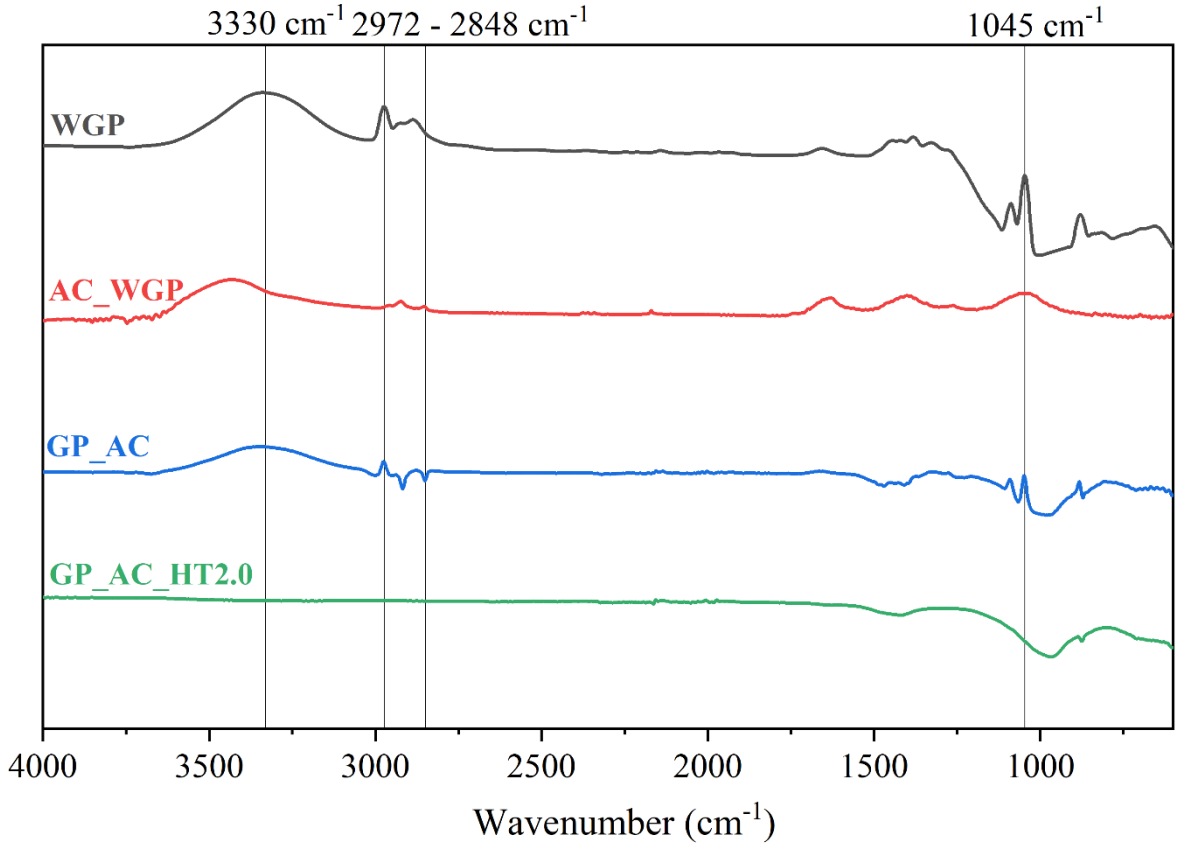

Figure 9: FT-IR spectra of the investigated organic materials.

The peaks observed between 2848 and 2972 cm⁻¹ correspond to –CH_2 and –CH_3 groups, while the peak around 1045 cm⁻¹ is associated with the vibrations of polysaccharides (C–O and C–O–C) [249]. In the AC_WGP sample, the decomposition of cellulose and part of the lignin can be observed through the reduction of the O–H and C–H bands, reflecting the formation of a more condensed and aromatic carbonaceous structure, which is characteristic of ACs. Sağlam *et al.* [185] produced AC from grape pomace by pyrolysis at 700°C for 120 min, followed by chemical activation using HCl. Their spectrum showed peaks at 1056 cm⁻¹ attributed to C–O vibrations, and a broad band around 3453 cm⁻¹ caused by O–H stretching vibrations, indicating the presence of moisture on the AC surface.

The spectrum of the GP_AC sample is dominated by the characteristic bands of the geopolymeric matrix, as previously observed in Figure 8. The bands around 1045 cm^{-1} differ from those observed in the pure samples, which may indicate difficulties in GP formation due to the incorporation of AC, as well as the integration of both materials [191].

Figure 10 presents the FT-IR spectra of the GP_M, GP_HT2.0, GP_AC, and GP_AC_HT2.0 samples after the CBZ adsorption process.

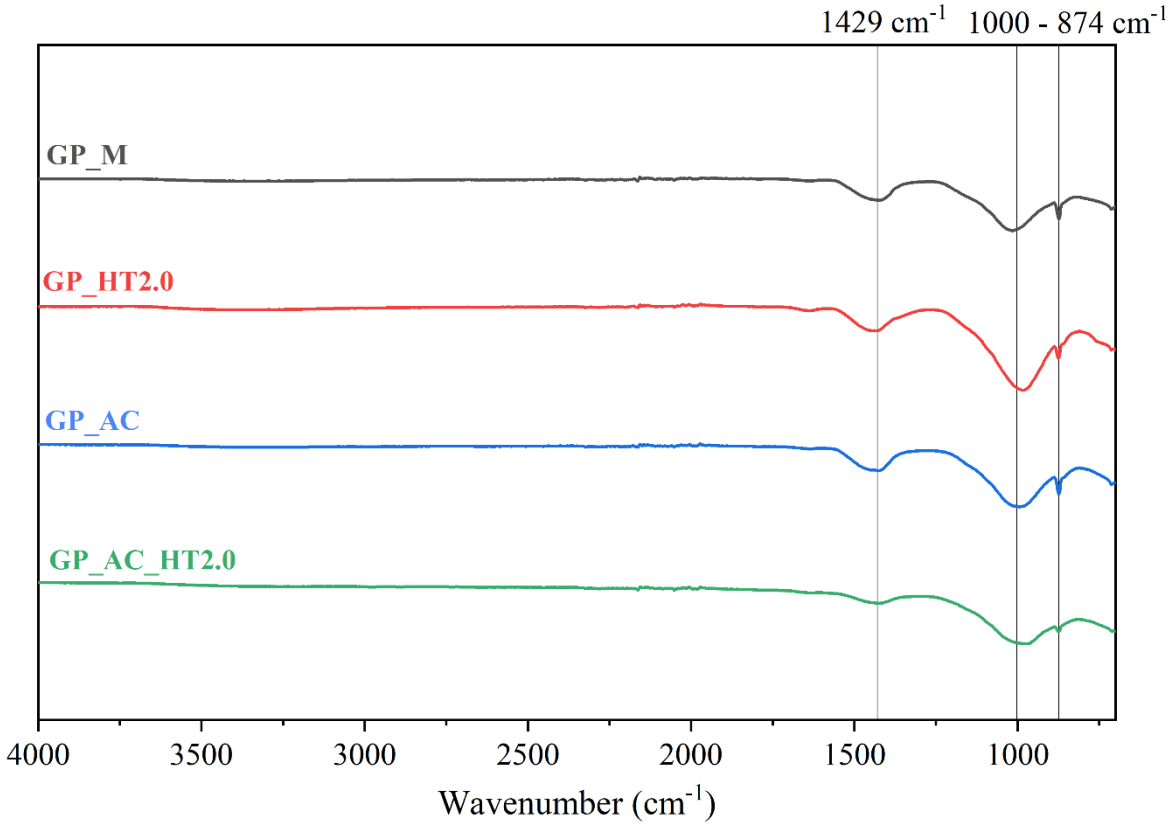

Figure 10: FT-IR spectra of the samples after adsorption (saturated).

The saturation of the samples with CBZ reveals structural modifications associated with the interaction between the pharmaceutical compound and the materials, as observed in the FT-IR spectra. An intensification and modification of the band at 1429 cm^{-1} can be observed, attributed to the C=C stretching vibrations of CBZ, as well as changes in the region around 1000 cm^{-1}, resulting from the overlap between the asymmetric stretching vibrations of the geopolymeric network (Si–O–Al/Si–O–Si) and the adsorbed molecule (C–N stretching vibrations). The band at approximately 874 cm^{-1} becomes more pronounced and is attributed to the out-of-plane deformation of aromatic C–H bonds of CBZ, confirming the presence of the adsorbed molecule on the surface of the materials [250].

5.2.1.3. Acid-base Characterization

The pH_{PZC}, acidity, and basicity are crucial parameters for understanding the surface properties of the materials. These parameters describe how the surface charges and interacts with ions across pH, crucial for adsorption applications [206]; pH_{PZC} shows that the surface may be positively charged, negatively charged, or have no charge at specific pH values; the acidity and basicity of a material are quantified by the concentration of acidic and basic sites on its surface, usually expressed in micromoles per gram (μmol g^{-1}) [229]. These parameters are shown in Table 6 for each material studied (pH_{PZC} graphs in APPENDIX).

Table 6: Values of pH_{PZC}, basicity, and acidity.

Sample	pH_{PZC}	Basicity (μmol g^{-1})	Acidity (μmol g^{-1})
FA	9.96	2500	515
GP_M	9.67	2387.5	470
GP_HT1.0	10.28	2434.5	1065
GP_HT1.5	9.81	2447.5	860
GP_HT2.0	9.75	2353.5	875
GP_HT2.5	10.02	2445	610
WGP	3.83	20	2370
AC_WGP	9.78	2315	140
GP_AC	9.86	2457.5	345
GP_AC_HT2.0	10.64	2425	895

The pH_{PZC} value for all GPs were in the range of approximately 9 to 10, indicating a predominantly basic surface character. This suggests that the GPs will exhibit a positive surface charge at pH values below the pH_{pzc} due to an increased hydrogen ion (H^+) concentration. Conversely, when the solution pH exceeds this value, the GPs carry a negative surface charge as hydroxide ions (OH^-) concentration increases [251]. The pH_{PZC} is a key parameter for describing variable-charge surfaces, as it directly influences electrostatic interactions between the adsorbent and ionic species in solution [206]. These results are in agreement with Manickam *et al*. [52], who prepared FA–biomass ash-based GPs activated with sodium silicate and NaOH, followed by HT in 1 M NaOH at 100 °C for 48 h, producing a zeolitic material with a pH_{pzc} of 10.3.

Notably, the materials subjected to HT, GP_HT1.0, GP_HT1.5, GP_HT2.0, and, GP_HT2.5, did not exhibit significant changes in pH_{PZC} (10.28, 9.81, 9.75, 10.02, respectably), indicating that this treatment did not alter the intrinsic basicity comparable to that of the pristine material (GP_M, 9.67).

The WGP exhibited a low pH_{PZC} value (3.8), attributed to the high content of acidic oxygen-containing functional groups, such as organic acids, phenolic compounds, and carboxylic functionalities inherent to its lignocellulosic structure [252], which agrees with the high concentration of acidic sites (2370 μmol g^{-1}) observed for the WGP, evidencing the strong acidic character of the material. After pyrolysis and subsequent physical activation with CO_2, the pH_{PZC} increased markedly to approximately 9, indicating a significant modification of the surface chemistry due to the thermal removal of acidic groups and increased aromaticity of the carbon matrix [185]. Additionally, the presence of inorganic mineral species typical of vitivinicultural residues, such as potassium and calcium, retained as oxides or carbonates after thermal treatment, further contributes to the enhanced surface basicity. This behavior is corroborated by the high density of basic sites measured for AC_WGP (2315 μmol g^{-1}), confirming the predominance of basic functionalities on the AC surface.

In contrast, the GP_AC and GP_AC_HT2.0 did not exhibit a significant change in basicity compared to their individual precursors, namely the AC and the GP. The basicity of the GP_AC was 2457.5 μmol g^{-1}, indicating that the incorporation process did not substantially alter the nature or density of basic surface sites. This result suggests that the basic functionalities of both precursor materials were largely preserved within the composite materials structure, with no evident synergistic or antagonistic effects arising from the combination of AC and GP.

4.2.2. Morphological Analysis

The morphology of the FA and GP materials (Figure 11a to f) was investigated using SEM/EDS microscopy. The microstructure of FA (Figure 11a) revealed an intricate and multifaceted morphology, characterized by an amalgamation of discrete and agglomerated particles that appear predominantly rounded and spherical, while varying in size and shape. These particles are frequently interspersed with interconnected pores, further complicating the overall structure [253]. The spherical particles are a typical feature of FA generated during high-temperature combustion processes, in which molten mineral droplets rapidly solidify upon cooling [206]. The SEM images of FA provide a fundamental basis for understanding the transformations occurring during geopolymerization, as the reactivity of the material is governed by its morphological heterogeneity.

In the SEM images, clear morphological differences are observed between the GP without HT (Figure 11b, GP_M) and the materials subjected to HT. The untreated sample GP_M still contains several spherical particles typical of unreacted FA (highlighted by the red

circles in the micrograph). Despite the presence of these residual particles, the GP matrix appears relatively dense and cohesive, indicating a degree of geopolymerization.

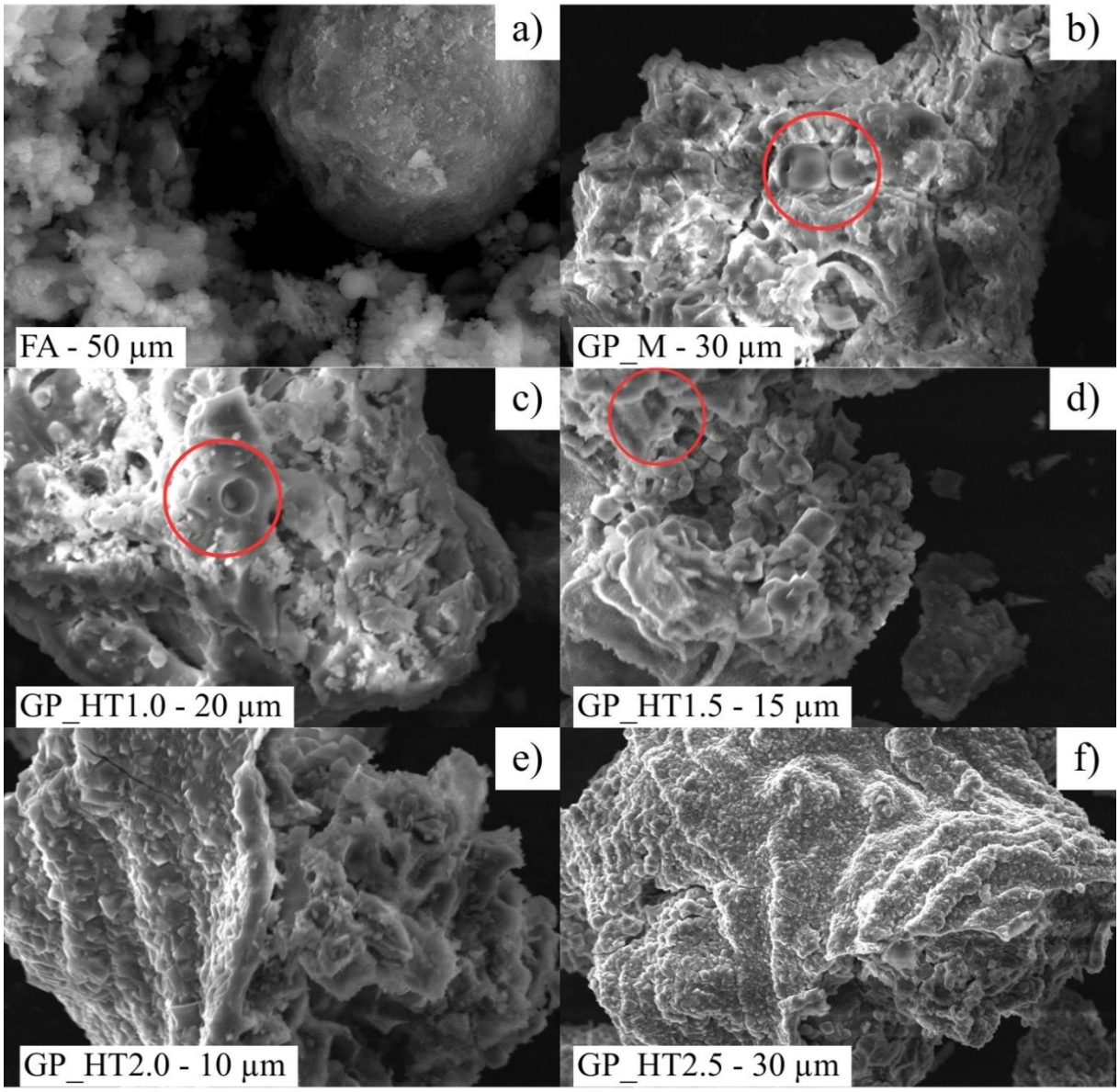

Figure 11: SEM micrographs of a) FA, b) GP_M, c) GP_HT1.0, d) GP_HT1.5, e) GP_HT2.0, and f) GP_HT2.5.

In contrast, GP_HT1.0 (Figure 11c) displays pronounced cavities. These voids are likely associated with the partial dissolution and subsequent removal of reaction products during the HT, which increases the porosity of the matrix. The samples exposed to more intense hydrothermal conditions, namely GP_HT2.0 (Figure 11e) and GP_HT2.5 (Figure 11f), exhibit a markedly different surface morphology. Their microstructures are characterized by a more homogeneous surface composed of angular, block-like crystalline aggregates. This morphology suggests substantial structural reorganization, driven by enhanced dissolution and recrystallization processes under stronger alkaline conditions. These

microstructural features are consistent with the XRD results, which identified Na-Faujasite a zeolite mineral characterized by its cubic FAU crystalline structure [254], exclusively in GP_HT2.0 and GP_HT2.5. Similarly, Li *et al.*, [242] also reported Faujasite formation in their materials, and their SEM images showed cubic crystals with well-defined edges, consistent with the morphology observed in the present study.

In addition, the morphology of AC_WGP and GP–carbon composite was presented in Figure 12a to c. The micrograph corresponding to AC_WGP (Figure 12a) reveals a highly irregular surface, characterized by the presence of cavities, fissures, and pores of varying dimensions, which are typical features of carbonaceous materials [255]. Hassani *et al.* [181] produced AC from grape seed bagasse via chemical activation using potassium hydroxide (KOH) and showed that the activation temperature conditions are effective in creating well-developed pores on the surface.

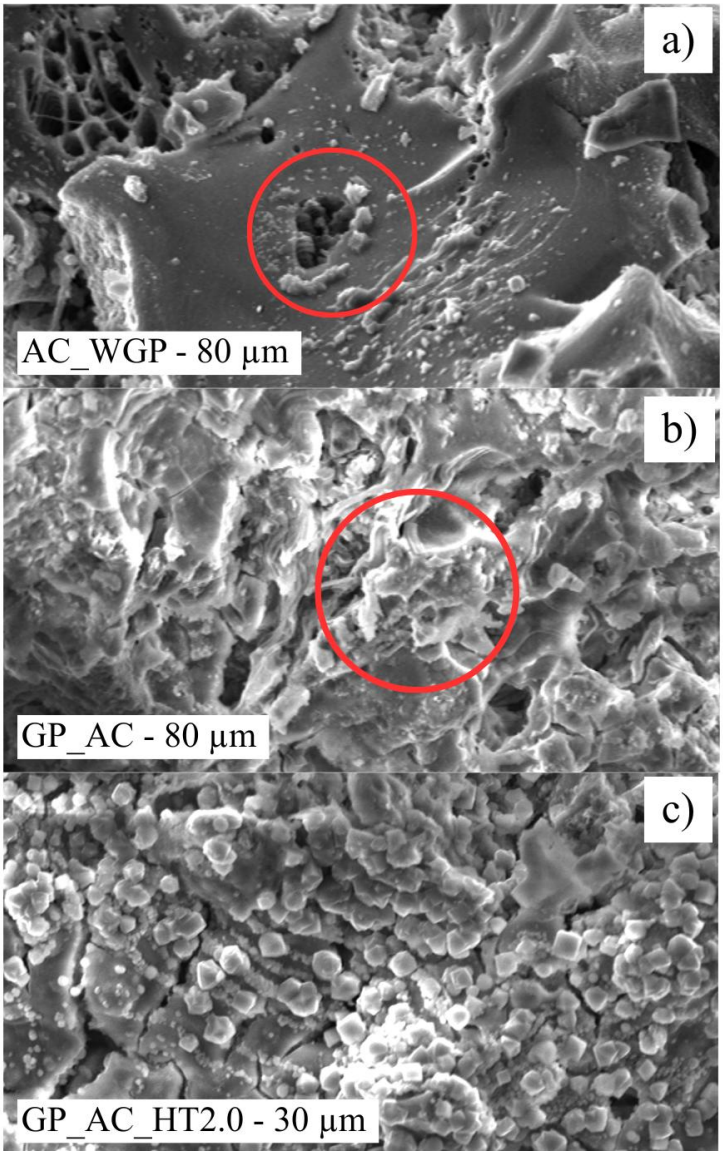

Figure 12: SEM micrographs of a) AC_WGP, b) GP_AC, and c) GP_AC_HT2.0.

After the incorporation of AC into the geopolymeric matrix, as observed in Figure 12b, a significant modification of the surface morphology compared to AC_WGP is evident. The AC particles are partially encapsulated by the GP matrix, resulting in a more compact structure with less clearly defined individual particles. The surface exhibits a more irregular and fragmented appearance, reflecting the interaction between the AC and the aluminosilicate phase of the GP [214]. This incorporation suggests a good dispersion of AC within the matrix, which is essential to ensure the accessibility of adsorptive sites as well as the structural stability of the material [256].

The sample subjected to HT (GP_AC_HT2.0, Figure 12c) exhibits an even more refined and homogeneous morphology, characterized by the formation of more uniform granular structures and a reduction in large voids or fissures. This behavior indicates that the HT promoted reorganization and densification of the geopolymeric matrix, possibly associated with the advancement of polycondensation reactions and the partial recrystallization of secondary phases. The presence of AC remains evident but is more efficiently integrated into the matrix, which not only enhances mechanical stability but also increases the accessibility of adsorptive sites and creates additional diffusion pathways, resulting in a superior adsorption capacity compared to the other materials.

Overall, the morphological evolution observed by SEM demonstrates that the incorporation of AC and the subsequent HT result in a heterogeneous, rough, and structurally integrated surface. These features are widely associated in the literature with enhanced adsorption capacity, due to the increased contact area and the greater availability of accessible active sites.

5.2.3. Textural Analysis

Textural properties analysis for the material was summarized in Table 7. The structure and physicochemical properties of GP materials are intrinsically governed by the nature of the raw materials used and their role in the geopolymerization reaction [257]. Yan et al. demonstrated that GPs derived from FA can exhibit specific surface area ranging from 15.6 $m^2\ g^{-1}$ [258] to 63.46 $m^2\ g^{-1}$ [259]. The pore characteristics of the GP materials indicate that the GP_M (30 $m^2\ g^{-1}$) developed in the present study are in good agreement with the structural and textural features reported in the literature.

Furthermore, the hydrothermally treated materials (GP_HT1.0, GP_HT1.5, GP_HT2.0, and GP_HT2.5) exhibited higher specific surface area (S_{BET}) and total pore volume values when compared to the precursor material (GP_M). This behavior highlights

the significant role of the HT treatment in promoting surface development and pore formation within the GP matrix.

Table 7: Textural properties analysis for the materials.

Sample	S_{BET} ($m^2\ g^{-1}$)	$S_{Langmuir}$ ($m^2\ g^{-1}$)	S_{mic} ($m^2\ g^{-1}$)	S_{ext} ($m^2\ g^{-1}$)	V_{total} ($cm^3\ g^{-1}$)
FA	13	248	-	1	0.010
GP_M	30	232	-	7	0.074
GP_HT1.0	57	437	3	54	0.155
GP_HT1.5	95	539	9	86	0.156
GP_HT2.0	181	527	68	113	0.195
GP_HT2.5	49	158	22	26	0.076
AC_WGP	427	632	254	173	0.225
GP_AC	48	188	12	36	0.110
GP_AC_HT2.0	139	138	77	62	0.138

The results indicate that the increase in surface area follows an approximately proportional trend only up to a certain NaOH concentration. The S_{BET} increases from 57 $m^2\ g^{-1}$ (GP_HT1.0) to 95 $m^2\ g^{-1}$ (GP_HT1.5), reaching a maximum value of 181 $m^2\ g^{-1}$ at a NaOH concentration of 2.0 M (GP_HT2.0). Beyond this point, the trend is not maintained, at 2.5 M, the surface area decreases markedly, with GP_HT2.5 displaying an S_{BET} of only 49 $m^2\ g^{-1}$. Thus, the samples GP_HT1.0 and GP_HT1.5 show comparable pore volumes (0.155 and 0.156 $cm^3\ g^{-1}$, respectively), reflecting only a modest increase consistent with their moderate S_{BET} values. A substantial rise in V_{total} occurs at a NaOH concentration of 2.0 M, where GP_HT2.0 reaches 0.195 $cm^3\ g^{-1}$, in agreement with its higher surface area and indicating extensive pore development. However, as also observed for S_{BET}, this effect does not persist at higher alkalinity: GP_HT2.5 exhibits a significant reduction in pore volume (0.076 $cm^3\ g^{-1}$), suggesting that excessive NaOH concentration may induce structural densification or collapse of previously formed pores.

The faujasite GP produced by Liu *et al.* [223], reached a S_{BET} of 174 $m^2\ g^{-1}$ using a 1 M NaOH solution during the HT. In contrast, the GP thermally treated with 1 M NaOH in the present study achieved a significantly lower S_{BET} of 57 $m^2\ g^{-1}$, which may be attributed to differences in the GP formulation. However, when the HT treatment was carried out with 2 M NaOH, the resulting material displayed a considerably higher S_{BET} of 181 $m^2\ g^{-1}$, greater than that reported by Liu *et al.* [223]. Regarding other GP-derived zeolites, Khalid *et al.* [22], reported a maximum S_{BET} of 90 $m^2\ g^{-1}$ for a zeolitized GP containing the analcime phase after

24 h of HT at 100 °C using 8 M NaOH. In contrast, He *et al*. [53], obtained only 30 $m^2 g^{-1}$ for a Li-ABW-type GP, where the HT was conducted in a 200 mL Teflon-lined autoclave containing the GP membrane and 50 mL of LiOH solution.

This study employed slow pyrolysis followed by physical activation with CO_2, resulting in a material with S_{BET} of 427 $m^2 g^{-1}$ (AC_WGP). Although no studies have developed AC using this exact approach, the obtained value falls within the range reported in the literature. Sardella *et al.* [260], employed thermal carbonization at 500 °C for 2 h under a nitrogen atmosphere to produce ACs from three different grape-derived residues, the resulting materials exhibited S_{BET} of 266 $m^2 g^{-1}$ for grape pomace, 300 $m^2 g^{-1}$ for grape stalk, and 798 $m^2 g^{-1}$ for grape lex. Mabrouk *et al.* [184], also reported an AC produced from grape seeds wastes at 800 °C for 3 h, chemically activated with H_3PO_4, which exhibited a S_{BET} of 543 $m^2 g^{-1}$. On the other hand, Sağlam *et al.* [185], produced AC from grape pomace by pyrolysis at 700°C for 120 min, followed by chemical activation using HCl, resulting in a S_{BET} of 44 $m^2 g^{-1}$.

The development of GPs incorporating AC is still scarcely reported in the literature. The GP_AC produced in the present work showed improved performance in terms of increased surface area compared to the precursor (GP_M – 30 $m^2 g^{-1}$), exhibiting an S_{BET} of 48 $m^2 g^{-1}$. The GP further subjected to HT (GP_AC_HT2.0) presented an S_{BET} of 139 $m^2 g^{-1}$; that is, the HT increased the surface area by approximately threefold.

Chen *et al.* [214], used a commercial wood-based AC with a S_{BET} of 1157 $m^2 g^{-1}$ and incorporated it into the synthesis of GP materials produced from MK and silica fume, as a result, the obtained material exhibited S_{BET} values ranging from 90 to 234 $m^2 g^{-1}$. The surface areas increased with increasing doses of AC. However, at the same AC dosages, the pore volumes, especially the micropores, decreased as the alkalinity of the activator increased. The study states that a strong alkaline activator could destroy and modify the original structure of the AC.

Khan *et al.* [261], synthesized GP materials from FA and MK, using H_3PO_4 as the activating solution, and obtained materials with a S_{BET} of approximately 5 $m^2 g^{-1}$. In a subsequent study, the author incorporated AC into the GP matrix, resulting in a significant increase in S_{BET}, reaching 47 $m^2 g^{-1}$ [191]. Finally, Gong *et al.* [262], developed a FA-GP-based composite incorporated with AC, obtained in situ from residual fiberboard powder. The resulting AC–GP composite exhibited textural properties with a specific surface area of 199 $m^2 g^{-1}$

4.2.4. Thermogravimetric Analysis

Figure 13a to e and Figure 14a to d illustrates the TGA results, along with the first-order derivative thermogravimetric analysis (DTG), providing a detailed overview of the weight loss and thermal transitions of the samples across the temperature range.

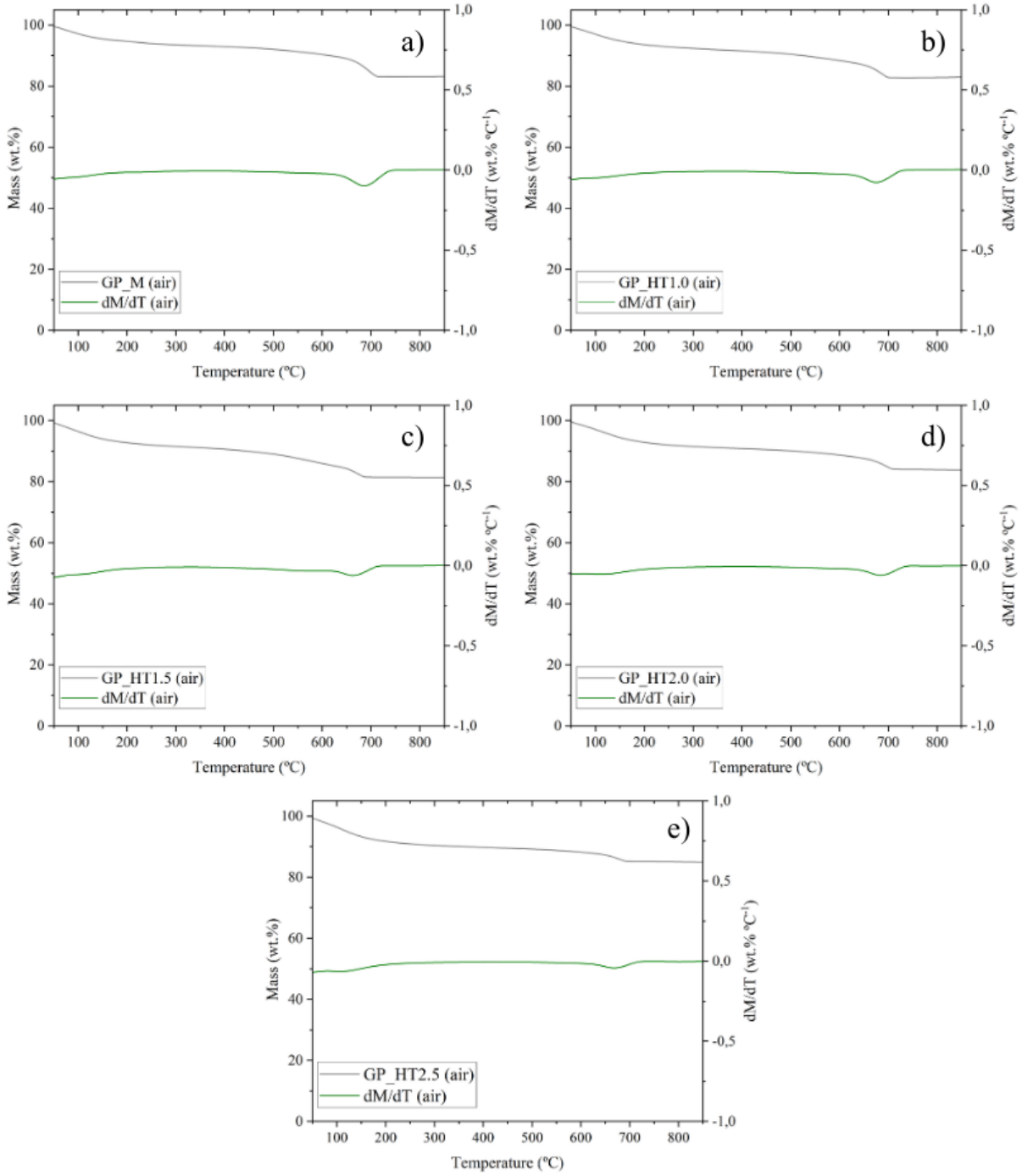

Figure 13: Thermogravimetric analysis in air (TGA and DTG) for: a) GP_M, b) GP_HT1.0, c) GP_HT1.5, d) GP_HT2.0, and e) GP_HT2.5.

Regarding thermal behavior, all materials exhibited expected behavior, each material maintaining its thermal stability even at elevated temperatures, consistent with their inorganic nature (Figure 13a to e). The DTG analysis reveals a mass loss at around 100 °C, for all samples attributed to water evaporation, which is expected and consistent with the findings in the literature [263,264]. The decrease in mass before 150 °C is indicative of the evaporation of both chemically bound water. Following this, there is a gradual but minor mass loss due to the elimination of hydroxyl groups (-OH) and chemically bonded water. However, around 700 °C, another peak in mass loss is observed. According to He *et al.* [263], this second weight loss, typically occurring between 300 and 650 °C, is related to the dehydroxylation of Si-OH and Al-OH groups.

The thermogravimetric behavior of the samples shown in Figure 14a to d differs from that of inorganic materials due to the presence of carbon in the analyzed materials. All samples exhibit mass loss in the temperature range from 100 to 200 °C, which is mainly attributed to the removal of physically adsorbed water [191]. The pronounced mass reduction observed between 200 and 500 °C is associated with the dehydration and depolymerization of the cellulose present, as well as with the onset of material carbonization. For the AC_WGP sample, this behavior occurs more gradually, indicating the vaporization of compounds that were not completely volatilized during the pyrolysis process [185].

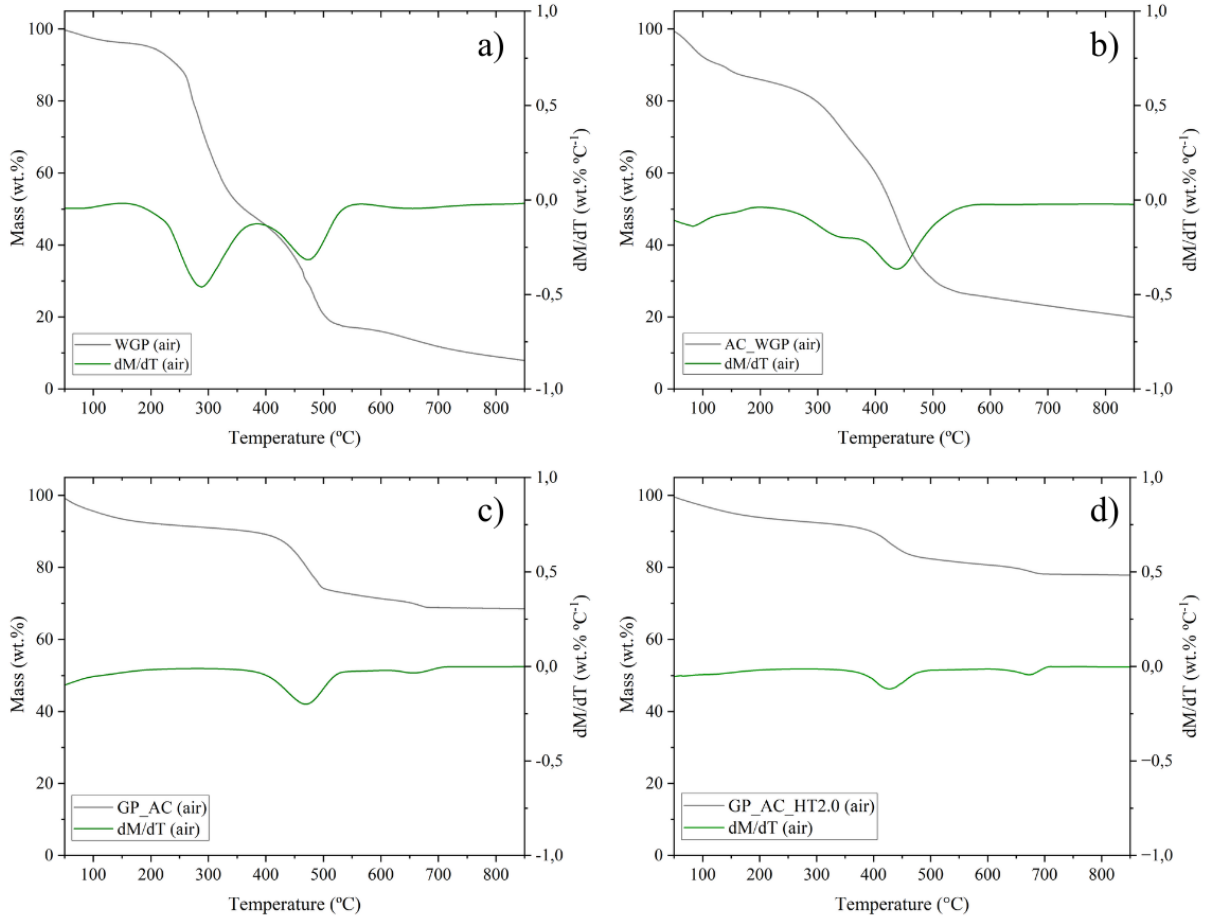

Figure 14: Thermogravimetric analysis in air (TGA and DTG) for: a) WGP, b) AC_ WGP, c) GP_AC, and d) GP_AC_HT2.0.

The GP-containing membranes exhibit good thermal stability, even after the incorporation of AC_WGP. In the temperature range between 200 and 400 °C, the mass loss is related to the decomposition of surface oxygen-containing functional groups and the degradation of less thermally stable organic fractions [41]. The differences observed in the intensity and position of the main DTG peak indicate that the HT promoted structural reorganization, leading to the prior removal of volatile compounds and an increase in the thermal stability of the material.

4.2.5. Elemental and Chemical Composition

5.2.5.1. Elemental Analysis

The CHNS elemental analysis was essential for the chemical characterization of the organic materials, allowing the determination of the mass percentage of carbon, nitrogen, hydrogen, and sulfur. This analysis made it possible to confirm the chemical composition of the precursor biomass (WGP), the produced AC (AC_WGP), and the GP-composite (GP_AC

and GP_AC_HT2.0), shown in Table 8. This analysis ensures the reliability of the obtained materials and highlights possible changes in their elemental structure throughout the conversion process. Where proximate analysis presents M (moisture), V.M. (volatile matter), F.C. (fixed carbon); and ultimate ansalysis presents C (carbon), N (nitrogen), H (hydrogen), S (sulfur), and O (oxygen).

Table 8: Proximate and ultimate analysis of CNHS-elemental analysis for WGP and AC_WGP (dried basis).

Sample	Proximate analysis				Ultimate analysis				
	M (wt.%)	**V.M. (wt.%)**	**F.C. (wt.%)**	**Ashes (wt.%)**	**C (wt.%)**	**N (wt.%)**	**H (wt.%)**	**S (wt.%)**	**O* (wt.%)**
WGP	2.64	73.29	16.68	7.38	49.49	1.64	5.89	0	42.98
AC_WGP	7.71	23.15	50.26	18.88	56.37	2.06	0	0	41.57
GP_AC	3.99	13.77	13.74	68.50	11.95	0.28	0.52	0	87.25
GP_AC_HT2.0	0.71	-	-	77.72	8.01	0.14	0.78	0	13.35

*Oxygen was determined as the difference: O = 100 - C - N - H - S - Ashes.

As expected, carbon is the predominant element in both WGP (49.49 wt.%) and the derived product AC_WGP (56.37 wt.%). In the present study, the WGP used exhibited a carbon content of 49.49 % and an oxygen content of 42.98 %. These values are comparable to those reported by Sardella *et al.* [260], in which the biomass presented a carbon content of 52.22 % and an oxygen content of 31.70 %. Although no studies were found that faithfully reproduce the AC production process employed in this work, a comparable study by Sağlam *et al.* [185], using a similar biomass precursor, reported CNHS values within a similar range with carbon and oxygen contents of 51.63% and 12.63%, respectively. In the present study, the AC exhibited higher carbon and oxygen contents, reaching 56.37% and 41.57%, respectively.

Furthermore, GP_AC exhibited a carbon content of 11.95% and an oxygen content of 87.25%, indicating a predominantly oxidized matrix. In CNHS analysis, oxygen is determined by difference and therefore reflects the non-carbonaceous fraction of the material. In geopolymeric systems, this high oxygen proportion is mainly associated with the inorganic mineral phase, particularly aluminosilicate oxides such as SiO_2 and Al_2O_3, rather than exclusively with oxygen-containing surface functional groups. For the GP_AC_HT2.0 material, a further reduction in carbon content (8.01%) and a relative increase in oxygen content (13.35%) were observed. This decrease in oxygen content is mainly associated with the reorganization of inorganic aluminosilicate phases during HT.

Although no data have been reported in the literature for directly comparable systems, the results indicate that the HT significantly affects the surface chemistry of GP_AC, altering its elemental composition and potentially its physicochemical properties.

4.2.5.2. X-ray fluorescence

The chemical composition of the FA, GP_M, GP_HT2.0, GP_AC, and GP_AC_HT2.0 was determined by XRF and shown in Table 9.

Table 9: Chemical composition of the samples determined by XRF, expressed as oxides and normalized to 100%.

	SiO_2 (wt. %)	**Al_2O_3 (wt. %)**	**CaO (wt. %)**	**K_2O (wt. %)**	**Fe_2O_3 (wt. %)**	**Na_2O (wt. %)**	**MgO (wt. %)**
FA	22.49	8.18	9.72	1.31	14.63	0.42	-
GP_M	43.20	13.98	64.23	7.25	12.14	0.76	1.33
GP_HT2.0	43.78	15.51	64.47	4.48	12.99	1.12	1.29
GP_AC	32.41	12.30	68.14	10.86	8.79	1.60	1.17
GP_AC_HT2.0	36.40	13.31	73.11	6.55	10.45	1.03	1.38

All geopolymeric samples present high CaO contents, varying from 64.23% (GP_M) to 73.11% (GP_AC_HT2.0), confirming a calcium-rich system in which Ca acts as a network modifier [265]. When compared to GP_M, the hydrothermally treated sample GP_HT2.0 shows a slight increase in CaO (64.47%) content, accompanied by a modest increase in SiO_2 (43.78%) and Al_2O_3 (15.51%) contents. This slight rise in SiO_2 and Al_2O_3 suggests enhanced dissolution and reorganization of aluminosilicate species under alkaline conditions, which is consistent with the XRD identification of zeolitic phases (faujasite), confirming structural rearrangement rather than changes in the overall composition

The incorporation of AC in the geopolymeric matrix (GP_AC) results in a higher CaO (68.14%) content and a reduction in SiO_2 (32.41%) when compared to the GP_M. After HT, GP_AC_HT2.0 exhibits a further increase in CaO (73.11%) content and a comparatively lower SiO_2 (36.40%) content. These results indicate that both AC incorporation and HT influence the oxide distribution within the system.

5.3. ADSORPTIVE MODELING

For the adsorption kinetics tests, four experiments were conducted considering the precursor materials (GP_M and GP_AC) and the developed materials (GP_HT2.0 e GP_AC_HT2.0).

5.3.1. Adsorption Kinetics

The adsorption kinetics of CBZ at an initial concentration of 100 mg L^{-1} were evaluated using the kinetic models presented in Table 3. The kinetic parameters obtained

from these models (Table 10) provide insights into the rate-controlling mechanisms and the effect of material modification on CBZ uptake.

Table 10: Parameters of adsorption kinetic models for PFO, PSO and ID.

		Pseudo-first order			Pseudo-second order			Intraparticle diffusion		
	q_{exp} (mg g^{-1})	q_e (mg g^{-1})	K_1 (min^{-1})	r_1^2	q_e (mg g^{-1})	K_2 (min^{-1})	r_2^2	I (mg g^{-1})	K_{id} (mg g^{-1} $min^{-1/2}$)	r_3^2
GP_M	3.7	3.6	0.017	0.97	4.2	0.004	0.95	0.4	0.18	0.84
GP_HT2.0	28.8	27.8	0.051	0.99	29.4	0.003	0.99	11.1	1.02	0.66
GP_AC	33.6	31.5	0.008	0.97	39.7	0.0002	0.98	0.8	1.54	0.99
GP_AC_HT2.0	30.8	28.6	0.047	0.95	30.6	0.0024	0.98	10.1	1.13	0.76

The ID model exhibited lower coefficient of determination (r_2^2 = 0.84 - GP_M; 0.66 - GP_HT2.0; 0.99 - GP_AC; 0.76 - GP_AC_HT2.0) compared to the PSO model (r_2^2 = 0.95 - GP_M; 0.99 - GP_HT2.0; 0.98 - GP_AC; 0.98 - GP_AC_HT2.0), and did not adequately describe the entire adsorption process, indicating that pore diffusion contributes to the overall kinetics but is not the sole rate-limiting step. A similar behavior was reported by Gong *et al*. [262] who attributed this effect to the predominance of surface adsorption in structurally heterogeneous materials.

Overall, the PSO model provided the best fit for all materials showing high coefficient of determination and good agreement between experimental and calculated adsorption capacities. Similar results were reported by Baghdadi *et al*. [266], who observed r_2^2 values higher than 0.99 for CBZ adsorption onto carbon-based materials (magnetic AC), indicating a process controlled by the availability of active sites. Chen et al. [267] applied biochar in the removal of CBZ, and the fitting was 0.99 for the PSO model, while for the PFO model it was 0.88. The Figure 15a and b illustrate the graph describing the fit PFO and PSO model relative to the experimental data evaluated.

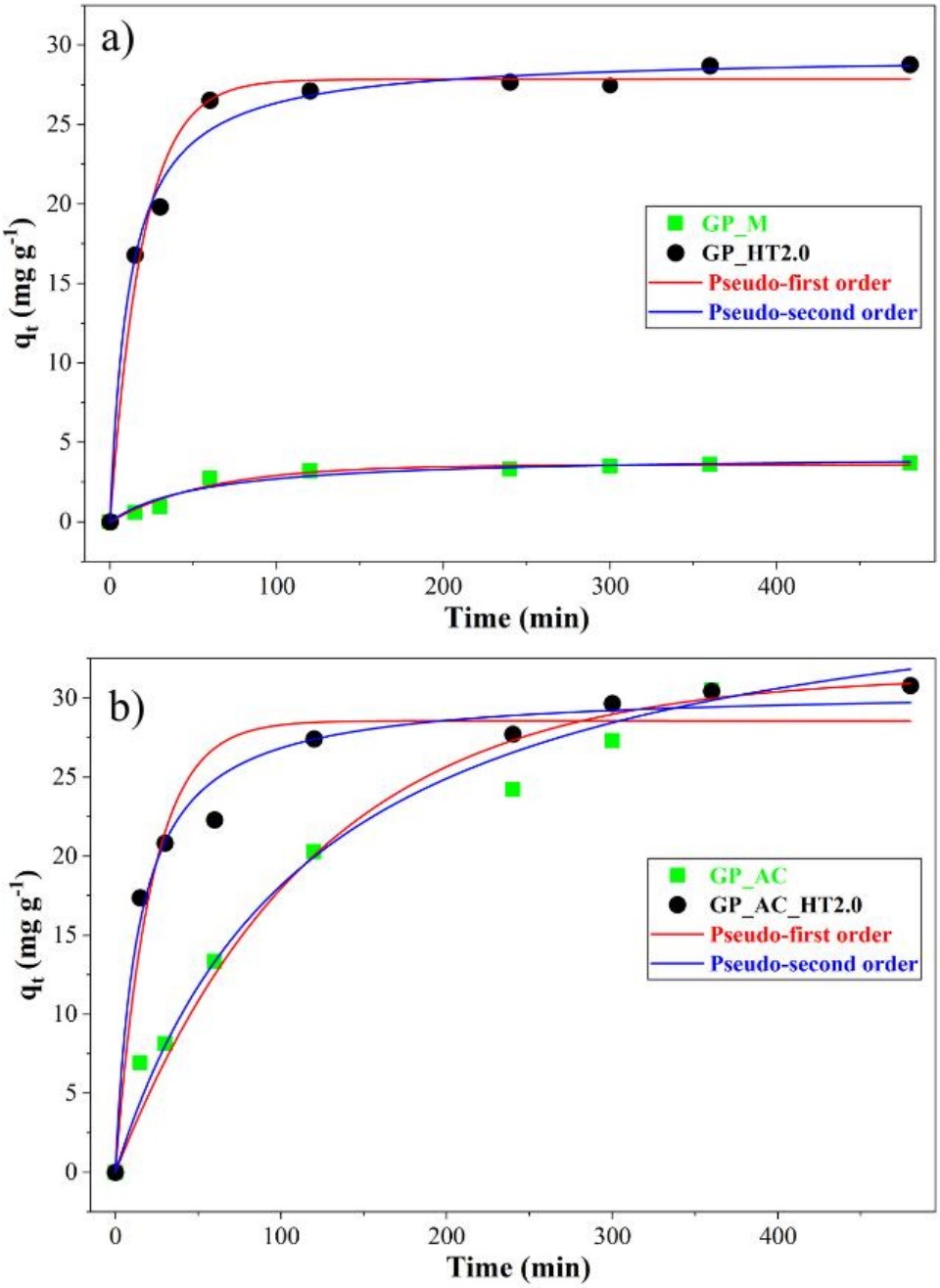

Figure 15: Fitting the kinetic models to the experimental data for CBZ: a) GP_M, and GP_HT2.0, and b) GP_AC, and GP_AC_HT2.0.

The superior fit to the PSO model suggests that the adsorption kinetics are mainly related to the occupation of active sites on the adsorbent surface rather than being exclusively governed by diffusion phenomena. This behavior is consistent with the textural properties obtained from BET analysis (Table 7), which revealed an increase in specific surface area, indicating a greater availability and accessibility of adsorption sites. The experimental adsorption capacity of GP_M (3.7 mg g^{-1}) compared with the zeolite-forming GP, GP_HT2.0 (28.8 mg g^{-1}), shows a significant increase in CBZ adsorption capacity, consistent with the increase in surface area from S_{bet} = 30 to S_{bet} = 181 m^2 g^{-1}, respectively. The low adsorption

capacity exhibited by GP_M can also be explained by its high surface basicity (2387.5 μmol g^{-1}) relative to its acidity (470 μmol g^{-1}), which imparts a strongly hydrophilic character to the material. This favors the adsorption of water molecules and reduces hydrophobic interactions with the aromatic structure of CBZ [268].

Structural information obtained from XRD also supports this interpretation. The formation of zeolitic phases after HT, particularly Na-faujasite (GP_HT2.0, Figure 7), indicates structural reorganization and the generation of specific adsorption sites. GP_AC, with S_{BET} = 48 m^2 g^{-1}, presented an adsorption capacity of q_{exp} = 33.6 mg g^{-1}, whereas GP_AC_HT2.0, despite its higher S_{BET} = 139 m^2 g^{-1}, showed a slightly lower capacity q_{exp} = 30.8 mg g^{-1}. This behavior suggests that the presence of AC and the alkaline HT may partially leach the geopolymeric matrix while increasing surface area. However, this treatment also increased the pHpzc of the material, rising from 9.86 (GP_AC) to 10.64 (GP_AC_HT2.0), which may influence the adsorption process and partially offset the benefit of the higher surface area, resulting in a slight reduction in adsorption capacity.

These properties indicate that surface area alone does not control the adsorption process, and the application of GP_HT2.0 may be advantageous considering that TGA results (Figure 13d) showed that the zeolitic material exhibits good thermal stability at high temperatures. Nevertheless, GP_AC remains particularly attractive due to the intrinsic characteristics of AC, including its S_{BET} = 427 m^2 g^{-1}, elemental analysis (higher carbon - 56.37 wt.% - and oxygen - 41.57 wt.%, contents, and pHpzc determination (9.78), contribute significantly to adsorption performance beyond the effect of surface area alone.

However, these crystalline domains may coexist with amorphous geopolymeric gel, producing a heterogeneous surface with sites of different energies, as discussed by Gong *et al*. [262] for heterogeneous geopolymeric systems. Therefore, the PSO behavior does not necessarily indicate chemisorption but reflects the strong dependence of adsorption on the density, accessibility, and energetic distribution of active sites across the heterogeneous geopolymeric matrix.

5.3.2. Equilibrium Isotherms

Equilibrium is reached when the solute concentration remains constant, indicating that there is no net transfer between the solute adsorbed and desorbed on the sorbent surface. Equilibrium adsorption isotherms represent the relationship between the sorbate concentration in the solid and liquid phases at a constant temperature [269].

The equilibrium isotherms were studied by fitting the Langmuir and Freundlich's models described by Table 4, to the experimental data. Table 11 presents the parameters obtained from the equilibrium fits for GP_M, GP_HT2.0, GP_AC, and GP_AC_HT2.0.

Table 11: Parameters of equilibrium models.

Material	Langmuir			Freundlich		
	q_{max} (mg g^{-1})	K_L (L mg^{-1})	r^2	K_F (L g^{-1})	n_F	r^2
GP_M	7.8	0.032	0.92	0.60	2.00	0.81
GP_HT2.0	10.3	0.022	0.88	0.64	1.90	0.79
GP_AC	10.4	1.399	0.96	4.96	4.19	0.91
GP_AC_HT2.0	23.4	1.689	0.92	12.47	4.59	0.74

Overall, the Langmuir model provided a better fit for all materials, with r^2 values of 0.92 (GP_M), 0.88 (GP_HT2.0), 0.96 (GP_AC), and 0.92 (GP_AC_HT2.0), whereas the Freundlich model yielded r^2 values of 0.81 (GP_M), 0.79 (GP_HT2.0), 0.91 (GP_AC), and 0.74 (GP_AC_HT2.0). Liu *et al.* [270] used magnetic sludge-derived biochar for CBZ adsorption and also reported a better fit to the Langmuir model (r^2 = 0.96), whereas the Freundlich model showed a lower linear coefficient of determination (r^2 = 0.91).

The q_{max} parameter represents the theoretical maximum adsorption capacity, and the best-performing material was GP_AC_HT2.0, with q_{max} = 23.4 mg g^{-1}. This significant increase, resulting from the incorporation of AC and HT compared to GP_M, can be corroborated by the higher specific surface area of the materials (S_{BET} = 139 m^2 g^{-1} for GP_AC_HT2.0 and 30 m^2 g^{-1} for GP_M), which represents an almost fivefold increase in surface area. An increase in the K_L parameter, which is associated with adsorbent–adsorbate affinity, was also observed, following the same trend as the q_{max} values. The hypothesis of Langmuir model is that adsorption is the single layer adsorption, all adsorption sites are the same, and the adsorption particles are completely independent [267]. Ferreira et *al.* synthesized FA-GP and applied it to the removal of gallic acid, obtaining q_{max} values up to 75.8 mg g^{-1}, with both models adequately describing the experimental equilibrium data.

Regarding the Freundlich model, the n_F values were greater than 1 (1.9 – 4.59), indicating favorable adsorption. The highest value was observed for GP_AC_HT2.0 (n_F = 4.59), suggesting greater surface heterogeneity. The enhanced adsorption capacity at low concentrations for the composites is further confirmed by the increase in K_F values, which were 4.96 for GP_AC and 12.47 for GP_AC_HT2.0.

The non-linear fittings of the models are shown in Figure 16a and b and Figure 17. The lowest r^2 value for the Freundlich model was obtained for GP_AC_HT2.0 (r^2 0.74),

indicating that the model does not adequately describe the behavior at higher concentrations (Figure 17), thereby reinforcing the occurrence of site saturation.

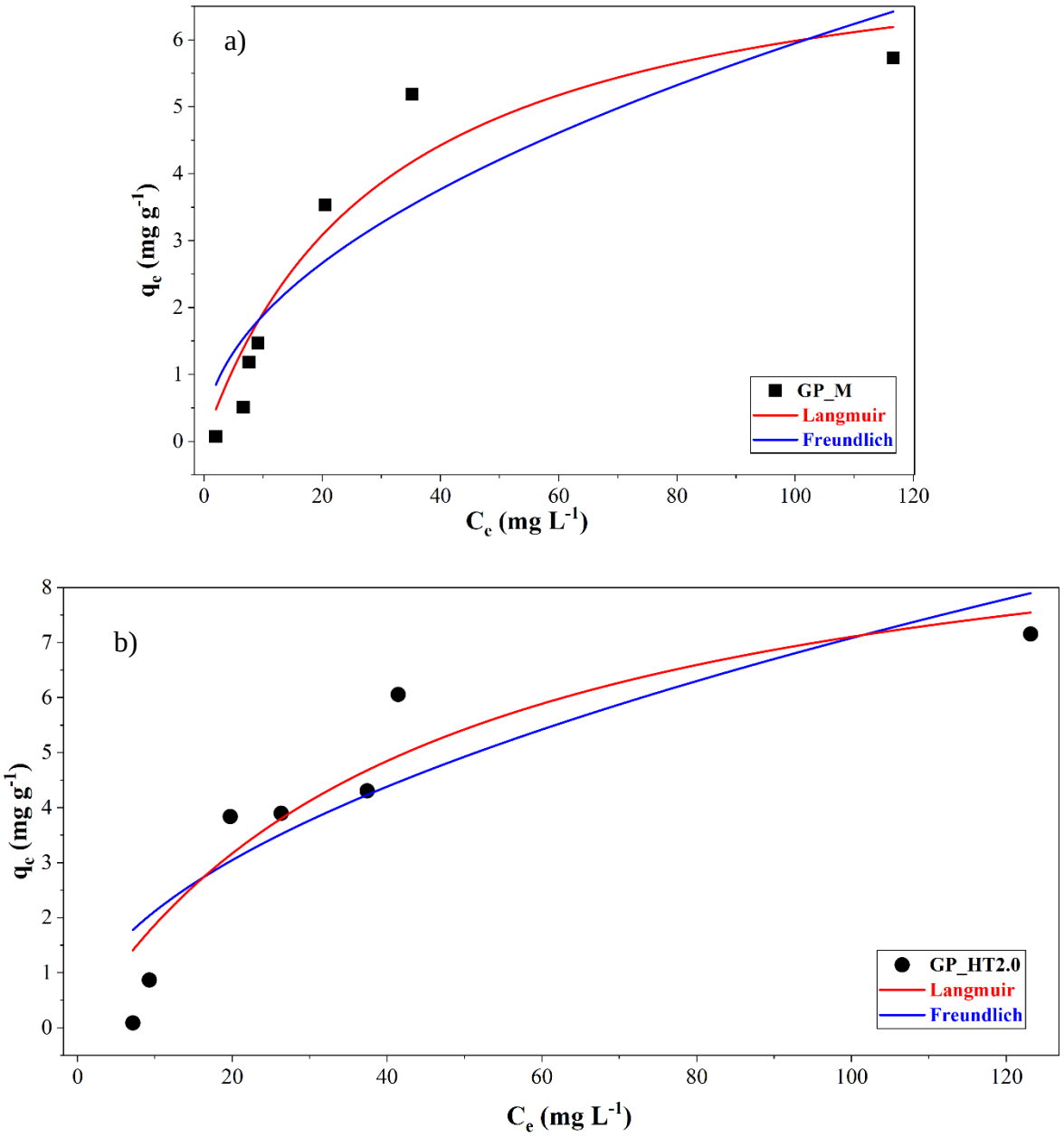

Figure 16: Fitting the equilibrium isotherms to the experimental data for CBZ: a) GP_M, and b) GP_HT2.0.

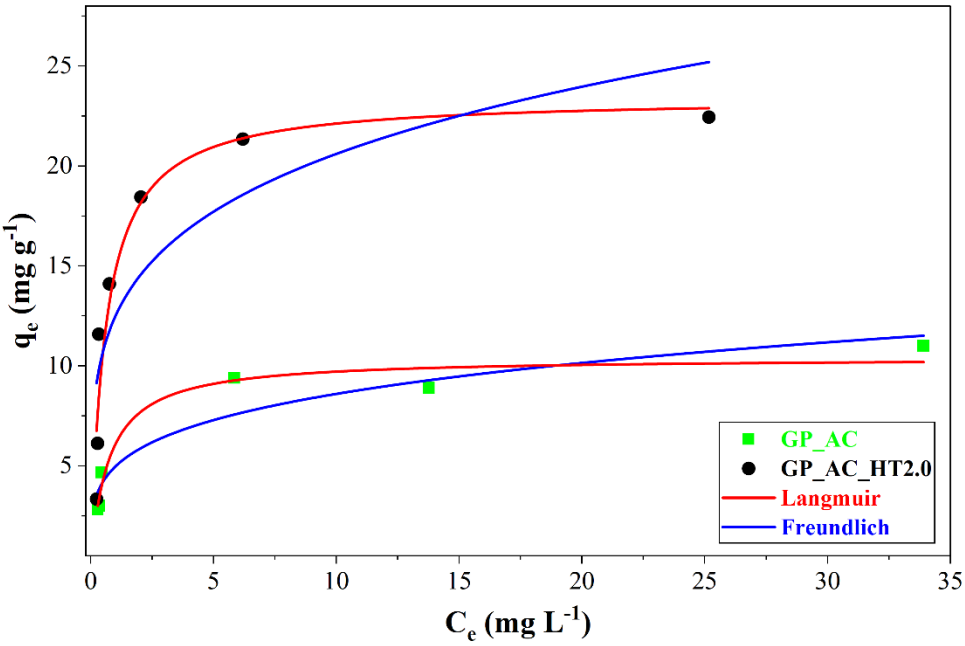

Figure 17: Fitting the equilibrium isotherms to the experimental data for CBZ by GP_AC, and GP_AC_HT2.0.

This saturation can be explained by the high efficiency of the material (q_{max} = 23.4 mg g^{-1}), whereby CBZ is rapidly removed from the liquid phase, significantly reducing the residual concentration and leading the system to equilibrium before the surface is completely saturated. Thus, the observed plateau may reflect a limitation imposed by the drug's solubility (~ 100 mg L^{-1} [271]) rather than the absolute exhaustion of the solid's adsorption capacity.

6. CONCLUSIONS AND FUTURE WORK

In this work, geopolymers matrix were successfully produced from fly ash derived from the incineration of municipal solid waste, yielding a specific surface area of 30 $m^2 g^{-1}$. Activated carbon was also successfully obtained via slow pyrolysis followed by physical activation with CO_2, using residues from the local winery, and exhibited a specific surface area of 427 $m^2 g^{-1}$.

Upon applying hydrothermal treatment and varying the NaOH (1.0, 1.5, 2.0, and 2.5 M) solution, the formation of zeolites (Na-faujasite) was identified by X-ray diffraction. The presence of crystalline phases occurred at NaOH concentrations of 2 and 2.5 M; however, the increase in surface area was not proportional to the concentration of NaOH, resulting in 181 $m^2 g^{-1}$ for GP_HT2.0 and 49 $m^2 g^{-1}$ for GP_HT2.5, indicating the existence of an optimal condition of NaOH concentration for zeolite formation under the employed conditions (70 °C and 24 h).

The incorporation of activated carbon into the geopolymeric matrix increased the specific surface area to 48 $m^2 g^{-1}$ (GP_AC). After hydrothermal treatment using the optimal NaOH concentration (2.0 M) determined for GP_M, the material exhibited a surface area of 139 $m^2 g^{-1}$ (GP_AC_HT2.0). However, no zeolitic phase formation was detected in GP_AC_HT2.0, indicating that the hydrothermal conditions promoted textural development rather than structural reorganization into crystalline zeolites. In contrast, materials containing activated carbon may experience partial structural degradation associated with the decomposition or loss of the carbonaceous phase during thermal treatment.

The kinetic study demonstrated that all materials followed the pseudo-second-order model (r^2 = 0.95 – 0.99), suggesting that the adsorption process was governed by the availability of active sites rather than solely by mass transfer limitations. The adsorption capacity increased with increasing surface area, rising from 3.7 mg g^{-1} (GP_M) to 28.8 mg g^{-1} (GP_HT2.0) for the no carbon-composite geopolymeric materials. In contrast, the activated carbon–incorporated materials did not follow the same trend, exhibiting capacities of 33.6 mg g^{-1} (GP_AC) and 30.8 mg g^{-1} (GP_AC_HT2.0). The equilibrium adsorption study further revealed that the Langmuir model provided the best fit to the experimental data (r^2 = 0.88 – 0.96), indicating favorable adsorption and a strong affinity between the adsorbent and carbamazepine.

Overall, this work contributes to filling gaps identified in the current state of the art regarding the application of geopolymeric materials for the removal of emerging contaminants, such as carbamazepine. The study highlights the innovation of converting

geopolymers into optimized zeolites through variation of NaOH concentration during hydrothermal treatment, as well as the analysis of the synergistic effects of incorporating activated carbon into the geopolymeric matrix, approaches that remain scarcely explored in the scientific literature.

6.1 FUTURE WORK

Although the results obtained in this study demonstrate the potential of the developed carbon-composite zeolitic geopolymer-based materials for adsorption applications, further investigations are required to fully assess their applicability under realistic operating conditions. Future research should focus on:

- Explore the application of the materials for the removal of others emerging contaminants such as sulfamethoxazole, caffeine, ibuprofen, among others;
- Apply the materials in membrane form in continuous systems to evaluate breakthrough curves;
- Investigate material regeneration and assess their performance over multiple adsorption–desorption cycles;
- Scale up the results to evaluate the life cycle of the developed materials.

7. REFERENCES

[1] P. Woodhouse, M. Muller, Water Governance—An Historical Perspective on Current Debates, World Dev. 92 (2017) 225–241. https://doi.org/10.1016/j.worlddev.2016.11.014.

[2] Y. Su, W. Gao, D. Guan, T. Zuo, Achieving Urban Water Security: a Review of Water Management Approach from Technology Perspective, Water Resources Management 34 (2020) 4163–4179. https://doi.org/10.1007/s11269-020-02663-9.

[3] N. Shehata, D. Egirani, A.G. Olabi, A. Inayat, M.A. Abdelkareem, K.-J. Chae, E.T. Sayed, Membrane-based water and wastewater treatment technologies: Issues, current trends, challenges, and role in achieving sustainable development goals, and circular economy, Chemosphere 320 (2023) 137993. https://doi.org/10.1016/j.chemosphere.2023.137993.

[4] A.M. Shitole, S. Tiwari, H. Sinhmar, E. Bellos, Emerging trends in sustainable adsorption systems: Materials, optimization, and applications in carbon capture, cooling, storage, and atmospheric water harvesting, Renewable and Sustainable Energy Reviews 221 (2025) 115899. https://doi.org/10.1016/j.rser.2025.115899.

[5] X. Li, L. Li, J. Jiang, W. Mei, Z. Wang, Q. Gao, H. Zhou, L. Wei, Q. Zhao, Seeking breakthroughs in advanced oxidation processes for waste activated sludge dewatering: A critical review of developments, bibliometrics and sustainable solutions, Chinese Chemical Letters (2025) 110847. https://doi.org/10.1016/j.cclet.2025.110847.

[6] Á. de J. Ruíz-Baltazar, Advancements in nanoparticle-modified zeolites for sustainable water treatment: An interdisciplinary review, Science of The Total Environment 946 (2024) 174373. https://doi.org/10.1016/j.scitotenv.2024.174373.

[7] H. Khan, M. Usama, M.I. Khan, F. Wahab, I. Ahmad, A. Hamid, S. Hussain, A. Maqbool, From pollutant to purifier: Leveraging plastic waste-derived activated carbon for sustainable water remediation solutions, J. Environ. Manage. 375 (2025) 124202. https://doi.org/10.1016/j.jenvman.2025.124202.

[8] F. Hosseinzadeh, H. Hashemi, H. Sarpoolaky, Sustainable ceramic membrane for water and wastewater treatment: A comprehensive review of environmental, social, and economic aspects, Desalination 615 (2025) 119231. https://doi.org/10.1016/j.desal.2025.119231.

[9] B. Schubert, P. Heininger, M. Keller, E. Claus, M. Ricking, Monitoring of contaminants in suspended particulate matter as an alternative to sediments, TrAC

Trends in Analytical Chemistry 36 (2012) 58–70. https://doi.org/10.1016/j.trac.2012.04.003.

[10] Z. Liu, J. Fu, A. Liu, W.-X. Zhang, Influence of natural organic matter on nanoscale zero-valent iron for contaminants removal in water: A critical review, Chemical Engineering Journal 488 (2024) 150836. https://doi.org/10.1016/j.cej.2024.150836.

[11] O.R. Umeh, E.M. Ibo, C.I. Eke, H.C. Afeku-Amenyo, D.U. Ophori, A review of the sidelined pollutant: Reviving the fight against heavy metal contamination in an era of emerging contaminants, Toxicol. Rep. 15 (2025) 102073. https://doi.org/10.1016/j.toxrep.2025.102073.

[12] S. Li, B. Yuan, M. Zhang, J. Du, X. Hu, X. Ning, Z. Duan, Y. Wen, A review of multi-contaminant risks in textile dyeing sludge pyrolysis: Transformation mechanisms and mitigation strategies, J. Hazard. Mater. 494 (2025) 138632. https://doi.org/10.1016/j.jhazmat.2025.138632.

[13] M.N. Goukeh, D. Ssekimpi, B.K. Asefaw, Z. Zhang, Occurrence of per- and polyfluorinated substances, microplastics, pharmaceuticals and personal care products as emerging contaminants in landfill leachate: A review, Total Environment Engineering 3 (2025) 100019. https://doi.org/10.1016/j.teengi.2025.100019.

[14] J.O. Osuoha, B.O. Anyanwu, C. Ejileugha, Pharmaceuticals and personal care products as emerging contaminants: Need for combined treatment strategy, Journal of Hazardous Materials Advances 9 (2023) 100206. https://doi.org/10.1016/j.hazadv.2022.100206.

[15] E.M. Ijanu, M.A. Kamaruddin, F.A. Norashiddin, Coffee processing wastewater treatment: a critical review on current treatment technologies with a proposed alternative, Appl. Water Sci. 10 (2020) 11. https://doi.org/10.1007/s13201-019-1091-9.

[16] Y. Liu, Y. Mo, X. Zhao, S. Wang, L. Wang, H. Guo, A mini review on treatment alternatives removing organic pollutants for reverse osmosis concentrate from industrial wastewater sources, J. Environ. Chem. Eng. 13 (2025) 116339. https://doi.org/10.1016/j.jece.2025.116339.

[17] M. Ahmaruzzaman, V.K. Gupta, Rice Husk and Its Ash as Low-Cost Adsorbents in Water and Wastewater Treatment, Ind. Eng. Chem. Res. 50 (2011) 13589–13613. https://doi.org/10.1021/ie201477c.

[18] M.A.H. Bhuyan, R. Busquets, L.C. Campos, T. Luukkonen, Separation of microplastics from water using superhydrophobic silane-coupling-agent-modified geopolymer foam, Sep. Purif. Technol. 339 (2024) 126709. https://doi.org/10.1016/j.seppur.2024.126709.

[19] M.A.A.M. Hamzah, N. Yusof, W.N.W. Salleh, F. Aziz, J. Jaafar, A.F. Ismail, Reutilization of ash waste for development of enhanced membrane technology, J. Environ. Chem. Eng. 12 (2024) 112629. https://doi.org/10.1016/j.jece.2024.112629.

[20] M. Sadiq, A. Naveed, M. Arif, S. Hassan, S. Afridi, M. Asif, S. Sultana, N. Amin, M. Younas, M.N. Khan, H. Jiang, S. Gul, Geopolymerization: a promising technique for membrane synthesis, Mater. Res. Express 8 (2021) 112002. https://doi.org/10.1088/2053-1591/ac30e4.

[21] A.M. Elgarahy, A. Maged, M.G. Eloffy, M. Zahran, S. Kharbish, K.Z. Elwakeel, A. Bhatnagar, Geopolymers as sustainable eco-friendly materials: Classification, synthesis routes, and applications in wastewater treatment, Sep. Purif. Technol. 324 (2023) 124631. https://doi.org/10.1016/j.seppur.2023.124631.

[22] H.R. Khalid, N.K. Lee, S.M. Park, N. Abbas, H.K. Lee, Synthesis of geopolymer-supported zeolites via robust one-step method and their adsorption potential, J. Hazard. Mater. 353 (2018) 522–533. https://doi.org/10.1016/j.jhazmat.2018.04.049.

[23] Y. Duan, P. Cong, Research on the durability of geopolymers based on bibliometrics, Journal of Traffic and Transportation Engineering (English Edition) (2025). https://doi.org/10.1016/j.jtte.2025.02.003.

[24] I. Giannopoulou, P.M. Robert, K.-M. Sakkas, M.F. Petrou, D. Nicolaides, High temperature performance of geopolymers based on construction and demolition waste, Journal of Building Engineering 72 (2023) 106575. https://doi.org/10.1016/j.jobe.2023.106575.

[25] I. Perná, M. Novotná, T. Hanzlíček, J. Rafl, M. Nováková, The application of geopolymers in the renovation of the historical ceramic tiles in the pilgrimage church of St. John of Nepomuk (Czech Republic), Case Studies in Construction Materials 22 (2025) e04161. https://doi.org/10.1016/j.cscm.2024.e04161.

[26] Md.H. Islam, D. Law, Y. Patrisia, C. Gunasekara, Blended brown coal and Class F fly ash based geopolymer, Case Studies in Construction Materials 23 (2025) e05036. https://doi.org/10.1016/j.cscm.2025.e05036.

[27] X. Cai, J. Yin, X. Xu, D. Zhang, Y. Wang, Rheological, mechanical, and microstructural properties of engineered geopolymer composite (EGC) made with ground granulated blast furnace slag (GGBFS) and fly ash, Journal of Materials Research and Technology 35 (2025) 1996–2010. https://doi.org/10.1016/j.jmrt.2025.01.166.

[28] L. Shao, M. Yi, H. Wei, R. Ji, L. He, Y. Jiang, K. Wang, Synthesis of sodium silicate-activated metakaolin geopolymer microspheres (SS@MGMs) for efficient F− removal

from acidic wastewater, Appl. Clay Sci. 276 (2025) 107958. https://doi.org/10.1016/j.clay.2025.107958.

[29] H. Zeng, J. Liang, S. Li, S. Han, Z. Li, J. Zhang, D. Li, Acid-resistant iron sludge-based fly ash geopolymer foam for efficient arsenic removal with pH self-regulation, Environ. Res. 285 (2025) 122432. https://doi.org/10.1016/j.envres.2025.122432.

[30] M. Zareechian, H. Siad, M. Lachemi, M. Sahmaran, Advancements in cleaner production of one-part geopolymers: A comprehensive review of mechanical properties, durability, and microstructure, Constr. Build. Mater. 409 (2023) 133876. https://doi.org/10.1016/j.conbuildmat.2023.133876.

[31] L.-Y. Xu, J.-C. Lao, L.-P. Qian, M. Khan, T.-Y. Xie, B.-T. Huang, Low-carbon high-strength engineered geopolymer composites (HS-EGC) with full-volume fly ash precursor: Role of silica modulus, Journal of CO2 Utilization 88 (2024) 102948. https://doi.org/10.1016/j.jcou.2024.102948.

[32] J. Liu, J.-H. Doh, D.E.L. Ong, S. Wang, Y. Yang, H.L. Dinh, G. Zi, Correlation between dissolubilities of Si, Al, and Fe from aluminosilicate precursor and strength of fly ash-based geopolymer, Constr. Build. Mater. 393 (2023) 132107. https://doi.org/10.1016/j.conbuildmat.2023.132107.

[33] W. Chen, H. Zhu, Y. Li, F. Liu, Q. Li, Y. Mao, A. Yang, Geopolymers prepared from industrial solid waste: Comprehensive properties and application prospects, Environ. Res. 278 (2025) 121518. https://doi.org/10.1016/j.envres.2025.121518.

[34] H. Lin, J. Zhang, R. Wang, W. Zhang, J. Ye, Adsorption properties and mechanisms of geopolymers and their composites in different water environments: A comprehensive review, Journal of Water Process Engineering 62 (2024) 105393. https://doi.org/10.1016/j.jwpe.2024.105393.

[35] H.X. Su, C.J. Li, Y.J. Zhang, Facile synthesis of geopolymer-based hierarchical porous materials for efficient adsorption-photocatalysis of dye wastewater, J. Environ. Chem. Eng. 12 (2024) 114809. https://doi.org/10.1016/j.jece.2024.114809.

[36] A.M.A. Ahmed, I.M. Mantawy, Additive construction of low embodied carbon concrete: Geopolymer concrete, Journal of Building Engineering 111 (2025) 112984. https://doi.org/10.1016/j.jobe.2025.112984.

[37] J. Carvalheiras, R.M. Novais, J.A. Labrincha, Metakaolin/red mud-derived geopolymer monoliths: Novel bulk-type sorbents for lead removal from wastewaters, Appl. Clay Sci. 232 (2023) 106770. https://doi.org/10.1016/j.clay.2022.106770.

[38] F. Matalkah, M.B. Hani, I. Al-Momani, Synthesis of porous volcanic tuff-based geopolymer for nickel and cobalt removal, Results Chem. 15 (2025) 102179. https://doi.org/10.1016/j.rechem.2025.102179.

[39] S. Yan, M. Zhang, D. Fu, C. He, S. Wang, X. Zhai, Synthesis of red mud/metakaolin based geopolymer for adsorption of methylene blue and tetracycline hydrochloride from water, Colloids Surf. A Physicochem. Eng. Asp. 722 (2025) 137155. https://doi.org/10.1016/j.colsurfa.2025.137155.

[40] A. Marubini, R. Mhlarhi, J.N. Edokpayi, Adsorptive Removal of Crystal Violet Dye from Aqueous Solution Using a Vermiculite-Based Geopolymer, Sci. Afr. 28 (2025) e02701. https://doi.org/10.1016/j.sciaf.2025.e02701.

[41] A.P. Ferreira, A.P. Baldo, A.S. Silva, A.P.S. Natal, A.J.B. Bezerra, J.L. Diaz de Tuesta, P. Marin, J.A. Peres, H.T. Gomes, Enhancing single and multi-component adsorption efficiency of pharmaceutical emerging contaminants using bio waste-derived carbon materials and geopolymers, Journal of Water Process Engineering 75 (2025) 107914. https://doi.org/10.1016/j.jwpe.2025.107914.

[42] Y. Dong, J. Liu, Adsorption and solidification / stabilization of phenol by slag-based geopolymer-biochar composite, Desalination Water Treat. 323 (2025) 101327. https://doi.org/10.1016/j.dwt.2025.101327.

[43] H.-Z. Jin, C.-X. Qiu, Y.-S. Li, B. Liu, J.-Y. Liu, Q. Chen, X.-F. Lu, C.-X. Li, Q.-K. Wang, Structural and functional design of geopolymer adsorbents : a review, Tungsten (2023). https://doi.org/10.1007/s42864-023-00213-5.

[44] S.A. Rasaki, Z. Bingxue, R. Guarecuco, T. Thomas, Y. Minghui, Geopolymer for use in heavy metals adsorption, and advanced oxidative processes: A critical review, J. Clean. Prod. 213 (2019) 42–58. https://doi.org/10.1016/j.jclepro.2018.12.145.

[45] D.G. Della Rocca, R.M. Peralta, R.A. Peralta, E. Rodríguez-Castellón, R. de Fatima Peralta Muniz Moreira, Adding value to aluminosilicate solid wastes to produce adsorbents, catalysts and filtration membranes for water and wastewater treatment, J. Mater. Sci. 56 (2021) 1039–1063. https://doi.org/10.1007/s10853-020-05276-0.

[46] G. Venkatesan, U.J. Alengaram, S. Ibrahim, M.S.I. Ibrahim, Effect of Fly Ash characteristics, sodium-based alkaline activators, and process variables on the compressive strength of siliceous Fly Ash geopolymers with microstructural properties: A comprehensive review, Constr. Build. Mater. 437 (2024) 136808. https://doi.org/10.1016/j.conbuildmat.2024.136808.

[47] D.M. Degefu, Z. Liao, U. Berardi, H. Doan, Salient parameters affecting the performance of foamed geopolymers as sustainable insulating materials, Constr. Build. Mater. 313 (2021) 125400. https://doi.org/10.1016/j.conbuildmat.2021.125400.

[48] C. Iong, J.-B.M. Dassekpo, F.N. Gyakari, X. Zha, L. Li, Y. Li, J. Wang, F.-L. Zhang, Effects of thermal conditioning and alkali molars on the properties changes of mesoporous fly ash geopolymers, Constr. Build. Mater. 471 (2025) 140676. https://doi.org/10.1016/j.conbuildmat.2025.140676.

[49] A. Naveed, F. Saeed, M. Khraisheh, M. Al Bakri, Noor-Ul-Amin, S. Gul, Porosity control of self-supported geopolymeric membrane through hydrogen peroxide and starch additives, Desalination Water Treat. 152 (2019) 11–15. https://doi.org/10.5004/dwt.2019.23895.

[50] Y. Song, R. Zhang, Y. Wang, X. Weichen, L. Fan, Permeability property study on slag-based geopolymers early-curing in corrosive environments: Effects of full pore distribution, pore throat size, and connectivity, Constr. Build. Mater. 458 (2025) 139711. https://doi.org/10.1016/j.conbuildmat.2024.139711.

[51] H. Jin, J. Liu, Y. Guo, K. Hong, M. Zhu, C. Li, Q. Wang, Nanoscale intergrowth of adsorption-photocatalysis active sites of geopolymer/Ag9(SiO4)2NO3 for efficient synergistic capture and photocatalytic degradation of tetracycline, J. Environ. Chem. Eng. 13 (2025) 116319. https://doi.org/10.1016/j.jece.2025.116319.

[52] C. Manickam, A. Chuwongwittaya, M. Jaideekard, M. Thala, C. Kumprom, N. Setthaya, K. Juengsuwattananon, P. Wattanachai, M. Murayama, P. Chindaprasirt, A. Siyasukh, K. Pimraksa, Geopolymer/zeolite-P materials prepared from high-CaO fly ash, biomass ash, and metakaolin using geopolymerization with a hydrothermal process for environmental clean-up, Constr. Build. Mater. 456 (2024) 139255. https://doi.org/10.1016/j.conbuildmat.2024.139255.

[53] P.Y. He, Y.J. Zhang, H. Chen, Z.C. Han, L.C. Liu, Low-cost and facile synthesis of geopolymer-zeolite composite membrane for chromium(VI) separation from aqueous solution, J. Hazard. Mater. 392 (2020) 122359. https://doi.org/10.1016/j.jhazmat.2020.122359.

[54] A. De Rossi, L. Simão, M.J. Ribeiro, R.M. Novais, J.A. Labrincha, D. Hotza, R.F.P.M. Moreira, In-situ synthesis of zeolites by geopolymerization of biomass fly ash and metakaolin, Mater. Lett. 236 (2019) 644–648. https://doi.org/10.1016/j.matlet.2018.11.016.

[55] A. Nikolov, I. Rostovsky, H. Nugteren, Geopolymer materials based on natural zeolite, Case Studies in Construction Materials 6 (2017) 198–205. https://doi.org/10.1016/j.cscm.2017.03.001.

[56] Q. Wan, F. Rao, S. Song, R.E. García, R.M. Estrella, C.L. Patiño, Y. Zhang, Geopolymerization reaction, microstructure and simulation of metakaolin-based geopolymers at extended Si/Al ratios, Cem. Concr. Compos. 79 (2017) 45–52. https://doi.org/10.1016/j.cemconcomp.2017.01.014.

[57] P. Wang, X. Wei, H. Chen, F. Xie, X. Shen, P. Zheng, F. Yan, W. Bai, Z. Zhang, Microstructural evolution and immobilization mechanisms of geopolymers incorporating cationic and oxyanionic heavy metals (Pb2+, Zn2+, Cr2O72−, and AsO2−), J. Environ. Chem. Eng. 13 (2025) 117784. https://doi.org/10.1016/j.jece.2025.117784.

[58] S.R. Satpathy, S. Bhattacharyya, Adsorptive dye removal using clay-based geopolymer: Effect of activation conditions on geopolymerization and removal efficiency, Materials Science and Engineering: B 319 (2025) 118348. https://doi.org/10.1016/j.mseb.2025.118348.

[59] Z. Ji, G. Zhang, R. Liu, J. Qu, H. Liu, Potential applications of solid waste-based geopolymer materials: In wastewater treatment and greenhouse gas emission reduction, J. Clean. Prod. 443 (2024) 141144. https://doi.org/10.1016/j.jclepro.2024.141144.

[60] M. Starkl, N. Brunner, S. Das, A. Singh, Sustainability Assessment for Wastewater Treatment Systems in Developing Countries, Water (Basel). 14 (2022) 241. https://doi.org/10.3390/w14020241.

[61] T. Fazal, A. Razzaq, F. Javed, A. Hafeez, N. Rashid, U.S. Amjad, M.S. Ur Rehman, A. Faisal, F. Rehman, Integrating adsorption and photocatalysis: A cost effective strategy for textile wastewater treatment using hybrid biochar-TiO2 composite, J. Hazard. Mater. 390 (2020) 121623. https://doi.org/10.1016/j.jhazmat.2019.121623.

[62] H. Muzioreva, T. Gumbo, N. Kavishe, T. Moyo, I. Musonda, Decentralized wastewater system practices in developing countries: A systematic review, Util. Policy 79 (2022) 101442. https://doi.org/10.1016/j.jup.2022.101442.

[63] A. Hafeez, Z. Shamair, N. Shezad, F. Javed, T. Fazal, S. ur Rehman, A.A. Bazmi, F. Rehman, Solar powered decentralized water systems: A cleaner solution of the industrial wastewater treatment and clean drinking water supply challenges, J. Clean. Prod. 289 (2021) 125717. https://doi.org/10.1016/j.jclepro.2020.125717.

[64] M. Mishra, S. Desul, C.A.G. Santos, S.K. Mishra, A.H.M. Kamal, S. Goswami, A.M. Kalumba, R. Biswal, R.M. da Silva, C.A.C. dos Santos, K. Baral, A bibliometric

analysis of sustainable development goals (SDGs): a review of progress, challenges, and opportunities, Environ. Dev. Sustain. 26 (2023) 11101–11143. https://doi.org/10.1007/s10668-023-03225-w.

[65] K. Obaideen, N. Shehata, E.T. Sayed, M.A. Abdelkareem, M.S. Mahmoud, A.G. Olabi, The role of wastewater treatment in achieving sustainable development goals (SDGs) and sustainability guideline, Energy Nexus 7 (2022) 100112. https://doi.org/10.1016/j.nexus.2022.100112.

[66] A.S. Kazora, K.A. Mourad, Assessing the Sustainability of Decentralized Wastewater Treatment Systems in Rwanda, Sustainability 10 (2018) 4617. https://doi.org/10.3390/su10124617.

[67] W.A.H. Altowayti, S. Shahir, N. Othman, T.A.E. Eisa, W.M.S. Yafooz, A. Al-Dhaqm, C.Y. Soon, I.B. Yahya, N.A.N. binti Che Rahim, M. Abaker, A. Ali, The Role of Conventional Methods and Artificial Intelligence in the Wastewater Treatment: A Comprehensive Review, Processes 10 (2022) 1832. https://doi.org/10.3390/pr10091832.

[68] R. Singh, J. Ryu, W. Hyoung Lee, J.-H. Kang, S. Park, K. Kim, Wastewater-borne viruses and bacteria, surveillance and biosensors at the interface of academia and field deployment, Crit. Rev. Biotechnol. 45 (2025) 413–433. https://doi.org/10.1080/07388551.2024.2354709.

[69] A.B. Rios-Miguel, T.J.H.M. van Bergen, C. Zillien, A.M.J. Ragas, R. van Zelm, M.S.M. Jetten, A.J. Hendriks, C.U. Welte, Predicting and improving the microbial removal of organic micropollutants during wastewater treatment: A review, Chemosphere 333 (2023) 138908. https://doi.org/10.1016/j.chemosphere.2023.138908.

[70] M.A. Díaz, D. Blanco, R. Chandia-Jaure, D. Lobos Calquin, A. Decinti, P. Naranjo, M.B. Almendro-Candel, Excess of Nutrients in Prefabricated or Compact Wastewater Treatment Plants: Review, Solution Alternative, and Modeling for Verification, Water (Basel). 16 (2024) 1354. https://doi.org/10.3390/w16101354.

[71] European Environment Agency, Country profiles on urban waste water treatment: Portugal, 2024. https://water.europa.eu/freshwater/countries/uwwt/portugal (accessed July 14, 2025).

[72] J. Almeida, A. Monahan, J. Dionísio, F. Delgado, C. Magro, Sustainability assessment of wastewater reuse in a Portuguese military airbase, Science of The Total Environment 851 (2022) 158329. https://doi.org/10.1016/j.scitotenv.2022.158329.

[73] European Commission, Urban wastewater, (2024). https://environment.ec.europa.eu/topics/water/urban-wastewater_en (accessed June 1, 2025).

[74] European Environment Agency, Waterbase - UWWTD: Urban Waste Water Treatment Directive – reported data, (2024). https://www.eea.europa.eu/en/datahub/datahubitem-view/6244937d-1c2c-47f5-bdf1-33ca01ff1715 (accessed June 1, 2025).

[75] European Commission, Council Directive of 21 May 1991 concerning urban waste water treatment (91/271/EEC), Belgium, 1991. https://eur-lex.europa.eu/legal-content/PT/TXT/?uri=CELEX:32024L3019 (accessed June 20, 2025).

[76] Official Gazette of the Portuguese Republic, Decree-Law No 11/2023 of 10 February, Portugal, 2025. https://diariodarepublica.pt/dr/detalhe/decreto-lei/11-2023-207272800?utm_source=chatgpt.com (accessed June 20, 2025).

[77] European Union, Directive (EU) 2024/3019 of the European Parliament and of the Council of 27 November 2024 concerning urban wastewater treatment, 2024. https://eur-lex.europa.eu/eli/dir/2024/3019/oj (accessed June 1, 2025).

[78] F. Florides, M. Giannakoudi, G. Ioannou, D. Lazaridou, E. Lamprinidou, N. Loukoutos, M. Spyridou, E. Tosounidis, M. Xanthopoulou, I.A. Katsoyiannis, Water Reuse: A Comprehensive Review, Environments 11 (2024) 81. https://doi.org/10.3390/environments11040081.

[79] N.K. Khanzada, R.A. Al-Juboori, M. Khatri, F.E. Ahmed, Y. Ibrahim, N. Hilal, Sustainability in Membrane Technology: Membrane Recycling and Fabrication Using Recycled Waste, Membranes (Basel). 14 (2024) 52. https://doi.org/10.3390/membranes14020052.

[80] A.S. Codina, E.C. Lumbaque, J. Radjenovic, Electrochemical removal of contaminants of emerging concern with manganese oxide-functionalized graphene sponge electrode, Chemical Engineering Journal 508 (2025) 160940. https://doi.org/10.1016/j.cej.2025.160940.

[81] J.S. Sudarsan, K. Dogra, R. Kumar, N.P. Raval, M. Leifels, S. Mukherjee, M.H. Trivedi, M.S. Jain, J. Zang, D. Barceló, J. Mahlknecht, M. Kumar, Tricks and tracks of prevalence, occurrences, treatment technologies, and challenges of mixtures of emerging contaminants in the environment: With special emphasis on microplastic, J. Contam. Hydrol. 265 (2024) 104389. https://doi.org/10.1016/j.jconhyd.2024.104389.

[82] S. Khan, Mu. Naushad, M. Govarthanan, J. Iqbal, S.M. Alfadul, Emerging contaminants of high concern for the environment: Current trends and future research, Environ. Res. 207 (2022) 112609. https://doi.org/10.1016/j.envres.2021.112609.

[83] C. Das, Prevalence and Impact of Emerging Chemical Contaminants in the Life Style Products on Human Health, Oriental Journal of Physical Sciences 9 (2024) 07–18. https://doi.org/10.13005/OJPS09.01.03.

[84] N. Morin-Crini, E. Lichtfouse, G. Liu, V. Balaram, A.R.L. Ribeiro, Z. Lu, F. Stock, E. Carmona, M.R. Teixeira, L.A. Picos-Corrales, J.C. Moreno-Piraján, L. Giraldo, C. Li, A. Pandey, D. Hocquet, G. Torri, G. Crini, Worldwide cases of water pollution by emerging contaminants: a review, Environ. Chem. Lett. 20 (2022) 2311–2338. https://doi.org/10.1007/s10311-022-01447-4.

[85] A.K. Priya, S. Antony, G.M.S. Kumar, S. Sivamoorthi, S. Vineesh, Anthropogenic impacts on the contamination in the coastal region: A review, Mater. Today Proc. 37 (2021) 2236–2238. https://doi.org/10.1016/j.matpr.2020.07.681.

[86] M. Li, S. Huang, X. Yu, W. Zhao, S. Lyu, Q. Sui, Discharge of pharmaceuticals from a municipal solid waste transfer station: Overlooked influence on the contamination of pharmaceuticals in surface waters, Science of The Total Environment 839 (2022) 156317. https://doi.org/10.1016/j.scitotenv.2022.156317.

[87] W. Calzadilla, L.C. Espinoza, M.S. Diaz-Cruz, A. Sunyer, M. Aranda, C. Peña-Farfal, R. Salazar, Simultaneous degradation of 30 pharmaceuticals by anodic oxidation: Main intermediaries and by-products, Chemosphere 269 (2021) 128753. https://doi.org/10.1016/j.chemosphere.2020.128753.

[88] A.M. Botero-Coy, D. Martínez-Pachón, C. Boix, R.J. Rincón, N. Castillo, L.P. Arias-Marín, L. Manrique-Losada, R. Torres-Palma, A. Moncayo-Lasso, F. Hernández, 'An investigation into the occurrence and removal of pharmaceuticals in Colombian wastewater,' Science of The Total Environment 642 (2018) 842–853. https://doi.org/10.1016/j.scitotenv.2018.06.088.

[89] Y. Chen, M. Lin, D. Zhuang, Wastewater treatment and emerging contaminants: Bibliometric analysis, Chemosphere 297 (2022) 133932. https://doi.org/10.1016/j.chemosphere.2022.133932.

[90] B.A. Mohamed, H. Hamid, C. V. Montoya-Bautista, L.Y. Li, Circular economy in wastewater treatment plants: Treatment of contaminants of emerging concerns (CECs) in effluent using sludge-based activated carbon, J. Clean. Prod. 389 (2023) 136095. https://doi.org/10.1016/j.jclepro.2023.136095.

[91] T.K. Kasonga, M.A.A. Coetzee, I. Kamika, V.M. Ngole-Jeme, M.N. Benteke Momba, Endocrine-disruptive chemicals as contaminants of emerging concern in wastewater and surface water: A review, J. Environ. Manage. 277 (2021) 111485. https://doi.org/10.1016/j.jenvman.2020.111485.

[92] A. Majumder, A.K. Gupta, P.S. Ghosal, M. Varma, A review on hospital wastewater treatment: A special emphasis on occurrence and removal of pharmaceutically active compounds, resistant microorganisms, and SARS-CoV-2, J. Environ. Chem. Eng. 9 (2021) 104812. https://doi.org/10.1016/j.jece.2020.104812.

[93] Y. Luo, W. Guo, H.H. Ngo, L.D. Nghiem, F.I. Hai, J. Zhang, S. Liang, X.C. Wang, A review on the occurrence of micropollutants in the aquatic environment and their fate and removal during wastewater treatment, Science of The Total Environment 473–474 (2014) 619–641. https://doi.org/10.1016/j.scitotenv.2013.12.065.

[94] K. Ślósarczyk, F. Wolny, A.J. Witkowski, Monitoring pharmaceuticals and personal care products to assess water quality changes and pollution sources in a drinking water reservoir catchment, Water Resour. Ind. 33 (2025) 100283. https://doi.org/10.1016/j.wri.2025.100283.

[95] J.A. Rodríguez-Hernández, R.G. Araújo, I.Y. López-Pacheco, L.I. Rodas-Zuluaga, R.B. González-González, L. Parra-Arroyo, J.E. Sosa-Hernández, E.M. Melchor-Martínez, M. Martínez-Ruiz, D. Barceló, L.M. Pastrana, H.M.N. Iqbal, R. Parra-Saldívar, Environmental persistence, detection, and mitigation of endocrine disrupting contaminants in wastewater treatment plants – a review with a focus on tertiary treatment technologies, Environmental Science: Advances 1 (2022) 680–704. https://doi.org/10.1039/D2VA00179A.

[96] R.K. Mishra, S.S. Mentha, Y. Misra, N. Dwivedi, Emerging pollutants of severe environmental concern in water and wastewater: A comprehensive review on current developments and future research, Water-Energy Nexus 6 (2023) 74–95. https://doi.org/10.1016/j.wen.2023.08.002.

[97] K. Skalska-Tuomi, L. Kaijanen, J.M. Monteagudo, M. Mänttäri, Efficient removal of pharmaceuticals from wastewater: Comparative study of three advanced oxidation processes, J. Environ. Manage. 375 (2025) 124276. https://doi.org/10.1016/j.jenvman.2025.124276.

[98] A. Mary Ealias, G. Meda, K. Tanzil, Recent Progress in Sustainable Treatment Technologies for the Removal of Emerging Contaminants from Wastewater: A Review on Occurrence, Global Status and Impact on Biota, Rev. Environ. Contam. Toxicol. 262 (2024) 16. https://doi.org/10.1007/s44169-024-00067-z.

[99] A.S. Silva, P.Z. Filho, A.P. Ferreira, F.F. Roman, A.P. Baldo, M. Rauhauser, J.L. Diaz de Tuesta, A.I. Pereira, A.M.T. Silva, J.M.T. Pietrobelli, M.S. Kalmakhanova, D.D. Snow, H.T. Gomes, Occurrence of micropollutants in surface water and removal by catalytic wet peroxide oxidation enhanced filtration using polymeric membranes

loaded with carbon nanotubes, Chemical Engineering Journal Advances 21 (2025) 100707. https://doi.org/10.1016/j.ceja.2025.100707.

[100] I.B. Gomes, J.-Y. Maillard, L.C. Simões, M. Simões, Emerging contaminants affect the microbiome of water systems—strategies for their mitigation, NPJ Clean Water 3 (2020) 39. https://doi.org/10.1038/s41545-020-00086-y.

[101] L. Zhang, J. Ling, M. Lin, Carbon neutrality: a comprehensive bibliometric analysis, Environmental Science and Pollution Research 30 (2023) 45498–45514. https://doi.org/10.1007/s11356-023-25797-w.

[102] H. Ghaempanah, K.I. Penev, A. Geraili, J.G. Burneo, K. Mequanint, Controlled release of carbamazepine at therapeutically relevant doses using photocrosslinkable polyanhydrides, Int. J. Pharm. 679 (2025) 125728. https://doi.org/10.1016/j.ijpharm.2025.125728.

[103] A. Majumder, A. Bhatnagar, A. Kumar Gupta, Simultaneous removal of sulfamethoxazole, 17β-estradiol, and carbamazepine from hospital wastewater using a combination of a continuous constructed wetland-based system followed by photocatalytic reactor, Chemical Engineering Journal 466 (2023) 143255. https://doi.org/10.1016/j.cej.2023.143255.

[104] J. Trognon, C. Albasi, J.-M. Choubert, A critical review on the pathways of carbamazepine transformation products in oxidative wastewater treatment processes, Science of The Total Environment 912 (2024) 169040. https://doi.org/10.1016/j.scitotenv.2023.169040.

[105] R. Kumar, A.K. Vuppaladadiyam, E. Antunes, A. Whelan, R. Fearon, M. Sheehan, L. Reeves, Emerging contaminants in biosolids: Presence, fate and analytical techniques, Emerg. Contam. 8 (2022) 162–194. https://doi.org/10.1016/j.emcon.2022.03.004.

[106] A. Majumder, P. Otter, D. Röher, A. Bhatnagar, N. Khalil, A.K. Gupta, R. Bresciani, C.A. Arias, Combination of advanced biological systems and photocatalysis for the treatment of real hospital wastewater spiked with carbamazepine: A pilot-scale study, J. Environ. Manage. 351 (2024) 119672. https://doi.org/10.1016/j.jenvman.2023.119672.

[107] A. Majumder, B. Gupta, A.K. Gupta, Pharmaceutically active compounds in aqueous environment: A status, toxicity and insights of remediation, Environ. Res. 176 (2019) 108542. https://doi.org/10.1016/j.envres.2019.108542.

[108] J. Lofty, V. Muhawenimana, C.A.M.E. Wilson, P. Ouro, Microplastics removal from a primary settler tank in a wastewater treatment plant and estimations of contamination

onto European agricultural land via sewage sludge recycling, Environmental Pollution 304 (2022) 119198. https://doi.org/10.1016/j.envpol.2022.119198.

[109] P. Kundu, N. Dutta, S. Bhattacharya, Application of microalgae in wastewater treatment with special reference to emerging contaminants: a step towards sustainability, Frontiers in Analytical Science 4 (2024). https://doi.org/10.3389/frans.2024.1513153.

[110] M. Pei, B. Zhang, Y. He, J. Su, K. Gin, O. Lev, G. Shen, S. Hu, State of the art of tertiary treatment technologies for controlling antibiotic resistance in wastewater treatment plants, Environ. Int. 131 (2019) 105026. https://doi.org/10.1016/j.envint.2019.105026.

[111] J.A. Silva, Wastewater Treatment and Reuse for Sustainable Water Resources Management: A Systematic Literature Review, Sustainability 15 (2023) 10940. https://doi.org/10.3390/su151410940.

[112] L.D.V. Melo, E.P. da Costa, C.C. Pinto, G.R. Barroso, S.C. Oliveira, Adequacy analysis of drinking water treatment technologies in regard to the parameter turbidity, considering the quality of natural waters treated by large-scale WTPs in Brazil, Environ. Monit. Assess. 191 (2019) 384. https://doi.org/10.1007/s10661-019-7526-9.

[113] L.D. Abo, M. Jayakumar, A.S. Jeyapaul, M. Rangaraju, H.A. Areti, A. Assefa Adugna, Comprehensive review on co-integration of conventional systems and advanced oxidation processes for industrial and agricultural wastewater treatment applications, Environmental Advances 20 (2025) 100638. https://doi.org/10.1016/j.envadv.2025.100638.

[114] A. V. Baskar, N. Bolan, S.A. Hoang, P. Sooriyakumar, M. Kumar, L. Singh, T. Jasemizad, L.P. Padhye, G. Singh, A. Vinu, B. Sarkar, M.B. Kirkham, J. Rinklebe, S. Wang, H. Wang, R. Balasubramanian, K.H.M. Siddique, Recovery, regeneration and sustainable management of spent adsorbents from wastewater treatment streams: A review, Science of The Total Environment 822 (2022) 153555. https://doi.org/10.1016/j.scitotenv.2022.153555.

[115] S. Dogruel, N. Chavoshi, N. Bilgin-Saritas, A. Khataee, E. Topuz, E. Pehlivanoglu, Degradation and ecotoxicity of favipiravir and oseltamivir in the presence of microplastics during ozonation and catalytic ozonation of synthetic municipal wastewater effluents, Journal of Chemical Technology & Biotechnology 100 (2025) 955–966. https://doi.org/10.1002/jctb.7831.

[116] A.L.R. Gomes, S. Ribeirinho-Soares, L.M. Madeira, O.C. Nunes, C.S.D. Rodrigues, Disinfection of Secondary Urban Wastewater Using Hydrogen Peroxide Combined

with UV/Visible Radiation: Effect of Operating Conditions and Assessment of Microorganism Competition, Water (Basel). 17 (2025) 596. https://doi.org/10.3390/w17040596.

[117] S.A. Moezzi, S. Rastgar, M. Faghani, Z. Ghiasvand, A. Javanshir Khoei, Optimization of carbon membrane performance in reverse osmosis systems for reducing salinity, nitrates, phosphates, and ammonia in aquaculture wastewater, Chemosphere 376 (2025) 144304. https://doi.org/10.1016/j.chemosphere.2025.144304.

[118] M. Kamali, K.M. Persson, M.E. Costa, I. Capela, Sustainability criteria for assessing nanotechnology applicability in industrial wastewater treatment: Current status and future outlook, Environ. Int. 125 (2019) 261–276. https://doi.org/10.1016/j.envint.2019.01.055.

[119] J. Lin, J. Li, Y. Xu, M. Xie, S. Zhao, W. Ye, Editorial: Wastewater treatment & resource recovery technologies, Front. Bioeng. Biotechnol. 11 (2023). https://doi.org/10.3389/fbioe.2023.1150044.

[120] A. Cristaldi, M. Fiore, P. Zuccarello, G. Oliveri Conti, A. Grasso, I. Nicolosi, C. Copat, M. Ferrante, Efficiency of Wastewater Treatment Plants (WWTPs) for Microplastic Removal: A Systematic Review, Int. J. Environ. Res. Public Health 17 (2020) 8014. https://doi.org/10.3390/ijerph17218014.

[121] J. Ianes, S. Piraldi, B. Cantoni, M. Antonelli, Micropollutants removal, residual risk, and costs for quaternary treatments in the framework of the Urban Wastewater Treatment Directive, Water Res. X 29 (2025) 100334. https://doi.org/10.1016/j.wroa.2025.100334.

[122] V. Medri, M.C. Marchioni, E. Landi, E. Papa, Development of membranes based on recycled geopolymer and zeolite through a cold sintering process, J. Eur. Ceram. Soc. 44 (2024) 7778–7790. https://doi.org/10.1016/j.jeurceramsoc.2024.05.053.

[123] N.M. Marin, M. Nita Lazar, M. Popa, T. Galaon, L.F. Pascu, Current Trends in Development and Use of Polymeric Ion-Exchange Resins in Wastewater Treatment, Materials 17 (2024) 5994. https://doi.org/10.3390/ma17235994.

[124] M.E. Argun, H. Ateş, M.Ş. Argun, Ö. Cakmakci, Management of sour cherry processing industry wastewater by super critical fluid method: Sequential recovery and treatment, Process Safety and Environmental Protection 199 (2025) 107318. https://doi.org/10.1016/j.psep.2025.107318.

[125] X. Zhang, Y. Chen, Q. Wang, Y. Sun, Advances in heavy metal wastewater treatment with biochar adsorption, Biofuels, Bioproducts and Biorefining (2025). https://doi.org/10.1002/bbb.2751.

[126] A.A. Siyal, M.R. Shamsuddin, M.I. Khan, N.E. Rabat, M. Zulfiqar, Z. Man, J. Siame, K.A. Azizli, A review on geopolymers as emerging materials for the adsorption of heavy metals and dyes, J. Environ. Manage. 224 (2018) 327–339. https://doi.org/10.1016/j.jenvman.2018.07.046.

[127] Y. So, S.Y. Kim, S. Kim, C. Park, Innovative approaches to high-speed ceramic membrane filtration for microplastic mitigation in urban wastewater treatment facilities, Sep. Purif. Technol. 363 (2025) 132013. https://doi.org/10.1016/j.seppur.2025.132013.

[128] G. Singh, G. Yadav, N. Yadav, S. Kapoor, B. Sharma, R.K. Sharma, R. Kumar, G.R. Chaudhary, Recent advancements in the synthesis of anion exchange membranes and their potential applications in wastewater treatment, Adv. Colloid Interface Sci. 336 (2025) 103376. https://doi.org/10.1016/j.cis.2024.103376.

[129] G. Fomo, T.N. Madzimbamuto, T.V. Ojumu, Applications of Nonconventional Green Extraction Technologies in Process Industries: Challenges, Limitations and Perspectives, Sustainability 12 (2020) 5244. https://doi.org/10.3390/su12135244.

[130] K.-Y. Khaw, M.-O. Parat, P.N. Shaw, J.R. Falconer, Solvent Supercritical Fluid Technologies to Extract Bioactive Compounds from Natural Sources: A Review, Molecules 22 (2017) 1186. https://doi.org/10.3390/molecules22071186.

[131] K.J. Castañeda-Retavizca, K. O'Dowd, E. Jambrina-Hernández, S. Nahim-Granados, P. Plaza-Bolaños, S. Malato, M.I. Polo-López, S.C. Pillai, I. Oller, Urban wastewater treatment by ozonation: Disinfection by-products and toxicity assessment, J. Environ. Chem. Eng. 13 (2025) 115970. https://doi.org/10.1016/j.jece.2025.115970.

[132] D. Sauter, A. Steuer, K. Wasmund, B. Hausmann, U. Szewzyk, A. Sperlich, R. Gnirss, M. Cooper, T. Wintgens, Microbial Communities and Processes in Biofilters for Post-Treatment of Ozonated Wastewater Treatment Plant Effluent, SSRN Electronic Journal (2022). https://doi.org/10.2139/ssrn.4176865.

[133] M. Bourgin, B. Beck, M. Boehler, E. Borowska, J. Fleiner, E. Salhi, R. Teichler, U. von Gunten, H. Siegrist, C.S. McArdell, Evaluation of a full-scale wastewater treatment plant upgraded with ozonation and biological post-treatments: Abatement of micropollutants, formation of transformation products and oxidation by-products, Water Res. 129 (2018) 486–498. https://doi.org/10.1016/j.watres.2017.10.036.

[134] S. Husien, R.M. El-taweel, A.I. Salim, I.S. Fahim, L.A. Said, A.G. Radwan, Review of activated carbon adsorbent material for textile dyes removal: Preparation, and modelling, Current Research in Green and Sustainable Chemistry 5 (2022) 100325. https://doi.org/10.1016/j.crgsc.2022.100325.

[135] K. Kaya-Özkiper, A. Uzun, S. Soyer-Uzun, Tuning adsorption, structure and compressive strength of sepiolite- and metakaolin-based alkali activated monoliths for methylene blue removal from waste water, Surfaces and Interfaces 33 (2022) 102110. https://doi.org/10.1016/j.surfin.2022.102110.

[136] H. Karimi-Maleh, A. Ayati, R. Davoodi, B. Tanhaei, F. Karimi, S. Malekmohammadi, Y. Orooji, L. Fu, M. Sillanpää, Recent advances in using of chitosan-based adsorbents for removal of pharmaceutical contaminants: A review, J. Clean. Prod. 291 (2021) 125880. https://doi.org/10.1016/j.jclepro.2021.125880.

[137] D. Somashekara, L. Mulky, Sequestration of Contaminants from Wastewater: A Review of Adsorption Processes, ChemBioEng Reviews 10 (2023) 491–509. https://doi.org/10.1002/cben.202200050.

[138] S. Ho, Low-Cost Adsorbents for the Removal of Phenol/Phenolics, Pesticides, and Dyes from Wastewater Systems: A Review, Water (Basel). 14 (2022) 3203. https://doi.org/10.3390/w14203203.

[139] A. Bassam, R. Bassam, M. El Alouani, Y. Rachdi, H. Saufi, S. Belaaouad, Synthesis of geopolymer powder and beads based on red clay waste for the adsorption of methyl orange dye from aqueous solutions: Characterization, application of response surface methodology, and cost analysis, Sustain. Chem. Pharm. 39 (2024) 101575. https://doi.org/10.1016/j.scp.2024.101575.

[140] M.H. Dehghani, S. Ahmadi, S. Ghosh, A. Othmani, C. Osagie, M. Meskini, S.S. AlKafaas, A. Malloum, W.A. Khanday, A.O. Jacob, Ö. Gökkuş, A. Oroke, O. Martins Chineme, R.R. Karri, E.C. Lima, Recent advances on sustainable adsorbents for the remediation of noxious pollutants from water and wastewater: A critical review, Arabian Journal of Chemistry 16 (2023) 105303. https://doi.org/10.1016/j.arabjc.2023.105303.

[141] S. Jha, R. Gaur, S. Shahabuddin, I. Tyagi, Biochar as Sustainable Alternative and Green Adsorbent for the Remediation of Noxious Pollutants: A Comprehensive Review, Toxics 11 (2023) 117. https://doi.org/10.3390/toxics11020117.

[142] N. Ziemińska, B. Doczekalska, Biomass derived activated carbons in wastewater treatment – The aim of metallurgical industry, Desalination Water Treat. 318 (2024) 100320. https://doi.org/10.1016/j.dwt.2024.100320.

[143] X. Li, S. Chen, F. Zi, X. Hu, Adsorption properties and selectivity of resin with amine group for gold in thiosulfate solution, Sep. Purif. Technol. 372 (2025) 133510. https://doi.org/10.1016/j.seppur.2025.133510.

[144] X. Zhang, J. Yu, B. Jin, Y. Huang, Z. Wang, Experimental research on the gaseous PbCl2 adsorption by thermal alkali modified coal fly ash, J. Environ. Chem. Eng. 10 (2022) 107912. https://doi.org/10.1016/j.jece.2022.107912.

[145] Y. Hui, R. Liu, J. Lan, T. Sun, A. Xu, Recyclable chitosan adsorbent: Facile functionalization strategy, excellent removal capacity of dyes and adsorption mechanism, Chemosphere 359 (2024) 142291. https://doi.org/10.1016/j.chemosphere.2024.142291.

[146] X. Yang, L. Chen, G. He, M. Yang, S. Geng, Y. Sun, X. Feng, C. Ma, Q. Wei, H. Zhao, S. Jiang, Chitosan-loaded coconut fiber for highly-enhanced heavy metal adsorption from wastewater, Sep. Purif. Technol. 368 (2025) 133105. https://doi.org/10.1016/j.seppur.2025.133105.

[147] Y. Zhang, M. Zhao, Q. Cheng, C. Wang, H. Li, X. Han, Z. Fan, G. Su, D. Pan, Z. Li, Research progress of adsorption and removal of heavy metals by chitosan and its derivatives: A review, Chemosphere 279 (2021) 130927. https://doi.org/10.1016/j.chemosphere.2021.130927.

[148] A. Gamage, N. Jayasinghe, P. Thiviya, M.L.D. Wasana, O. Merah, T. Madhujith, J.R. Koduru, Recent Application Prospects of Chitosan Based Composites for the Metal Contaminated Wastewater Treatment, Polymers (Basel). 15 (2023) 1453. https://doi.org/10.3390/polym15061453.

[149] Z. Li, G. Lu, D. Du, D. Zhao, Harnessing low-cost adsorbents for removal of heavy metals and metalloids in contaminated water: Progress in the past decade and future perspectives, J. Clean. Prod. 518 (2025) 145845. https://doi.org/10.1016/j.jclepro.2025.145845.

[150] S. Sutar, J. Jadhav, A comparative assessment of the methylene blue dye adsorption capacity of natural biochar versus chemically altered activated carbons, Bioresour. Technol. Rep. 25 (2024) 101726. https://doi.org/10.1016/j.biteb.2023.101726.

[151] Y. Wang, Y. Liu, W. Zhan, K. Zheng, J. Wang, C. Zhang, R. Chen, Stabilization of heavy metal-contaminated soils by biochar: Challenges and recommendations, Science of The Total Environment 729 (2020) 139060. https://doi.org/10.1016/j.scitotenv.2020.139060.

[152] L. Velarde, M.S. Nabavi, E. Escalera, M.-L. Antti, F. Akhtar, Adsorption of heavy metals on natural zeolites: A review, Chemosphere 328 (2023) 138508. https://doi.org/10.1016/j.chemosphere.2023.138508.

[153] Y. Dehmani, B. Ba Mohammed, R. Oukhrib, A. Dehbi, T. Lamhasni, Y. Brahmi, A. El-Kordy, D.S.P. Franco, J. Georgin, E.C. Lima, A.A. Alrashdi, N. Tijani, S.

Abouarnadasse, Adsorption of various inorganic and organic pollutants by natural and synthetic zeolites: A critical review, Arabian Journal of Chemistry 17 (2024) 105474. https://doi.org/10.1016/j.arabjc.2023.105474.

[154] I. El Bojaddayni, M. Emin Küçük, Y. El Ouardi, I. Jilal, S. El Barkany, K. Moradi, E. Repo, K. Laatikainen, A. Ouammou, A review on synthesis of zeolites from natural clay resources and waste ash: Recent approaches and progress, Miner. Eng. 198 (2023) 108086. https://doi.org/10.1016/j.mineng.2023.108086.

[155] C. Cao, W. Xuan, S. Yan, Q. Wang, Zeolites synthesized from industrial and agricultural solid waste and their applications: A review, J. Environ. Chem. Eng. 11 (2023) 110898. https://doi.org/10.1016/j.jece.2023.110898.

[156] N.S. Kim, M. Numan, S.C. Nam, S.-E. Park, C. Jo, Dynamic adsorption/desorption of p-xylene on nanomorphic MFI zeolites: Effect of zeolite crystal thickness and mesopore architecture, J. Hazard. Mater. 403 (2021) 123659. https://doi.org/10.1016/j.jhazmat.2020.123659.

[157] Y. Pei, S. Mo, Q. Xie, N. Chen, Z. Yang, L. Huang, L. Ma, Stellerite-seeded facile synthesis of zeolite X with excellent aqueous Cd2+ and Ni2+ adsorption performance, Chin. J. Chem. Eng. 51 (2022) 61–74. https://doi.org/10.1016/j.cjche.2022.06.008.

[158] S. Lin, X. Jiang, Y. Zhao, J. Yan, Zeolite greenly synthesized from fly ash and its resource utilization: A review, Science of The Total Environment 851 (2022) 158182. https://doi.org/10.1016/j.scitotenv.2022.158182.

[159] W. Zhang, T. Zhang, Y. Lv, T. Jing, X. Gao, Z. Gu, S. Li, H. Ao, D. Fang, Recent Progress on the Synthesis and Applications of Zeolites from Industrial Solid Wastes, Catalysts 14 (2024) 734. https://doi.org/10.3390/catal14100734.

[160] Y. Zhao, S. Gu, L. Li, M. Wang, From waste to catalyst: Growth mechanisms of ZSM-5 zeolite from coal fly ash & rice husk ash and its performance as catalyst for tetracycline degradation in fenton-like oxidation, Environmental Pollution 345 (2024) 123509. https://doi.org/10.1016/j.envpol.2024.123509.

[161] A. Rozhkovskaya, J. Rajapakse, G.J. Millar, Optimisation of zeolite LTA synthesis from alum sludge and the influence of the sludge source, Journal of Environmental Sciences 99 (2021) 130–142. https://doi.org/10.1016/j.jes.2020.06.019.

[162] D. Bosch, J.O. Back, M. Spruck, L. Nohel, D. Gurtner, C. Margreiter, A. Hofmann, A. Bockreis, Addressing Europe’s new hunger for sustainable activated carbon in wastewater treatment: Micropollutant removal with residual wood-based adsorbents using different activation strategies, Chemical Engineering Research and Design 217 (2025) 108–120. https://doi.org/10.1016/j.cherd.2025.03.021.

[163] G. Duran-Jimenez, J. Rodriguez, L. Stevens, S. Altarawneh, A. Batchelor, L. Jiang, C. Dodds, Single-step preparation of activated carbons from pine wood, olive stones and nutshells by KOH and microwaves: Influence of ultra-microporous for high CO2 capture, Chemical Engineering Journal 499 (2024) 156135. https://doi.org/10.1016/j.cej.2024.156135.

[164] N. Noorani, S. Pourebrahimi, A. Mehrdad, Enhancing CO2 adsorption performance of cold oxygen plasma-treated almond shell-derived activated carbons through ionic liquid incorporation, Journal of CO2 Utilization 88 (2024) 102927. https://doi.org/10.1016/j.jcou.2024.102927.

[165] S. Poovaragan, S. Lakshmanan, K.L.V. Joseph, Sterculia foetida fruit shell based activated carbon for the effective removal of industrial effluents, Journal of the Indian Chemical Society 98 (2021) 100196. https://doi.org/10.1016/j.jics.2021.100196.

[166] C. Yogin Soodesh, A.K. Seriyala, Navjot, P. Chattopadhyay, N. Rozhkova, B. Michalkiewicz, S. Chatterjee, B. Roy, Carbonaceous catalysts (biochar and activated carbon) from agricultural residues and their application in production of biodiesel: A review, Chemical Engineering Research and Design 203 (2024) 759–788. https://doi.org/10.1016/j.cherd.2024.02.002.

[167] L. Sellaoui, L.F.O. Silva, M. Badawi, J. Ali, N. Favarin, G.L. Dotto, A. Erto, Z. Chen, Adsorption of ketoprofen and 2- nitrophenol on activated carbon prepared from winery wastes: A combined experimental and theoretical study, J. Mol. Liq. 333 (2021) 115906. https://doi.org/10.1016/j.molliq.2021.115906.

[168] S.R. Mishra, T. Mandal, P. Kumar, V. Verma, R.N. Senapati, M. Kumar, V. Singh, Microporous activated carbon from Madhuca Longifolia flower for efficient methylene blue dye removal in wastewater treatment, Surfaces and Interfaces 69 (2025) 106770. https://doi.org/10.1016/j.surfin.2025.106770.

[169] J. Jjagwe, P.W. Olupot, E. Menya, H.M. Kalibbala, Synthesis and Application of Granular Activated Carbon from Biomass Waste Materials for Water Treatment: A Review, Journal of Bioresources and Bioproducts 6 (2021) 292–322. https://doi.org/10.1016/j.jobab.2021.03.003.

[170] P. Samba, S. Schaefer, B. Cagnon, Impregnation by hydrothermal carbonization in the presence of phosphoric acid in the activated carbon production process from hemp residus: Impact on porous properties and ibuprofen adsorption, Journal of Industrial and Engineering Chemistry (2025). https://doi.org/10.1016/j.jiec.2025.02.060.

[171] A. Grich, A. Naboulsi, T. Bouzid, H. Yazid, A. Elbasraoui, A. Regti, M. El Himri, M. El Haddad, Doum fiber-derived activated carbon via H_3PO_4-assisted pyrolysis for

sulfamethoxazole removal: Box-Behnken Design optimization and mechanistic approach, Diam. Relat. Mater. 156 (2025) 112464. https://doi.org/10.1016/j.diamond.2025.112464.

[172] Y. Yin, Q. Liu, J. Wang, Y. Zhao, Recent insights in synthesis and energy storage applications of porous carbon derived from biomass waste: A review, Int. J. Hydrogen Energy 47 (2022) 39338–39363. https://doi.org/10.1016/j.ijhydene.2022.09.121.

[173] A. Khamkeaw, W. Sanprom, M. Phisalaphong, Activated carbon from bacterial cellulose by potassium hydroxide activation as an effective adsorbent for removal of ammonium ion from aqueous solution, Case Studies in Chemical and Environmental Engineering 8 (2023) 100499. https://doi.org/10.1016/j.cscee.2023.100499.

[174] J.J. Romero-Hernandez, M. Paredes-Laverde, J. Silva-Agredo, D.F. Mercado, Y. Ávila-Torres, R.A. Torres-Palma, Pharmaceutical adsorption on NaOH-treated rice husk-based activated carbons: Kinetics, thermodynamics, and mechanisms, J. Clean. Prod. 434 (2024) 139935. https://doi.org/10.1016/j.jclepro.2023.139935.

[175] I. Alouiz, M. Benhadj, E. Dahmane, M. Sennoune, M.-Y. Amarouch, D. Mazouzi, Elaboration of fibrous structured activated carbon from olive pomace via chemical activation and low-temperature pyrolysis, Heliyon 10 (2024) e38886. https://doi.org/10.1016/j.heliyon.2024.e38886.

[176] S. Sagadevan, T. Balakrishnan, M.Z. Rahman, T. Soga, H. Randriamahazaka, B. Kakavandi, M.R. Johan, Agricultural biomass-based activated carbons for efficient and sustainable supercapacitors, J. Energy Storage 97 (2024) 112878. https://doi.org/10.1016/j.est.2024.112878.

[177] J. Wang, A. Cahyadi, B. Wu, W. Pee, A.G. Fane, J.W. Chew, The roles of particles in enhancing membrane filtration: A review, J. Memb. Sci. 595 (2020) 117570. https://doi.org/10.1016/j.memsci.2019.117570.

[178] Z. Heidarinejad, M.H. Dehghani, M. Heidari, G. Javedan, I. Ali, M. Sillanpää, Methods for preparation and activation of activated carbon: a review, Environ. Chem. Lett. 18 (2020) 393–415. https://doi.org/10.1007/s10311-019-00955-0.

[179] O.Y. Bakather, Eco-friendly biosorbent for lead removal: Activated carbon produced from grape wood, Desalination Water Treat. 317 (2024) 100210. https://doi.org/10.1016/j.dwt.2024.100210.

[180] A.C. Deiana, M.F. Sardella, H. Silva, A. Amaya, N. Tancredi, Use of grape stalk, a waste of the viticulture industry, to obtain activated carbon, J. Hazard. Mater. 172 (2009) 13–19. https://doi.org/10.1016/j.jhazmat.2009.06.095.

[181] S.E.A. El Hassani, A. Driouich, H. Chaair, H. Mellouk, K. Digua, Optimization of activated carbon by chemical activation from grape seeds using the response surface methodology, Desalination Water Treat. 245 (2022) 144–157. https://doi.org/10.5004/dwt.2022.27961.

[182] C. Purnomo, D. Castello, L. Fiori, Granular Activated Carbon from Grape Seeds Hydrothermal Char, Applied Sciences 8 (2018) 331. https://doi.org/10.3390/app8030331.

[183] S. Bourahla, F. Nemchi, H. Belayachi, A. Belayachi, C. Harrats, M. Belhakem, Removal of the AO7 dye by adsorption on activated carbon based on grape marc: equilibrium, regeneration, and FTIR spectroscopy, Journal of the Iranian Chemical Society 20 (2023) 669–681. https://doi.org/10.1007/s13738-022-02705-6.

[184] S. Mabrouk, M. Fizer, R. Mariychuk, H. Dhaouadi, Grape seeds waste activated carbon as an adsorber of paracetamol drug residue: Experimental and theoretical approaches, J. Mol. Liq. 408 (2024) 125325. https://doi.org/10.1016/j.molliq.2024.125325.

[185] S. Sağlam, F.N. Türk, H. Arslanoğlu, Tetracycline (TC) removal from wastewater with activated carbon (AC) obtained from waste grape marc: activated carbon characterization and adsorption mechanism, Environmental Science and Pollution Research 31 (2024) 33904–33923. https://doi.org/10.1007/s11356-024-33493-6.

[186] P.Y. He, Y.J. Zhang, H. Chen, Z.C. Han, L.C. Liu, Low-cost and facile synthesis of geopolymer-zeolite composite membrane for chromium(VI) separation from aqueous solution, J. Hazard. Mater. 392 (2020) 122359. https://doi.org/10.1016/j.jhazmat.2020.122359.

[187] X. Zhang, X. Zhang, M. Ma, Y. Sun, C. Ma, Rapid performance optimization strategy of MK-FA-GBFS based geopolymer foam heavy-metal adsorbent, Constr. Build. Mater. 394 (2023) 132161. https://doi.org/10.1016/j.conbuildmat.2023.132161.

[188] F.Z. Karmil, Z. Naribi, A. Azifa, H. El Alaoui-Belghiti, Synthesis of lightweight porous fly ash geopolymer monoliths for phosphorus removal from aqueous media: Kinetics, safety, and economic feasibility, Journal of Industrial and Engineering Chemistry (2025). https://doi.org/10.1016/j.jiec.2025.03.056.

[189] G. Huang, M. Wang, Q. Liu, S. Zhao, H. Liu, F. Liu, L. Feng, J. Song, Simultaneous utilization of mine tailings and steel slag for producing geopolymers: Alkali-hydrothermal activation, workability, strength, and hydration mechanism, Constr. Build. Mater. 414 (2024) 135029. https://doi.org/10.1016/j.conbuildmat.2024.135029.

[190] I. Fatimah, P.W. Citradewi, R.M. Iqbal, S.A.I.S.M. Ghazali, A. Yahya, G. Purwiandono, Geopolymer from tin mining tailings waste using Salacca leaves ash as

activator for dyes and peat water adsorption, S. Afr. J. Chem. Eng. 43 (2023) 257–265. https://doi.org/10.1016/j.sajce.2022.11.008.

[191] M.I. Khan, S. Sufian, F. Hassan, R. Shamsuddin, M. Farooq, Phosphoric acid based geopolymer foam-activated carbon composite for methylene blue adsorption: isotherm, kinetics, thermodynamics, and machine learning studies, RSC Adv. 15 (2025) 1989–2010. https://doi.org/10.1039/D4RA05782A.

[192] B. Yuan, H. Hu, Y. Huang, B. Fu, H. Liu, G. Luo, Y. Zhao, H. Yao, Condensation and adsorption characteristics of gaseous selenium on coal-fired fly ash at low temperatures, Chemosphere 287 (2022) 132127. https://doi.org/10.1016/j.chemosphere.2021.132127.

[193] X. Zhao, H. Zhao, X. Huang, L. Wang, F. Liu, X. Hu, J. Li, G. Zhang, P. Ji, Effect and mechanisms of synthesis conditions on the cadmium adsorption capacity of modified fly ash, Ecotoxicol. Environ. Saf. 223 (2021) 112550. https://doi.org/10.1016/j.ecoenv.2021.112550.

[194] Q. Tian, K. Sasaki, Structural characterizations of fly ash-based geopolymer after adsorption of various metal ions, Environ. Technol. 42 (2021) 941–951. https://doi.org/10.1080/09593330.2019.1649469.

[195] Y. Song, J. Pan, M. Chen, Y. Wang, Z. Li, Y. Ge, Chitosan-modified geopolymer sub-microparticles reinforced multifunctional membrane for enhanced removal of multiple contaminants in water, J. Memb. Sci. 658 (2022) 120704. https://doi.org/10.1016/j.memsci.2022.120704.

[196] R. Zhang, F. Li, S. Zhou, Y. Hou, Carbon nanofiber dispersion in alkali solution and its reinforcement of alkali-activated volcanic ash-based geopolymers, J. Clean. Prod. 405 (2023) 137021. https://doi.org/10.1016/j.jclepro.2023.137021.

[197] S. Yan, F. Zhang, J. Kong, B. Wang, H. Li, Y. Yang, P. Xing, Mechanical properties of geopolymer composite foams reinforced with carbon nanofibers via modified hydrogen peroxide method, Mater. Chem. Phys. 253 (2020) 123258. https://doi.org/10.1016/j.matchemphys.2020.123258.

[198] H. Chen, Y.J. Zhang, P.Y. He, C.J. Li, L.C. Liu, Novel activated carbon route to low-cost geopolymer based porous composite with high mechanical resistance and enhanced CO2 capacity, Microporous and Mesoporous Materials 305 (2020) 110282. https://doi.org/10.1016/j.micromeso.2020.110282.

[199] Z. Ji, Y. Pei, Bibliographic and visualized analysis of geopolymer research and its application in heavy metal immobilization: A review, J. Environ. Manage. 231 (2019) 256–267. https://doi.org/10.1016/j.jenvman.2018.10.041.

[200] Y. Ettahiri, B. Bouargane, K. Fritah, B. Akhsassi, L. Pérez-Villarejo, A. Aziz, L. Bouna, A. Benlhachemi, R.M. Novais, A state-of-the-art review of recent advances in porous geopolymer: Applications in adsorption of inorganic and organic contaminants in water, Constr. Build. Mater. 395 (2023) 132269. https://doi.org/10.1016/j.conbuildmat.2023.132269.

[201] Z. Jwaida, A. Dulaimi, N. Mashaan, M.A. Othuman Mydin, Geopolymers: The Green Alternative to Traditional Materials for Engineering Applications, Infrastructures (Basel). 8 (2023) 98. https://doi.org/10.3390/infrastructures8060098.

[202] A.L. Freire, H.J. José, R. de F.P.M. Moreira, Potential applications for geopolymers in carbon capture and storage, International Journal of Greenhouse Gas Control 118 (2022) 103687. https://doi.org/10.1016/j.ijggc.2022.103687.

[203] L. Zhang, Y. Wang, B. Ding, J. Gu, N. Ukrainczyk, J. Cai, Development of geopolymer-based composites for geothermal energy applications, J. Clean. Prod. 419 (2023) 138202. https://doi.org/10.1016/j.jclepro.2023.138202.

[204] L. Ricciotti, A. Apicella, V. Perrotta, R. Aversa, Geopolymer Materials for Bone Tissue Applications: Recent Advances and Future Perspectives, Polymers (Basel). 15 (2023) 1087. https://doi.org/10.3390/polym15051087.

[205] B. Zhang, Durability of low-carbon geopolymer concrete: A critical review, Sustainable Materials and Technologies 40 (2024) e00882. https://doi.org/10.1016/j.susmat.2024.e00882.

[206] A.P. Ferreira, A.P.S. Natal, A.P. Baldo, A.S. Silva, J.L. Diaz de Tuesta, P. Marin, J.A. Peres, H.T. Gomes, Response surface method-driven design of experiments for the synthesis of fly ash-based geopolymers in the gallic acid optimized removal from wastewater, Chemical Engineering Journal Advances 21 (2025) 100703. https://doi.org/10.1016/j.ceja.2024.100703.

[207] S. Yang, Y. He, G. Xue, H. Yu, X. Cui, Fabrication of geopolymer microspheres and their Pb(II) adsorption performance by fixed-bed column method, Desalination Water Treat. 207 (2020) 300–308. https://doi.org/10.5004/dwt.2020.26433.

[208] T. Hertel, R.M. Novais, R. Murillo Alarcón, J.A. Labrincha, Y. Pontikes, Use of modified bauxite residue-based porous inorganic polymer monoliths as adsorbents of methylene blue, J. Clean. Prod. 227 (2019) 877–889. https://doi.org/10.1016/j.jclepro.2019.04.084.

[209] M. Xu, Y. He, Z. Liu, Z. Tong, X. Cui, Preparation of geopolymer inorganic membrane and purification of pulp-papermaking green liquor, Appl. Clay Sci. 168 (2019) 269–275. https://doi.org/10.1016/j.clay.2018.11.024.

[210] Y. Liu, X. Qiu, Y. Fan, S. Zhou, H. Wang, X. Zhu, Z. Wang, C. Yan, From natural clinoptilolite to hierarchical designed porous geopolymer-zeolite monoliths: Synthesis, characterization and formation mechanism, Constr. Build. Mater. 408 (2023) 133718. https://doi.org/10.1016/j.conbuildmat.2023.133718.

[211] Q. Yang, S. Chu, M. Li, Z. Zhou, Q. Su, X. Xue, Y. Han, H. Li, In-situ synthesized multifunctional petal-like geopolymer/Mo_2S_3 composite membrane for water purification and recovery, J. Hazard. Mater. 489 (2025) 137564. https://doi.org/10.1016/j.jhazmat.2025.137564.

[212] J. Wang, Y. Ge, Y. He, M. Xu, X. Cui, A porous gradient geopolymer-based tube membrane with high PM removal rate for air pollution, J. Clean. Prod. 217 (2019) 335–343. https://doi.org/10.1016/j.jclepro.2019.01.268.

[213] H. Chen, Y.J. Zhang, P.Y. He, L.C. Liu, DFT Studies on Al Distribution and Bronsted Acid Sites in Zeolite ECR-1, Integrated Ferroelectrics 207 (2020) 118–124. https://doi.org/10.1080/10584587.2020.1728670.

[214] H. Chen, Y.J. Zhang, P.Y. He, L.C. Liu, Synthesis, characterization, and selective CO2 capture performance of a new type of activated carbon-geopolymer composite adsorbent, J. Clean. Prod. 325 (2021) 129271. https://doi.org/10.1016/j.jclepro.2021.129271.

[215] C. Di Pietro, W.F. Cossio Guzman, E. Papa, E. Landi, F. Miccio, M. Minelli, V. Medri, Cold sintered geopolymer and geopolymer-zeolite composite sorbents for CO2 capture, J. Environ. Chem. Eng. 13 (2025) 117098. https://doi.org/10.1016/j.jece.2025.117098.

[216] X. Qiu, Y. Liu, D. Li, C. Yan, Preparation of NaP zeolite block from fly ash-based geopolymer via in situ hydrothermal method, Journal of Porous Materials 22 (2015) 291–299. https://doi.org/10.1007/s10934-014-9895-3.

[217] Z. Ren, L. Wang, Y. Li, J. Zha, G. Tian, F. Wang, H. Zhang, J. Liang, Synthesis of zeolites by in-situ conversion of geopolymers and their performance of heavy metal ion removal in wastewater:A review, J. Clean. Prod. 349 (2022) 131441. https://doi.org/10.1016/j.jclepro.2022.131441.

[218] N. Supamathanon, K. Boonserm, N. Osakoo, J. Wittayakun, S. Prayoonpokarach, N. Chanlek, W. Dungkaew, Potassium supported on zeolite-geopolymer hybrid materials as a new solid base catalyst for transesterification of soybean oil, Renew. Energy 202 (2023) 1460–1469. https://doi.org/10.1016/j.renene.2022.12.018.

[219] C. Luan, A. Zhou, Y. Li, D. Zou, P. Gao, T. Liu, CO2 avoidance cost of fly ash geopolymer concrete, Constr. Build. Mater. 416 (2024) 135193. https://doi.org/10.1016/j.conbuildmat.2024.135193.

[220] C. Bai, L. Wang, X. Zhang, D. Wang, Z. Zhang, T. Zheng, L. Zhang, P. Colombo, Zeolite/slag-based porous geopolymer sphere regenerable composites with enhanced mechanical strength and good dye removal performance, Mater. Lett. 360 (2024) 136026. https://doi.org/10.1016/j.matlet.2024.136026.

[221] H.S. Abdelbaset, S.A. Shama, R.M. Hegazey, E.A. Abdelrahman, Utilisation of wastes for low-cost synthesis of chitosan composites with nanosized sodium aluminium silicate hydrate and geopolymer/zeolite A for the removal of Hg(II) and Pb(II) ions from aqueous media, Int. J. Environ. Anal. Chem. 103 (2023) 182–200. https://doi.org/10.1080/03067319.2020.1855336.

[222] Y. Wang, L. Chen, S. Li, Z. Zhang, Synthesis of geopolymer-zeolite composite from municipal solid waste incineration fly ash and their performance for CO2 adsorption, Sep. Purif. Technol. 354 (2025) 129114. https://doi.org/10.1016/j.seppur.2024.129114.

[223] Y. Liu, C. Yan, X. Qiu, D. Li, H. Wang, A. Alshameri, Preparation of faujasite block from fly ash-based geopolymer via in-situ hydrothermal method, J. Taiwan Inst. Chem. Eng. 59 (2016) 433–439. https://doi.org/10.1016/j.jtice.2015.07.012.

[224] Y. Liu, C. Yan, Z. Zhang, Y. Gong, H. Wang, X. Qiu, A facile method for preparation of floatable and permeable fly ash-based geopolymer block, Mater. Lett. 185 (2016) 370–373. https://doi.org/10.1016/j.matlet.2016.09.044.

[225] E.F.L. Moraes, A.P.F. da Silva, J.L. Diaz de Tuesta, A.N. Silva, F. Orssatto, H.T. Gomes, Production of Polymeric Membranes Based on Activated Carbons for Wastewater Treatment, in: The 4th International Electronic Conference on Applied Sciences, MDPI, Basel Switzerland, 2023: p. 336. https://doi.org/10.3390/ASEC2023-16874.

[226] L. López-Pérez, V. Zarubina, I. Melián-Cabrera, The Brunauer–Emmett–Teller model on alumino-silicate mesoporous materials. How far is it from the true surface area?, Microporous and Mesoporous Materials 319 (2021) 111065. https://doi.org/10.1016/j.micromeso.2021.111065.

[227] Q.S. Pavão, P.G. Ribeiro, G.P. Maciel, S.H.G. Silva, S.R. Araújo, A.R. Fernandes, J.A.M. Demattê, P.W.M. e Souza Filho, S.J. Ramos, Portable XRF and Vis-NIR spectrometry for predicting chemical properties of forest soils in the Amazon: Insights into sensor data dimensionality reduction, Soil Advances 4 (2025) 100063. https://doi.org/10.1016/j.soilad.2025.100063.

[228] M.F. González, N. Saadatkhah, G.S. Patience, Experimental methods in chemical engineering: X-ray fluorescence— <scp>XRF</scp>, Can. J. Chem. Eng. 102 (2024) 2004–2018. https://doi.org/10.1002/cjce.25218.

[229] A.A. Siyal, R. Shamsuddin, A. Low, A. Hidayat, Adsorption Kinetics, Isotherms, and Thermodynamics of Removal of Anionic Surfactant from Aqueous Solution Using Fly Ash, Water Air Soil Pollut. 231 (2020) 509. https://doi.org/10.1007/s11270-020-04879-2.

[230] S. Lagergren, Zur Theorie der sogenannten Adsorption gelöster Stoffe, Bihang till Kongliga Svenska Vetenskaps-Akademiens Handlingar 24 (1898) 1–39.

[231] Y. S. Ho, G. McKay, Pseudo-second order model for sorption processes, Process Biochemistry 34 (1999) 451–465.

[232] W.J. Weber, J.C. Morris, Kinetics of Adsorption on Carbon from Solution, Journal of the Sanitary Engineering Division 89 (1963) 31–59. https://doi.org/10.1061/JSEDAI.0000430.

[233] M.S. Akhtar, S. Ali, W. Zaman, Innovative Adsorbents for Pollutant Removal: Exploring the Latest Research and Applications, Molecules 29 (2024) 4317. https://doi.org/10.3390/molecules29184317.

[234] I. Langmuir, THE ADSORPTION OF GASES ON PLANE SURFACES OF GLASS, MICA AND PLATINUM., J. Am. Chem. Soc. 40 (1918) 1361–1403. https://doi.org/10.1021/ja02242a004.

[235] M. Vigdorowitsch, A. Pchelintsev, L. Tsygankova, E. Tanygina, Freundlich Isotherm: An Adsorption Model Complete Framework, Applied Sciences 11 (2021) 8078. https://doi.org/10.3390/app11178078.

[236] L. Bouna, Y. Ettahiri, A. Elimbi, A. Benlhachemi, M. Cyr, Role of washing process in the improvement of surface properties of porous geopolymers, Journal of Porous Materials 31 (2024) 569–576. https://doi.org/10.1007/s10934-023-01533-0.

[237] M. Ramadan, A.O. Habib, M.M. Hazem, M.S. Amin, A. Mohsen, Synergetic effects of hydrothermal treatment on the behavior of toxic sludge-modified geopolymer: Immobilization of cerium and lead, textural characteristics, and mechanical efficiency, Constr. Build. Mater. 367 (2023) 130249. https://doi.org/10.1016/j.conbuildmat.2022.130249.

[238] C. Kuenzel, N. Ranjbar, Dissolution mechanism of fly ash to quantify the reactive aluminosilicates in geopolymerisation, Resour. Conserv. Recycl. 150 (2019) 104421. https://doi.org/10.1016/j.resconrec.2019.104421.

[239] S.Ş. Akın, S.K. Kirdeciler, F. Kazanç, B. Akata, Critical analysis of zeolite 4A synthesis through one-pot fusion hydrothermal treatment approach for class F fly ash, Microporous and Mesoporous Materials 325 (2021) 111338. https://doi.org/10.1016/j.micromeso.2021.111338.

[240] Z. Qin, S. Zeng, G. Melinte, T. Bučko, M. Badawi, Y. Shen, J. Gilson, O. Ersen, Y. Wei, Z. Liu, X. Liu, Z. Yan, S. Xu, V. Valtchev, S. Mintova, Understanding the Fundamentals of Microporosity Upgrading in Zeolites: Increasing Diffusion and Catalytic Performances, Advanced Science 8 (2021). https://doi.org/10.1002/advs.202100001.

[241] B. Reiprich, T. Weissenberger, W. Schwieger, A. Inayat, Layer-like FAU-type zeolites: A comparative view on different preparation routes, Front. Chem. Sci. Eng. 14 (2020) 127–142. https://doi.org/10.1007/s11705-019-1883-3.

[242] Y. Liu, C. Yan, X. Qiu, D. Li, H. Wang, A. Alshameri, Preparation of faujasite block from fly ash-based geopolymer via in-situ hydrothermal method, J. Taiwan Inst. Chem. Eng. 59 (2016) 433–439. https://doi.org/10.1016/j.jtice.2015.07.012.

[243] L. Li, S. Wang, Z. Zhu, Geopolymeric adsorbents from fly ash for dye removal from aqueous solution, J. Colloid Interface Sci. 300 (2006) 52–59. https://doi.org/10.1016/J.JCIS.2006.03.062.

[244] C.J. Li, Y.J. Zhang, H. Chen, P.Y. He, Q. Meng, Development of porous and reusable geopolymer adsorbents for dye wastewater treatment, J. Clean. Prod. 348 (2022) 131278. https://doi.org/10.1016/j.jclepro.2022.131278.

[245] M. Król, J. Minkiewicz, W. Mozgawa, IR spectroscopy studies of zeolites in geopolymeric materials derived from kaolinite, J. Mol. Struct. 1126 (2016) 200–206. https://doi.org/10.1016/J.MOLSTRUC.2016.02.027.

[246] L. Panda, S.S. Rath, D.S. Rao, B.B. Nayak, B. Das, P.K. Misra, Thorough understanding of the kinetics and mechanism of heavy metal adsorption onto a pyrophyllite mine waste based geopolymer, J. Mol. Liq. 263 (2018) 428–441. https://doi.org/10.1016/J.MOLLIQ.2018.05.016.

[247] N. Kozai, K. Tokunaga, T. Dohi, Y. Takahashi, Environmentally friendly geopolymers: Synthesis and characterization of pH-Controlled metakaolinite phosphate-based hardened bodies, J. Environ. Chem. Eng. 13 (2025) 119612. https://doi.org/10.1016/j.jece.2025.119612.

[248] H.J. Rao, Characterization Studies on Adsorption of Lead and Cadmium Using Activated Carbon Prepared from Waste Tyres, Nature Environment and Pollution Technology 20 (2021). https://doi.org/10.46488/NEPT.2021.v20i02.012.

[249] S.K. Shahcheragh, M.M. Bagheri Mohagheghi, A. Shirpay, Effect of physical and chemical activation methods on the structure, optical absorbance, band gap and urbach energy of porous activated carbon, SN Appl. Sci. 5 (2023) 313. https://doi.org/10.1007/s42452-023-05559-6.

[250] M. Suhasini, E. Sailatha, S. Gunasekaran, G.R. Ramkumaar, Molecular structure and spectroscopic characterization of Carbamazepine with experimental techniques and DFT quantum chemical calculations, Spectrochim. Acta A Mol. Biomol. Spectrosc. 141 (2015) 252–262. https://doi.org/10.1016/j.saa.2015.01.059.

[251] A.A. Siyal, R. Shamsuddin, A. Low, A. Hidayat, Adsorption Kinetics, Isotherms, and Thermodynamics of Removal of Anionic Surfactant from Aqueous Solution Using Fly Ash, Water Air Soil Pollut. 231 (2020) 1–13. https://doi.org/10.1007/S11270-020-04879-2/FIGURES/5.

[252] R. Pardo, L. Taboada-Ruiz, E. Fuente, B. Ruiz, M. Díaz-Somoano, L.F. Calvo, S. Paniagua, Exploring the potential of conventional and flash pyrolysis methods for the valorisation of grape seed and chestnut shell biomass from agri-food industry waste, Biomass Bioenergy 177 (2023) 106942. https://doi.org/10.1016/j.biombioe.2023.106942.

[253] K. Khatib, L. Lahmyed, M. El Azhari, Synthesis, Characterization, and Application of Geopolymer/TiO2 Nanoparticles Composite for Efficient Removal of Cu(II) and Cd(II) Ions from Aqueous Media, Minerals 12 (2022) 1445. https://doi.org/10.3390/min12111445.

[254] Organic-bridged faujasite X zeolites ZOF-X, in: 2007: pp. 539–545. https://doi.org/10.1016/S0167-2991(07)80889-5.

[255] B. Dziejarski, D.F. Hernández-Barreto, J.C. Moreno-Piraján, L. Giraldo, J. Serafin, P. Knutsson, K. Andersson, R. Krzyżyńska, Upgrading recovered carbon black (rCB) from industrial-scale end-of-life tires (ELTs) pyrolysis to activated carbons: Material characterization and CO2 capture abilities, Environ. Res. 247 (2024) 118169. https://doi.org/10.1016/j.envres.2024.118169.

[256] A.E. Ogungbenro, D. V. Quang, K.A. Al-Ali, L.F. Vega, M.R.M. Abu-Zahra, Physical synthesis and characterization of activated carbon from date seeds for CO2 capture, J. Environ. Chem. Eng. 6 (2018) 4245–4252. https://doi.org/10.1016/j.jece.2018.06.030.

[257] X. Ge, X. Hu, C. Shi, The effect of different types of class F fly ashes on the mechanical properties of geopolymers cured at ambient environment, Cem. Concr. Compos. 130 (2022) 104528. https://doi.org/10.1016/j.cemconcomp.2022.104528.

[258] A. Purbasari, D. Ariyanti, E. Fitriani, Adsorption of anionic and cationic dyes from aqueous solutions on fly ash-based porous geopolymer, Global NEST Journal (2023). https://doi.org/10.30955/gnj.004363.

[259] Y. Liao, X. Ma, J. Zou, M. Zhao, D. Chen, D. Xu, B. Yuan, Preparation and adsorption properties of microsphere geopolymers derived from calcium carbide slag and fly ash, Sci. Rep. 15 (2025) 7021. https://doi.org/10.1038/s41598-025-85749-x.

[260] F. Sardella, M. Gimenez, C. Navas, C. Morandi, C. Deiana, K. Sapag, Conversion of viticultural industry wastes into activated carbons for removal of lead and cadmium, J. Environ. Chem. Eng. 3 (2015) 253–260. https://doi.org/10.1016/j.jece.2014.06.026.

[261] M.I. Khan, Teoh.K. Min, K. Azizli, S. Sufian, H. Ullah, Z. Man, Effective removal of methylene blue from water using phosphoric acid based geopolymers: synthesis, characterizations and adsorption studies, RSC Adv. 5 (2015) 61410–61420. https://doi.org/10.1039/C5RA08255B.

[262] J. Gong, S. Li, Y. Zhang, N. Zhang, Alkali-thermal co-activation synthesis of solid waste-derived activated carbon-geopolymer composites for enhanced tetracycline hydrochloride adsorption: Mechanisms and performance, J. Environ. Chem. Eng. 14 (2026) 120623. https://doi.org/10.1016/j.jece.2025.120623.

[263] R. He, N. Dai, Z. Wang, Thermal and Mechanical Properties of Geopolymers Exposed to High Temperature: A Literature Review, Advances in Civil Engineering 2020 (2020) 7532703. https://doi.org/10.1155/2020/7532703.

[264] O.A. Abdulkareem, A.M. Mustafa Al Bakri, H. Kamarudin, I. Khairul Nizar, A.A. Saif, Effects of elevated temperatures on the thermal behavior and mechanical performance of fly ash geopolymer paste, mortar and lightweight concrete, Constr. Build. Mater. 50 (2014) 377–387. https://doi.org/10.1016/J.CONBUILDMAT.2013.09.047.

[265] P. Rożek, M. Król, W. Mozgawa, Geopolymer-zeolite composites: A review, J. Clean. Prod. 230 (2019) 557–579. https://doi.org/10.1016/j.jclepro.2019.05.152.

[266] M. Baghdadi, E. Ghaffari, B. Aminzadeh, Removal of carbamazepine from municipal wastewater effluent using optimally synthesized magnetic activated carbon: Adsorption and sedimentation kinetic studies, J. Environ. Chem. Eng. 4 (2016) 3309–3321. https://doi.org/10.1016/j.jece.2016.06.034.

[267] D. Chen, S. Xie, C. Chen, H. Quan, L. Hua, X. Luo, L. Guo, Activated biochar derived from pomelo peel as a high-capacity sorbent for removal of carbamazepine from aqueous solution, RSC Adv. 7 (2017) 54969–54979. https://doi.org/10.1039/C7RA10805B.

[268] M.A. Décima, S. Marzeddu, M. Barchiesi, C. Di Marcantonio, A. Chiavola, M.R. Boni, A Review on the Removal of Carbamazepine from Aqueous Solution by Using

Activated Carbon and Biochar, Sustainability 13 (2021) 11760. https://doi.org/10.3390/su132111760.

[269] M.A.S. D. Barros, P. A., E. A., General Aspects of Aqueous Sorption Process in Fixed Beds, in: Mass Transfer - Advances in Sustainable Energy and Environment Oriented Numerical Modeling, InTech, 2013. https://doi.org/10.5772/51954.

[270] Y. Liu, Q. Li, H. Pan, L. Liang, L. Zhao, Q. Shi, C. Zhao, X. Liu, Adsorption of carbamazepine on self-endowed magnetic biochar produced from iron-rich sludge, RSC Adv. 15 (2025) 44486–44494. https://doi.org/10.1039/D5RA03580E.

[271] M.S. Alsalhi, K.L.A. Chan, Amino acid hydrotropes to increase the solubility of indomethacin and carbamazepine in aqueous solution, Int. J. Pharm. 617 (2022) 121591. https://doi.org/10.1016/j.ijpharm.2022.121591.

8. APPENDIX

APPENDIX A - HPLC Calibration.

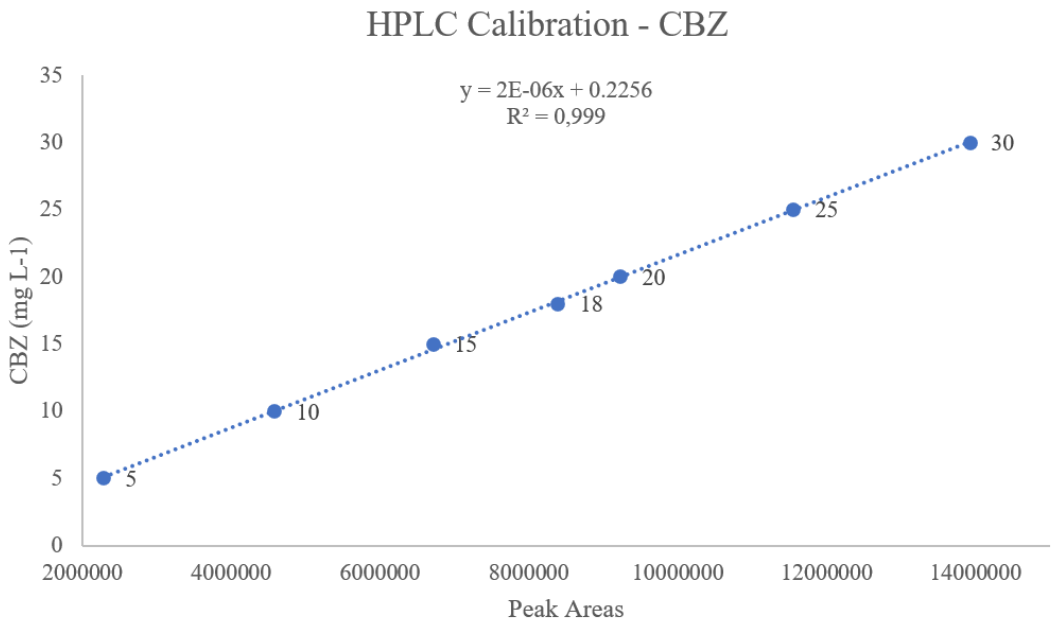

Figure 18: CBZ calibration curve obtained by HPLC.

APPENDIX B – pH_{pzc} graphs.

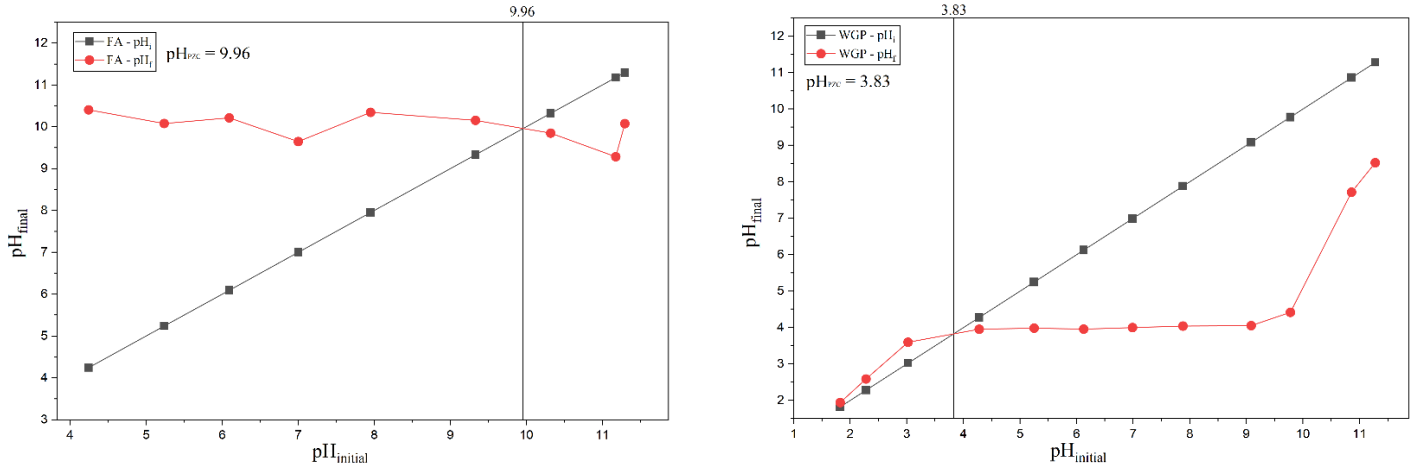

Figure 19: pH_{PZC} graph by FA and WGP.

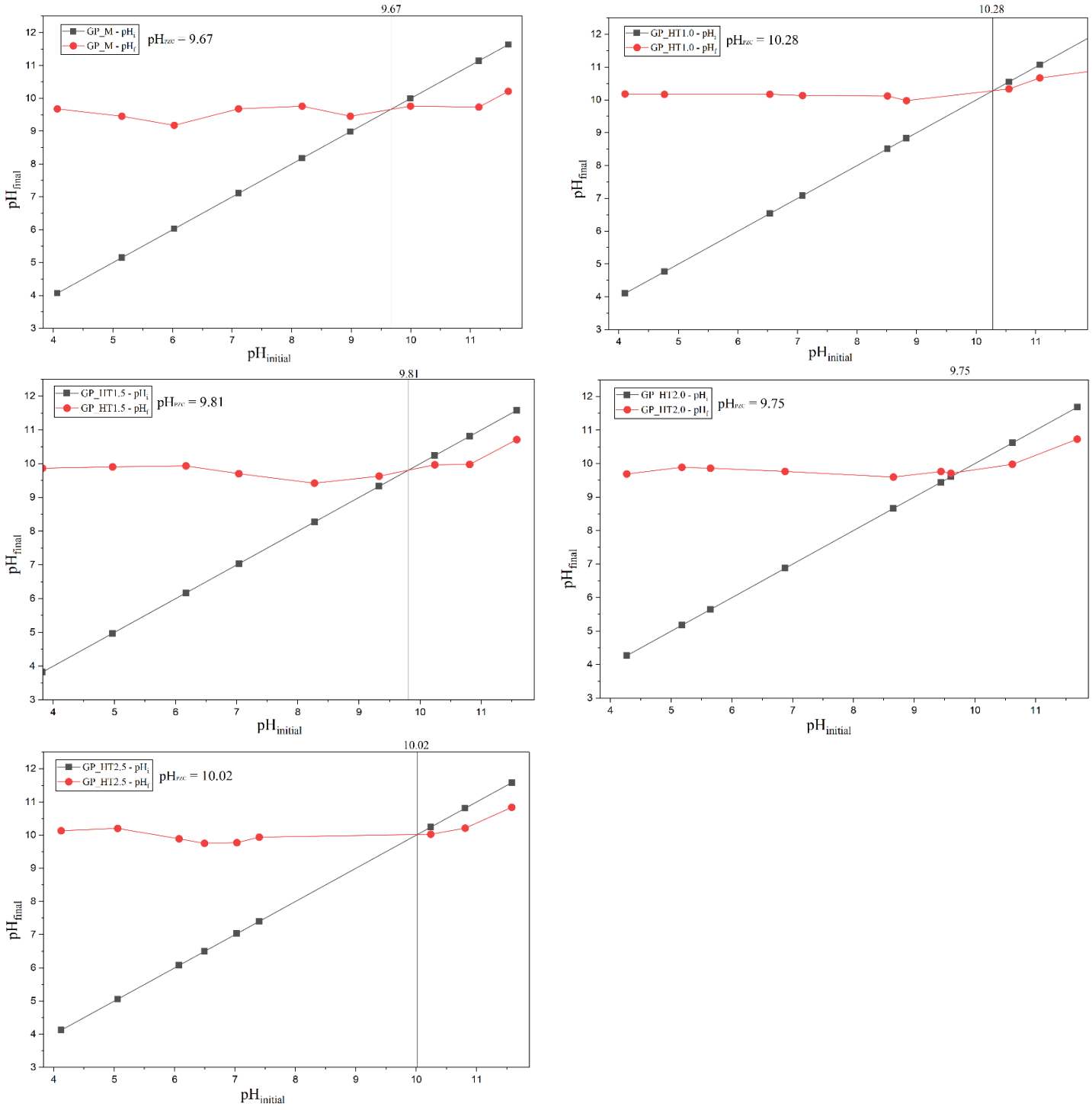

Figure 20: pH_{PZC} graph by GP_M, GP_HT1.0, GP_HT1.5, GP_HT2.0, and GP_HT2.5.

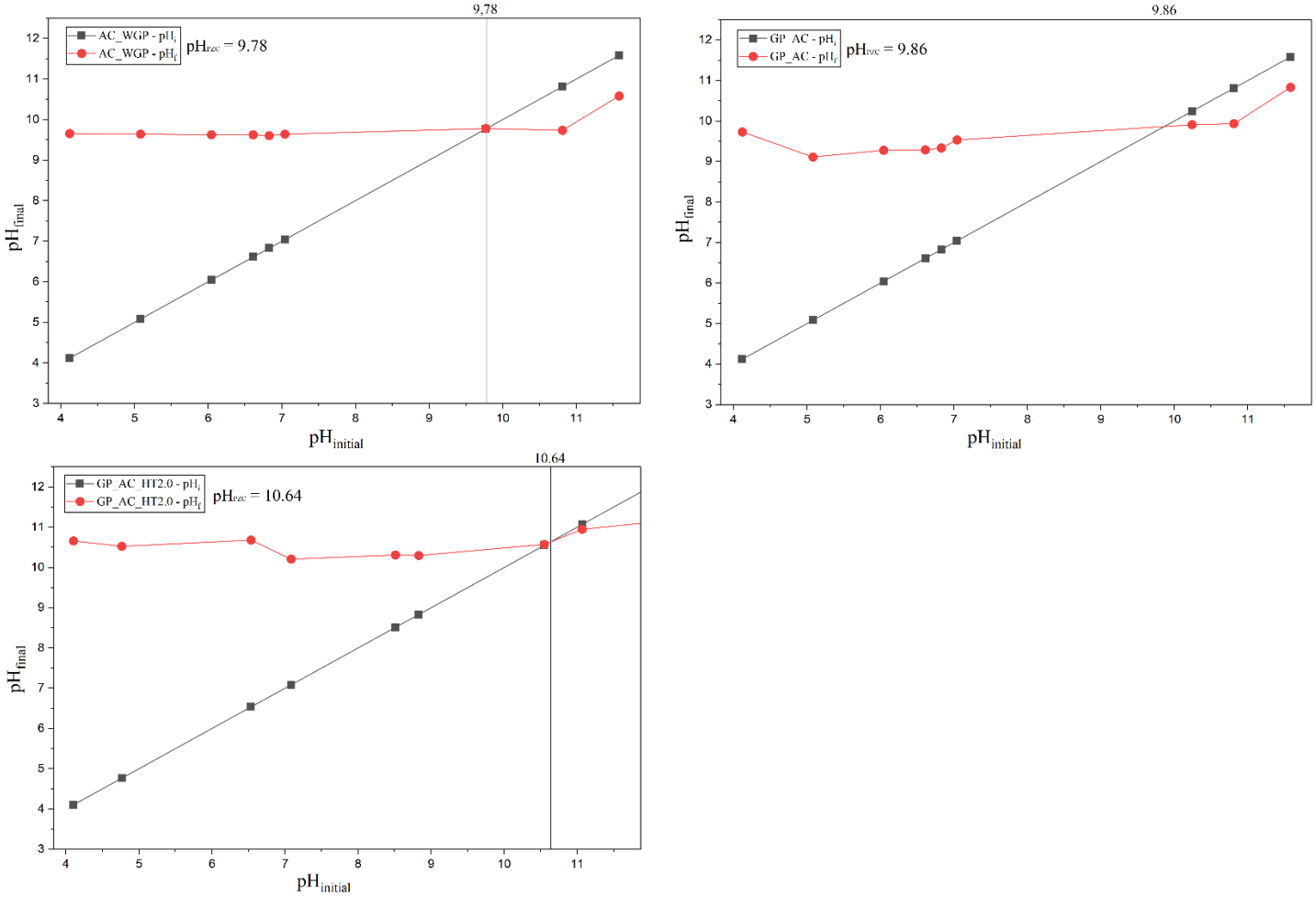

Figure 21: pH_{PZC} graph by AC_WGP, GP_AC, and GP_AC_HT2.0.